Characterization of Tmem128 – An activity regulated ER protein, interacting with the immediate early gene Arc/Arg3.1

Dissertation
zur Erlangung des akademischen Grades des
Doktors der Naturwissenschaften (Dr. rer. nat.)

Eingereicht im Fachbereich Biologie, Chemie, Pharmazie
der Freien Universität Berlin

vorgelegt von

Jakob Gutzmann

aus Berlin

Berlin, 2013

1st reviewer: Prof. Dr. Stephan Sigrist

2nd reviewer: Prof. Dr. Dietmar Kuhl

Date of Disputation: 15.08.2013

Table of contents

Acknowledgement

First of all I would like to thank Professor Dietmar Kuhl for providing me with the opportunity to conduct my doctoral research in his laboratory, for scientific liberty and for advice during my thesis. I would also like to thank Dietmar for the opportunity to apply for a scholarship and become a member of the DFG Research Training Group „GRK1123 - Cellular Mechanisms of Learning and Memory Consolidation in the Hippocampal Formation ". I met fellow scientists and friends in the GRK. Stephanie, Vanessa, Elisa „Black Magic", Elena, Jens, Gürsel, Micha, Benni, Sascha, and Johannes „Handle with Care". Thank you all!

I would also like to thank Prof. Stephan Sigrist for agreeing to be a reviewer of this thesis and for helpful advice during my time in the GRK1123.

Further I would like to thank PD Dr. Guido Hermey for the close and cordial cooperation on different projects and for his supervision of my work. Moreover I would like to thank Guido for interesting scientific discussions, hands-on support (Guido and Johnny Cash made TAP-analysis possible) and his help in analyzing and evaluating my thesis' data. And of course for his critical review of this manuscript.

Additionally I would like to thank all the members of the Institute for Molecular and Cellular Cognition. Particularly I would like to mention Lars Binkle, without whom I would not have been able to finish my thesis in the way I did.

I also owe thanks to the PhD students of the ZMNH, who made working there a very enjoyable experience. Luisa, Kay, Daniel, Sandra, Andrea, Anna, Tiemo, Florian, Sergio, Xiaoyan, Daniel, Francesca, Oli, Ben...

Last but not least, my thank goes to Can from „Fabulous Coffee" and Sandro from „Magris Antipasti".

Synopsis

Arc/Arg3.1 is highly and transiently expressed following activity-inducing stimuli that produce synaptic plasticity. Its mRNA is actively transported into those dendritic branches with a history of recent activity. Arc/Arg3.1 knockout mice show a severe deficit in the consolidation of neuronal plasticity and long-term memories whereas synaptic transmission and the formation of short-term memory are unaffected. Previously described interaction partners of Arc/Arg3.1 suggest a role for Arc/Arg3.1 in endocytosis and intracellular sorting of neuronal transmembrane proteins. Specifically, Arc/Arg3.1 has been implicated in activity-dependent changes of AMPA-type glutamate receptor levels in the postsynaptic membrane, a mechanism considered important for different forms of synaptic plasticity. More recently Arc/Arg3.1 has also been identified to regulate activity-dependent trafficking of Presenilin1, a component of the gamma-secretase complex that plays an important role in neuronal development, synaptic plasticity and the pathogenesis of Alzheimer's disease.

Mechanistically, however, it is still unclear how Arc/Arg3.1 influences intracellular trafficking. Since many of the functions of Arc/Arg3.1 involve membrane dynamics or transmembrane proteins like AMPA receptors and Presenilin1, I searched for membrane bound and transmembrane interaction partners of Arc/Arg3.1. Using a Split-Ubiquitin Yeast-2-Hybrid screen I identified RIP5 and Tmem128, two so far uncharacterized multiple-pass transmembrane proteins. I confirmed their interaction with Arc/Arg3.1 in additional experiments and determined the topology of RIP5 and Tmem128 within the ER membrane. In cultured neurons RIP5 and Tmem128 are localized to the endoplasmic reticulum (ER) and are also found to colocalize with Arc/Arg3.1 and PSD95 in a subset of spines. Using northern blot analysis and in situ hybridization I could demonstrate the expression of both genes in a variety of tissues and brain regions. Moreover, I generated an antibody against Tmem128 and used this to show that the protein is expressed in the hippocampus, the cerebellum and the cerebral cortex. Furthermore, Tmem128 expression is high in brains of neonate mice and decreases during adolescence. I used genomic analysis and RT-PCR to show that Tmem128 is alternatively spliced and that neurons express two mRNAs which encode an identical Tmem128 protein but harbor mutually exclusive 3'-UTRs. The use of individual exons as 3'UTRs has so far not been described in the literature and its biological significance is likely of regulatory nature. In accordance with that, the longer splice variant is induced by synaptic activity in cultured hippocampal neurons and in the hippocampus of mice and it is accompanied by increased protein levels of Tmem128. To gain further functional insight I generated Tmem128 knockout mice. These animals are overall healthy and showed no gross alterations in brain morphology as well as neuronal ER distribution. Furthermore, knockout animals showed normal expression levels of glial and interneuron markers as well as glutamate receptors in whole brain lysates and crude synaptic membranes. Given the

inducible expression of Tmem128, future experiments in the knockout mice will address the role of Tmem128 in activity-induced neuronal processes, many of which are directly or indirectly dependent on the endoplasmic reticulum.

Zusammenfassung

Aktivitätsinduzierende Stimuli, die synaptische Plastizität auslösen, sorgen für einen starken und transienten Anstieg in der Expression von Arc/Arg3.1. Die Arc/Arg3.1 mRNA wird dabei aktiv in die dendritischen Regionen transportiert, die dieser Aktivität ausgesetzt waren. Mäuse mit einer genetischen Deletion von Arc/Arg3.1 zeigen schwere Störungen in der Konsolidierung von synaptischer Plastizität und im Langzeitgedächtnis, während grundlegende synaptische Transmission und das Kurzzeitgedächtnis intakt sind. Beschriebene Interaktionspartner von Arc/Arg3.1 legen nahe, dass Arc/Arg3.1 an der Endozytose und intrazellulären Sortierung von neuronalen Transmembranproteinen beteiligt ist. Im Speziellen wurde Arc/Arg3.1 mit aktivitätsabhängigen Änderungen der Oberflächenexpression von Glutamatrezeptoren des AMPA Typs in Verbindung gebracht, ein Mechanismus, der für verschiedene Formen der synaptischen Plastizität wichtig ist. Kürzlich wurde auch gezeigt, dass Arc/Arg3.1 die aktivitätsabhängige intrazelluläre Sortierung von Presenilin1 reguliert, einer Komponente des gamma-Sekretase Komplexes, der eine Rolle in neuronaler Entwicklung spielt, sowie bei synaptischer Plastizität und der Pathogenese von Morbus Alzheimer.

Über welche Mechanismen Arc/Arg3.1 diese intrazellulären Sortierungsprozesse beeinflusst, ist noch immer unklar. Da die beschriebenen Funktionen von Arc/Arg3.1 Membrandynamiken beeinflussen und Transmembranproteine wie AMPA Rezeptoren und Presenilin mit einschließen, habe ich spezifisch nach membran-assoziierten neuen Interaktionspartnern für Arc/Arg3.1 gesucht. Unter Verwendung des Split-Ubiquitin Hefe-2-Hybrid Systems konnte ich RIP5 und Tmem128, zwei bis jetzt nicht charakterisierte Transmembranproteine, identifizieren. Ich habe die Interaktion dieser Proteine mit Arc/Arg3.1 in weiteren Experimenten bestätigen können und ihre Topologie innerhalb der ER Membran bestimmt. In kultivierten Neuronen sind RIP5 und Tmem128 im Endoplasmatischen Retikulum (ER) zu finden, sowie kolokalisiert mit Arc/Arg3.1 und PSD95 in einer Fraktion dendritischer Dornenfortsätze. Northern Blots und in situ Hybridisierungen ergaben, dass beide Gene in verschiedenen Geweben und Hirnregionen der Maus exprimiert werden. Zudem habe ich einen Antikörper gegen Tmem128 generiert, mit dem ich die Expression des Proteins in Hippokampus, Kleinhirn und Großhirnrinde bestätigen konnte. Entwicklungsabhängig ist die Expression von Tmem128 in den Gehirnen neugeborener Mäuse stark und nimmt im Laufe der ersten Lebenswochen ab. Darüber hinaus ergaben Genomanalyse und RT-PCRs, dass Tmem128 in Neuronen alternativ gespleißt wird. Beide mRNAs kodieren für das gleiche Protein, enthalten aber sich gegenseitig ausschließende 3'UTRs. Die Verwendung eigenständiger Exons für alternative 3'UTRs wurde bislang noch nicht beschrieben, ist jedoch vermutlich für die Regulation der Expression bedeutsam. Dies scheint auch für Tmem128 der Fall zu sein, da selektiv die längere der beiden Varianten durch synaptische Aktivität induziert wird. Dies konnte ich sowohl in kultivierten hippokampalen Neuronen als auch im intakten Hippokampus der Maus zeigen. Zusätzlich konnte ich die aktivitätsabhängige Induktion von Tmem128 im Hippokampus der Maus auf Proteinebene bestätigen. Zur

weiteren Charakterisierung der Proteinfunktion habe ich Tmem128 knockout-Mäuse generiert. Die genetisch veränderten Mäuse zeigen eine normale postnatale Entwicklung und keine Veränderungen in ihrer makroskopischen Gehirnanatomie sowie der Morphologie des neuronalen ER. Zudem exprimieren die knockout-Mäuse normale Level von Gliazell- und Interneuron-Markern sowie von Glutamatrezeptoren, soweit dies in Hirnlysaten und isolierten synaptischen Membranfraktionen erkennbar ist. Im Hinblick auf die induzierbare Expression von Tmem128 werden zukünftige Untersuchungen in den knockout-Mäusen die Funktion dieses Proteins in aktivitätsinduzierten neuronalen Prozessen untersuchen, von denen viele direkt oder indirekt vom endoplasmatischen Retikulum abhängen.

1 Introduction

1.1 Learning and memory

In order to adapt to a constantly changing environment, animals have evolved the ability to use past experiences to guide their decisions. This requires the storage and retrieval of specific information, a phenomenon we call learning and remembering. The organ in an animal's body that is responsible for this astounding feat is the brain, which is composed of two major cell types: Glia cells and neurons. The human brain consists of roughly 86 billion neurons with the average neuron forming between 1.000 and 10.000 connections to other neurons (Herculano-Houzel 2012). In the adult brain the vast majority of these connections appear in the form of a highly specialized structure: The chemical synapse. Even though there is a staggering diversity of synapse morphologies and types, the basic components and mechanism of action are always the same. Synapses are comprised of the presynaptic side, provided by the neuron sending information, and the postsynaptic side, provided by the neuron (or muscle cell) receiving information. Both sides are divided by the synaptic cleft and, very often, isolated from the surrounding extracellular space by astrocytic glia cells, thus forming the so called tripartite synapse (Araque et al. 1999; Dityatev and Rusakov 2011). Recently, there has been growing support for the idea that the synaptic cleft itself, or more precisely the glycoprotein rich extracellular matrix (ECM) which fills the synaptic cleft, also plays a major role in synapse function (Gundelfinger et al. 2010; Frischknecht and Gundelfinger 2012).

At the presynaptic side an electrical signal that is generated by the presynaptic neuron, called action potential (AP), is transduced into a chemical signal in the form of neurotransmitters. These neurotransmiters cross the synaptic cleft and are recognized by receptors on the postsynaptic side. If enough signals reach the postsynaptic cell, a new AP may be generated and propagated along the postsynaptic neuron to the next synapse. This cascade, although being orders of magnitude slower than a purely electrical signal, has the undisputable advantage of being modifiable. The amount of transmitter released by the presynaptic side, the dwell time of transmitter in the synaptic cleft, and, most importantly, the type, number and distribution of postsynaptic receptors are all regulated and can be adapted according to the circumstances - a phenomenon we call synaptic plasticity.

It is highly debated how and where in the brain memories are formed and stored, but given the extraordinary amount and complexity of synaptic connections, synaptic plasticity has emerged as a prime candidate for the physical correlate of learning and memory (Bliss and Collingridge 1993; Malenka and Bear 2004; Whitlock et al. 2006; Mayford et al. 2012). Most synaptic contacts are located on the dendritic tree, either on the dendritic shaft itself or on small membrane protrusions called dendritic spines. Because of the complicated branched architecture of the dendritic tree, and the vast number of synaptic contacts formed by the average neuron, neurons face enormous cell biological challenges. Among them are the large amount of lipids needed for the plasma membrane and the long distances that need

to be overcome in neuronal intracellular trafficking and transport. Also, in order to generate meaningful electrical and chemical signals with a high signal to noise ratio, neurons need the ability to control their intracellular and extracellular space. By tightly regulating the spatial distribution and the released amount of signaling molecules as well as the number and position of signaling receptors on the plasma membrane, neurons are able to sense and integrate a large number of different signals, excitatory, inhibitory or modulatory, from other neurons in order to decide whether or not to generate an action potential.

One intensely studied brain region in rodents is the hippocampal formation. Located in the temporal lobe of the mammalian brain and anatomically highly structured, the hippocampus is considered to be a crucial gateway in the brain for experiences and information to be consolidated into long-term memories (Eichenbaum 2000; van Strien et al. 2009). The hippocampal formation contains the Subiculum (Sb), the perirhinal and entorhinal cortices, as well as the hippocampus proper, which comprises the dentate gyrus (DG) and the cornu ammonis regions 1-3 (CA1-CA3). Although information reaches and leaves the hippocampus via various input and output projections, the main pathway for information processing is thought to be the trisynaptic loop: Axons from layer II of the entorhinal cortex (collectively termed the perforant path) connect to dendrites of the granule cell neurons in the DG. From there, information is passed on to pyramidal neurons of CA3 via the mossy fiber axon bundles. CA3 then projects via Schaffer collaterals onto pyramidal neurons of CA1, which in turn project, partially via the subiculum, back to the entorhinal cortex, thus closing the loop (Amaral and Witter 1989; Yeckel and Berger 1990) (Figure 1).

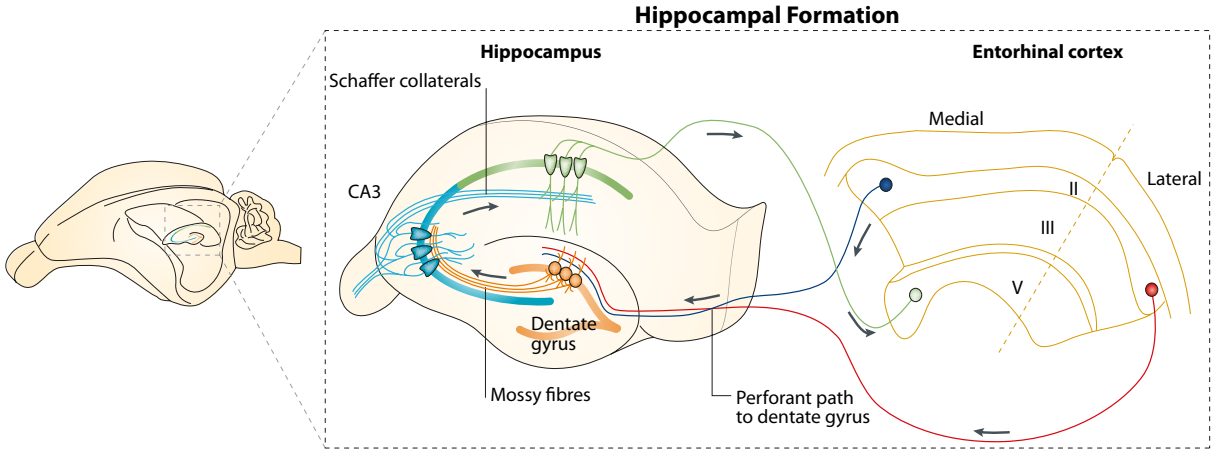

Figure 1: The hippocampal formation.

Schematic representation of the hippocampal formation and its position within the rodent brain. Only the main synaptic pathways into and out of the hippocampus are depicted. Arrows indicate the direction of information flow from the entorhinal cortex via the dentate gyrus to CA1 and CA3 back to the entorhinal cortex. Figure modified from Neves et al. (2009).

Brenda Milner and William Scoville first described the case of the now famous patient Henry Molaison (Scoville and Milner 1957), who had both hippocampi and neighboring brain regions removed as a matter of last resort to stop his temporal lobe epilepsy from spreading to other brain regions. This intervention resulted in almost complete anterograde amnesia, while his perceptual and cognitive capacities stayed intact (Corkin 1984). Brenda Milner and Suzanne Corkin kept working with Henry Molaison until his death in 2008 and deepened our understanding of the importance of the hippocampus for different forms of memory. Lesion studies in mammals have since established the hippocampus as a crucial region for the formation of a number of spatial and non-spatial associative memories (Eichenbaum 2013).

Changes in the strength of synaptic connections as a result of sensory experience have long been hypothesized as correlates of information storage (Hebb 1949; Stent 1973) and indeed, physiological studies have uncovered the potential of hippocampal neurons to undergo strong and long lasting forms of synaptic plasticity (Bliss and Lomo 1973). Involving physiology and morphology of the synapse, the synaptic strength increases when synapses undergo long-term potentiation (LTP), a Hebbian type of plasticity. Named after the Canadian psychologist Donald Hebb, who more than 60 years ago formulated the theory that the correlated activity of a presynaptic and a postsynaptic neuron would strengthen the connection between the two (Hebb 1949), LTP now serves as a model for associative memory (Bliss and Collingridge 1993; Pastalkova et al. 2006). The alternative direction of modification, i.e. the weakening of synaptic strength after uncorrelated pre- and postsynaptic activity, was proposed by Gunther Stent (Stent 1973). Long-lasting forms of this decrease in synaptic strength are called long-term depression (LTD).

Different forms of synaptic plasticity have been described to date and the molecular basis for each form of plasticity varies. However, given the ubiquity of various short- and long-lasting forms of synaptic plasticity in diverse brain regions and circuits, it is highly likely that the brain takes advantage of these mechanisms to perform complicated computations and to store and retrieve information (Bliss and Collingridge 1993; Malenka and Bear 2004; Fusi et al. 2005; Neves et al. 2008).

1.2 Molecular mechanisms underlying synaptic plasticity

Glutamate, the major excitatory neurotransmitter in the vertebrate central nervous system, is recognized by different postsynaptic receptors that can be categorized into ionotropic receptors, which form ion channels, and metabotropic receptors, which activate second messenger cascades. The two main classes of ionotropic receptors are NMDA receptors (NMDARs) and non-NMDA receptors of which the AMPA type receptor is the most prevalent. Named after the selective agonists AMPA (α-amino-3-hydroxy-5-methyl-4-isoxazole-propionic acid) and NMDA (N-methyl D-Aspartate), both types of receptors

are heterotetramers of transmembrane protein subunits and form ion selective pores in the postsynaptic membrane (Wisden and Seeburg 1993; Hollmann and Heinemann 1994). In the hippocampus, most AMPAR are composed of heterodimers of the subunits GluA1 and 2 or GluA2 and 3. While AMPARs open upon glutamate binding and mediate the main ionic conductance of the postsynaptic cell, NMDARs require an additional signal for channel opening. In the resting state the pore of the NMDAR is blocked by a Mg^{2+} ion and only by depolarization of the postsynaptic membrane is this block released and the NMDAR will conduct current upon glutamate binding (Mayor et al. 1984; Nowak et al. 1984; Mayer et al. 1992). The NMDAR thus acts as a coincidence detector for presynaptic activity (glutamate release) and postsynaptic activity (membrane depolarization), while the AMPARs are mainly responsible for the strength of the electrical signal that is generated on the postsynaptic side upon glutamate binding.

Because of the special characteristics of the NMDAR, it has often been described as the molecular sensor responsible for Hebbian plasticity at single synapses. Only by correlated activation of the pre- and postsynaptic neuron does the NMDAR open. In contrast to the majority of AMPARs (depending on their subunit composition), NMDARs permit Ca^{2+}, as well as Na^{+} to enter the cell. The effect of Ca^{2+} on the electrical charge of the postsynaptic membrane is marginal but it acts as a powerful signaling molecule. Intracellular Ca^{2+} can be bound by a number of proteins which then act as cofactors for enzymes in plasticity related processes (Malenka et al. 1988; Berridge 1998; Mikhaylova et al. 2006).

1.2.1 AMPA receptor trafficking

One of the local effects of Ca^{2+} influx in the spine is the regulated phosphorylation and dephosphorylation of synaptic proteins by Ca^{2+} dependent kinases. This can lead to the regulated insertion or deletion of AMPAR from the postsynaptic membrane, termed AMPAR trafficking, which emerged as the leading mechanism underlying postsynaptic LTP and LTD (Hey-Kyoung Lee et al. 2003; Collingridge et al. 2004; Shepherd and Huganir 2007). Functional properties and trafficking behavior of AMPARs depend on their subunit composition and the most structurally and functionally divergent element of the individual subunits is their intracellular c-terminus (Malinow and Malenka 2002; Collingridge et al. 2004; Derkach et al. 2007).

Several posttranslational modifications and interacting proteins of the GluA C-termini have been identified as being involved in the trafficking of AMPARs. Some proteins anchor AMPARs to the postsynaptic density (PSD), an electron dense layer of scaffolding proteins and signaling complexes beneath the postsynaptic membrane (Opazo et al. 2010; Opazo and Choquet 2011). Other proteins post-translationally modify AMPARs to change their electrophysiological properties (Barria et al. 1997; Benke et al. 1998; Banke et al. 2000;

Derkach et al. 2007). Again other proteins aid in the recycling, sorting and extrasynaptic/ endosomal storage of AMPARs (Ehlers 2000; José A Esteban 2003; H.-Y. Man et al. 2007; Y. Yang et al. 2008).

However, although much has been learnt about synaptic plasticity and AMPAR trafficking, for many cellular circumstances it is still unclear which rules govern the composition of the postsynaptic signaling complex and thus control the signal integrating ability of the neuron.

1.2.2 Calcium activated transcription

In addition to these local effects, Ca^{2+} influx into the postsynaptic neuron can alter cellular function by activating new gene transcription. Flexner et al. had shown in 1963 that the formation of long-term memories is dependent on novel protein synthesis and Ca^{2+} is an ideal candidate to regulate this process (J. B. Flexner et al. 1963; Berridge 1998). Ca^{2+} influx activates a number of signaling pathways that converge on transcription factors within the nucleus, which in turn control the expression of a large number of neuronal activity-regulated genes (Greer and Greenberg 2008). Prominent examples of Ca^{2+} dependent transcriptional activators are cAMP response-elemet [CRE] binding protein (CREB) (Sheng et al. 1991; Arthur et al. 2004), Serum response factor (SRF) (Treisman 1987) and Myocyte enhancer factor 2 (MEF2) (McKinsey et al. 2002). CREB is regulated through phosphorylation by different kinases and induces stimulus dependent transcription of various plasticity related genes (Sheng et al. 1990; Fujino et al. 2003). CREB has been shown to play an essential role in translating synaptic activity to increased expression of memory relevant genes (Dash et al. 1990; Kaang et al. 1993; Won and A. J. Silva 2008; Mayford et al. 2012).

SRF and MEF2 are also regulated by Ca^{2+} dependent phosphorylation (Rivera et al. 1993; Xia et al. 1996; Chawla et al. 2003; Linseman et al. 2003) and regulate, among other genes, the activity dependent transcription of Arc/Arg3.1 (Ramanan et al. 2005; Flavell et al. 2006; Kawashima et al. 2009).

1.3 Arc/Arg3.1

In order to identify target genes that are important in synaptic plasticity and thus presumably for learning and memory, changes of gene expression levels in the mammalian brain, and especially the hippocampus, have been analyzed before and after neuronal activity (Nedivi et al. 1993; Qian et al. 1993; Altar et al. 2004; Li et al. 2004; Hong et al. 2004; Park et al. 2006, Hermey et al.). These screens for activity regulated genes revealed one class of tightly regulated genes called immediate early genes (IEG). IEGs had originally been identified in non-neuronal cells as growth-factor responsive genes that might control the reentry of differentiated cells into the cell cycle (Hayward et al. 1981; Kelly et al. 1983; Greenberg and Ziff 1984; Sheng and Greenberg 1990). In the neuronal context, the transcription of

these genes is strongly increased within 10-60 minutes after activity inducing stimuli and it is independent of novel protein synthesis. Thus IEG transcription is only dependent on the posttranslational modifications of existing proteins like transcription factors. The termination of transcription, however, is dependent on protein synthesis, thereby making IEGs highly controlled and regulated genes (Sheng and Greenberg 1990). IEGs themselves are often transcription factors like Npas4 and the zinc-finger containing proteins zif268 and c-fos (Morgan et al. 1987; Cole et al. 1989; Lin et al. 2008). But some, like tissue-plasminogen activator (tPA) or Homer1A, are known to be effector proteins (Qian et al. 1993; Kato et al. 1997; Vazdarjanova et al. 2002). The induction of IEGs by diverse plasticity inducing stimuli is so strong and reliable, that the expression of c-fos, Arc/Arg3.1, and other IEGs is now routinely used to mark and identify neurons that have been recently activated (Guzowski et al. 2005; Wang et al. 2006).

1.3.1 Identification of Arc/Arg3.1

The Activity regulated gene of 3.1 kb (Arg3.1) is an IEG that has been identified by such a screen for plasticity responsive genes in our laboratory (Link et al. 1995). Arg3.1 has been identified in parallel in the laboratory of Paul Worley under the name of Activity regulated and cytoskeleton associated protein (Arc) (Lyford et al. 1995). Arc/Arg3.1 has since been established as an important player in the consolidation of long term memories and its cellular correlate LTP. Arc/Arg3.1 transcription increases within 30 minutes after neuronal activity and stays elevated until 4-8 hours after the end of the stimulus. Various physiological and artificial stimuli lead to an increase in Arc/Arg3.1 mRNA and protein levels in the cortex and hippocampus. Arc/Arg3.1 is unique among IEGs because its mRNA is selectively targeted to dendritic regions of dentate gyrus granule cells that have received synaptic inputs (C. S. Wallace et al. 1998) and it is therefore likely that Arc/Arg3.1 plays an important role in the transformation of strong synaptic activity into increased synaptic efficacy.

The genetic deletion of Arc/Arg3.1 in mice in our laboratory has further strengthened this hypothesis. We could show that Arc/Arg3.1 knockout mice lack the ability to stabilize plastic changes like LTP and LTD on the network level and that they are unable to form long lasting memories in a variety of behavioral paradigms (Plath et al. 2006). Arc/Arg3.1 has no known enzymatic activity and it has yet to be elucidated by which mechanisms Arc/Arg3.1 influences synaptic strength and physiology. However, several interacting proteins for Arc/Arg3.1 have been identified which implicate Arc/Arg3.1 as a regulator of synaptic efficacy and thus help to explain why Arc/Arg3.1 is essential for the consolidation of long term memories.

1.3.2 Arc/Arg3.1 in AMPAR dependent plasticity

A yeast-2-Hybrid screen carried out in the laboratory of Paul Worley identified Dynamin2 and Endophilin3 as interaction partners of Arc/Arg3.1 (Chowdhury et al. 2006). Both proteins are involved in the formation and endocytosis of vesicles. Subsequent experiments that aimed to elucidate the physiological function of these interactions demonstrated that transient overexpression of the three proteins in cultured hippocampal neurons led to a 30% decrease of the AMPAR subunit GluA1 in these neurons and to a 50% decrease of GluA1 at the cell surface. Conversely, analysis of neurons cultured from Arc/Arg3.1 knockout animals showed a ~2-fold increase in surface AMPARs compared to wild type controls and, despite the high availability of surface GluA1, a strong reduction in the rate of GluA1 internalization (Chowdhury et al. 2006).

Work of Hollis Cline showed that Arc/Arg3.1 not only influences AMPAR localization in cultured neurons, but also in cultured hippocampal slices where the neuronal network has a more physiological layout compared to dissociated neuronal cultures. In these experiments, enhanced expression of Arc/Arg3.1 was found to increase internalization of GluA2 containing AMPARs (Rial-Verde et al. 2006). The difference in AMPAR subunit specificity of Arc/Arg3.1 seen between dissociated neurons and slices might be reflective of the differences in recycling speed under baseline conditions seen for GluA1/2 heteromers (Shi et al. 2001). Rial Verde and colleagues therefore speculated, that Arc/Arg3.1 regulates the surface expression of different pools of AMPAR, depending on the history of activity of each synapse and thereby taking part in homeostatic regulatory mechanisms (Rial-Verde et al. 2006).

Further studies of the relationship between Arc/Arg3.1 and AMPA receptors supported this hypothesis and demonstrated, that Arc/Arg3.1 is necessary for activity induced homeostatic synaptic scaling (Shepherd et al. 2006). In this form of synaptic plasticity, neurons react to sustained increases or decreases of activity by globally adjusting their excitability at least in part through the synaptic removal or insertion of AMPARs (Turrigiano 2008). Thereby neurons can increase or decrease their overall firing behavior in response to synaptic inputs, without affecting individual synaptic weights.

In neurons cultured from Arc/Arg3.1 knockout mice this fundamental mechanism is disturbed. Reducing overall synaptic activity by application of the puffer fish toxin Tetrodotoxin (TTX), an antagonist of voltage gated sodium channels, has no effect on the surface levels of AMPARs while it strongly increases surface AMPAR in wild type neurons. Conversely, increasing synaptic activity by applying Bicuculline, an antagonist of the inhibitory GABA-A receptor, strongly decreases surface AMPARs in wild type neurons but has no effect on hippocampal cultures from Arc/Arg3.1 knockout animals. Activation of NMDARs with their co-agonist glycine, a form of chemically induced LTP, increases the surface presence of AMPARs in both

wild type and Arc/Arg3.1 knockout neurons, proving that general mechanisms of AMPAR trafficking are intact and that Arc/Arg3.1 is necessary only for certain activity dependent forms of AMPAR trafficking (Shepherd et al. 2006).

Arc/Arg3.1 has also been shown to be an important player in another type of AMPAR dependent type of plasticity, namely synapse-specific homeostatic plasticity. In this form of plasticity, a single synapse reacts to prolonged changes of input with an adaptive up- or down regulation of its AMPAR content. In a study in 2011, Béïque and colleagues described an experimental setting in which, by genetically inactivating a presynaptic neuron for a certain amount of time, the activation of a single postsynaptic spine showed profound up-regulation of their AMPAR content, specifically of AMPARs lacking the Ca^{2+} permeable GluA2 subunit. This phenomenon of synapse-specific homeostatic plasticity was occluded in neurons cultured from Arc/Arg3.1 knockout mice, presumably due to their already relatively high surface levels of GluA1 containing AMPARs (Béïque et al. 2011).

1.3.3 Arc/Arg3.1 in activity dependent gamma-secretase trafficking

However, regulation of AMPAR surface levels is not the only synaptic trafficking event that Arc/Arg3.1 has been implicated in. Alberi and colleagues described that upon synaptic activity, the Notch1 receptor is proteolytically processed and the transcriptionally active Notch1 intracellular domain (NICD1) is released (Alberi et al. 2011). This proteolytic cleavage is performed by a protease complex called gamma-secretase, which consists of the protease subunit Presenilin1 (PS1) as well as accessory proteins Pen-2, Aph-1 and Nicastrin (Kimberly et al. 2003). Notch1 signalling has been mostly studied in a developmental context (Stump et al. 2002), but it has also been implicated in adult neuronal functions, among them synaptic plasticity (Costa et al. 2003; de Bivort et al. 2009). It has so far been unclear, where Notch1 is expressed in mature brains and how Notch1 signaling is regulated and it remains unknown, how Notch1 or NICD1 affect synaptic plasticity. However, Alberi and colleagues clearly demonstrated that Notch1 and Arc/Arg3.1 are coexpressed in hippocampal neurons after synaptic activity and that the activity dependent processing of Notch1 to NICD1 is absent in Arc/Arg3.1 knockout neurons and can be rescued by virally reintroducing Arc/Arg3.1 in these neurons (Alberi et al. 2011).

Another very prominent target of the gamma-secretase protease complex is the Amyloid Precursor Protein (APP). Sequential processing of APP by different proteases can either be along the non-amyloidogenic pathway (Kojro and Fahrenholz 2005) or along the amyloidogenic pathway (Gandy 2005; Thinakaran and Koo 2008). Of which the latter leads to the generation of the amyloid peptide Aβ. The generation of Aβ from APP is one of the main mechanisms implicated in the development of Alzheimer's disease (AD) (Glenner and C. W.

Wong 1984; Goldgaber et al. 1987; Tanzi and Bertram 2005), and since the catalytic site of the gamma-secretase resides within the membrane, a critical factor in the amyloidogenic process is the presence of APP and gamma-secretase within the same membrane.

In a study in 2011, Wu and colleagues demonstrated that activity dependent processing of APP and increase of extracellular Aβ levels are dependent on the presence of Arc/Arg3.1. Moreover, Arc/Arg3.1 binds to PS1 and the interaction of both proteins is necessary for the increase of gamma-secretase activity after neuronal activity. Alzheimer's disease mouse models that were genetically modified to contain mutations in APP and PS1 were crossed to Arc/Arg3.1 knockout mice. At the age of 6 months, these mice had a severely reduced Aβ plaque load in the brain, compared to Arc/Arg3.1 wild type AD-mice. Interestingly, post mortem tissue samples from the brains of patients with AD showed increased levels of Arc/Arg3.1 compared to age matched control samples (Wu et al. 2011), which further emphasizes the connection between the expression levels of Arc/Arg3.1 and Aβ.

Taken together, these results demonstrate that Arc/Arg3.1 is a key regulator of diverse trafficking events that are essential for synaptic physiology and that are inducible by neuronal activity.

1.4 The endoplasmic reticulum

1.4.1 Morphology

With the advent of electron microscopy, a "lace-like reticulum" was identified in chick epithelial cells (Porter et al. 1945), which was later named the endoplasmic reticulum (ER) (Porter 1953; Palade and Porter 1954). Nowadays we know that this multifunctional organelle consists of a vast network of intracellular membranes which surrounds a common luminal space (Martone et al. 1993). The ER originates at the nucleus and emerges from the outer membrane of the nuclear envelope and its lumen is a continuation of the perinuclear space. Near to the nucleus the ER consists of sheet like cisterna and tubules that are connected by three-way junctions. Further out in the cell periphery the ER consist only of tubules (Shibata et al. 2006; Friedman and Voeltz 2011). The ER is tightly associated with the cytoskeleton and other membranous organelles, like the mitochondria, via protein complexes and it continuously exchanges material in the form of trafficking vesicles with the Golgi apparatus (Baumann and Walz 2001; Csordás et al. 2010; Lord et al. 2013).

The neuronal ER displays tremendous morphological complexity with networks of interconnected tubules entering dendrites and axons. This morphological complexity increases during development and is especially pronounced in dendritic areas of high spine density and at nodes of Ranvier in axons (Cui-Wang et al. 2012). In dendrites, the ER reaches even the finest dendritic branches and occasionally also enters the spine neck and head

(Figure 2) (Terasaki et al. 1994; Spacek and Harris 1997; Cooney et al. 2002; Toresson and Grant 2005). In a subset of spines the ER gives rise to an enigmatic organelle called spine apparatus (Gray 1959; Spacek 1985). The function of the spine apparatus remains elusive, but there is accumulating evidence that the spine apparatus serves as a Ca^{2+} source/sink in different forms of synaptic plasticity (Holbro et al. 2009; Vlachos et al. 2009).

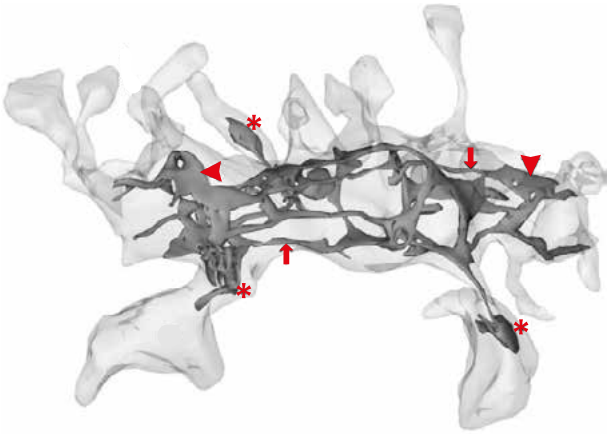

Figure 2: Dendritic ER.

Three-dimensional reconstruction of the smooth ER (sER) of a short dendritic branch demonstrates that the cisternae form a network with larger flat compartments (arrowheads) connected by thin extensions (arrows). Seventeen spines originate from this segment of dendrite. sER is found in only three spines (*), two of which are large mushroom spines with spine apparatuses. Modified after Cooney et al. (2002).

1.4.2 Protein synthesis

One of the major functions of the ER is the synthesis of transmembrane proteins and proteins destined for secretion or the use in endosomal compartments such as the lysosome. Microscopically this is visualized by ribosomes that associate with the ER and give it a studded appearance in electron micrographs (rough ER - rER). In the cell periphery the number of ribosomes associated with the ER decreases and the ER thus has a smoother appearance in electron micrographs (smooth ER - sER) (Shibata et al. 2006).

In neurons the importance of the ER for protein synthesis is highlighted by the fact that ER exit sites (ERES), where cargo leaves the ER for the Golgi apparatus (Hammond and Glick 2000), are distributed along the dendritic tree in addition to somatic regions (Aridor et al. 2004). The Golgi apparatus is needed for further modification and maturation of transmembrane proteins and, similar to the exit sites, so called Golgi outposts have evolved (Horton and Ehlers 2003). These outposts are usually situated at dendritic branch points. This system of ERES‘ and Golgi outposts is ideally suited for local translation and maturation of novel transmembrane proteins and it may have evolved in order to compensate for the vast transport distances in dendrites and axons. This applies to all newly synthesized proteins under baseline conditions, as well as to proteins that are specifically needed after the onset of a synaptic stimulus (Kang and Schuman 1996; Swanger and Bassell 2012).

Newly synthesized proteins can reach the synapse by different means. In the canonical route, proteins are synthesized in the somatic ER, post-translationally modified in the somatic golgi, and reach the synapse via post-golgi carrier vesicles that are transported by molecular motors along microtubules (Figure 3A, route 1). In the more recently described

non canonical route, proteins can be synthesized in the somatic ER, transported within the ER membrane to dendritic ERES and then be processed in golgi outposts (Figure 3A, route 2). Proteins can also be synthesized and processed locally from dendritic mRNA (Figure 3A, route 3) (Cajigas et al. 2010) and several examples of local translation or local release of different neurotransmitter receptors from the dendritic ER highlight the importance of this organelle in synaptic function (Ju et al. 2004; Carrel et al. 2008; Jeyifous et al. 2009; Ramírez et al. 2009).

1.4.3 Calcium signaling

The regulation of intracellular Ca^{2+} levels is vital for neuronal function and synaptic plasticity. And the best characterized organell involved in intracellular Ca^{2+} signaling is the smooth endoplasmic reticulum (Meldolesi 2001). The ER accumulates Ca^{2+} via its SERCA-pump (sarco/endoplasmic reticulum Ca^{2+}-ATPase) and the stimulus triggered rapid release of Ca^{2+} from the sER is evoked by stimulation of Ry-receptors (RyR) and IP_3-receptors (IP_3R). These are two largely homologous tetrameric receptor types on the sER, which are named for their affinity for either the plant alkaloid ryanodine or the cell metabolite inositol (1,4,5)-trisphosphate [Ins(1,4,5)P3 - IP_3] (Bardo et al. 2006). Under physiological conditions RyR are stimulated by intracellular Ca^{2+} in the 1-10µM range and inhibited by higher Ca^{2+} concentrations (Bezprozvanny et al. 1991). This Ca^{2+} induced Ca^{2+} release (CICR) and the analogous IICR, triggered by IP_3, play different roles in different types of neurons. In cerebellar Purkinje cells, RyR are mainly detected in the soma, whereas IP_3R can be found throughout the dendritic tree including spines (Sharp et al. 1993). In hippocampal neurons, however, IP3R are expressed throughout the cell, including spines and RyR can also be found everywhere, except the spine while expression levels depend on the exact type of hippocampal neuron (Sharp et al. 1993). And indeed, the importance of ER-dependent neuronal Ca^{2+} signaling for different forms of pre- and postsynaptic plasticity has been demonstrated in various studies (Llano et al. 2000; Miyata et al. 2000; Bardo et al. 2006; Holbro et al. 2009). Nakamura and colleagues highlighted the importance of IP_3R driven regenerative Ca^{2+} waves that travel from an activated spine to the soma (Figure 3B) (Oertner and Svoboda 2002; Nakamura et al. 2002). Because of this combination of local and long-range signaling, the ER has been conceptually described as a "neuron within a neuron" (Berridge 1998).

Interestingly, many of the known AD risk mutaions in Presenilin1 not only affect the generation of Aβ, but also influence IP_3 and Ryandine receptor function, as well as neuronal Ca^{2+} homeostasis in general, in a variety of ways (Chan et al. 2000; Cheung et al. 2008, 2010; Mattson 2010).

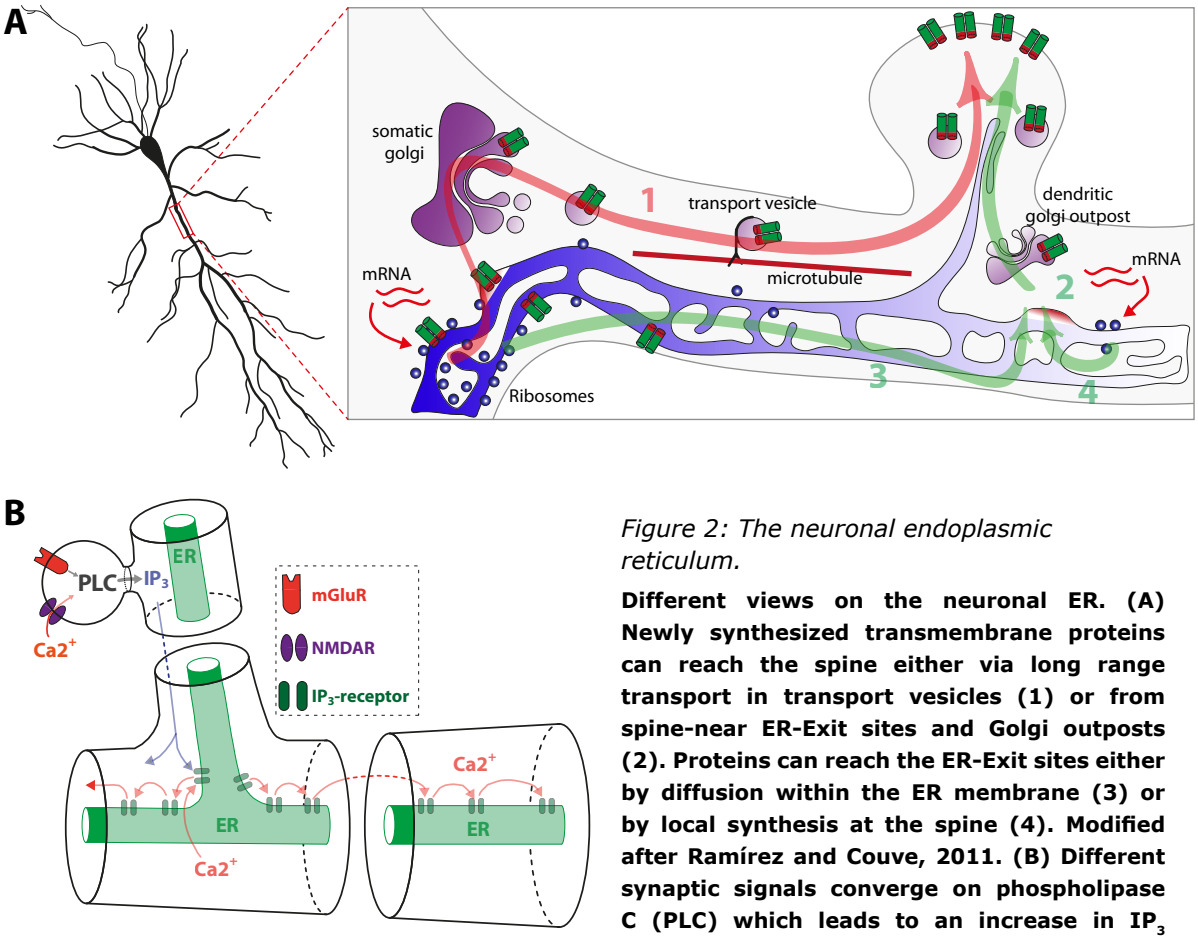

Figure 2: The neuronal endoplasmic reticulum.

Different views on the neuronal ER. (A) Newly synthesized transmembrane proteins can reach the spine either via long range transport in transport vesicles (1) or from spine-near ER-Exit sites and Golgi outposts (2). Proteins can reach the ER-Exit sites either by diffusion within the ER membrane (3) or by local synthesis at the spine (4). Modified after Ramírez and Couve, 2011. (B) Different synaptic signals converge on phospholipase C (PLC) which leads to an increase in IP_3 generation. This can trigger Ca^{2+} waves along the dendrite via repeated activation of IP_3-receptors by IP_3 near the activated spine and by Ca^{2+} further away from the spine. Modified after Oertner and Svoboda, 2002.

1.5 Aim of this study

The importance of Arc/Arg3.1 for different forms of synaptic plasticity and its involvement in activity dependent gamma-secretase trafficking is undisputed. However, the various forms of homeostatic plasticity are likely to be molecularly diverse and to rely on mechanisms that differ from those underlying activity dependent intracellular trafficking. The precise role of Arc/Arg3.1 in any of these processes is still elusive. The aim of this study was therefore to identify and characterize protein interaction partners of Arc/Arg3.1 that might shed light on the involvement of Arc/Arg3.1 in processes of subcellular organization and sorting.

2 Materials and Methods

2.1 Materials

2.1.1 Chemicals

Table 1 lists common buffers and media used throughout this thesis.

Table 1: Common buffer and media

PBS 10x		
reagent	**final concentration**	**amount**
NaCl	1.37M	80g
KCl	27mM	2.01g
Na_2HPO_4 (*$2H_2O$)	81mM	14.4g
KH_2PO_4	14.7mM	2g
Aqua dest		**ad 1000ml**
no pH adjustment necessary		

Antibiotics for LB media			
reagent	**stock concentration**	**final concentration**	**volume for 1l medium**
Kanamycin	50mg/ml in a.d.	50µg/ml	1ml
Ampicillin	100mg/ml in a.d.	100µg/ml	1ml
Tetracyclin	5mg/ml in EtOH	10µg/ml	2ml
Chloramphenicol	34mg/ml in EtOH	12.5µg/ml	367.7µl

SSC 20x		
reagent	**final concentration**	**amount**
NaCl	3M	175.3g
Trisodium citrate (*$2H_2O$)	0.3M	88.2g
Aqua dest		**ad 1000ml**
adjust pH to 7.0 (for RNA, add 1000µl DEPC over night and then autoclave)		

SOC medium			
reagent	**stock concentration**	**final concentration**	**volume /amount**
Pepton			20g
Yeast extract			5g
NaCl	5M	8.56mM	1712µl
KCl	1M	2.5mM	2.5ml
Aqua dest			**ad 1000ml**
adjust pH to 7.0 with NaOH, autoclave and let cool to ~60°C			
$MgCl_2$	2M	10mM	5ml
Glucose (filter sterilize through 0.22µm)	1M	20mM	20ml

Table 1: Common buffer and media

DNA gel loading buffer 10x

reagent	stock concentration	final concentration	volume /amount
TrisHCl pH 7.6	1M	10mM	100µl
Glycerin	100%	50%	5ml
EDTA pH8.0	500mM	60mM	1.2ml
Bromphenol blue or Xylene cyanol		0.25%	25mg
Aqua dest			**ad 10ml**

Protein sample buffer 5x

reagent	stock concentration	final concentration	volume / amount
TrisHCl pH6.8	1M	250mM	25ml
SDS		10%	10g
Glycerin	100%	50% (w/v)	50g
DTT		500mM	7.715g
Bromphenol blue	1%	0.01%	1ml
Aqua dest			**ad 100ml**

HANKS` medium

reagent	stock concentration	final concentration	volume / amount
HANKS` balanced salt solution (Sigma H9394)			1 bottle
$NaHCO_3$		4.17mM	350mg
HEPES		1mM	238.3mg
Aqua dest			**ad 1000ml**
adjust to pH7.3 - 7.4			

HANKS` medium plus FCS

reagent	final concentration	volume
HANKS` medium	80%	160ml
FCS	20%	40ml

Dissociation buffer

reagent	stock concentration	final concentration	volume / amount
NaCl	5M	137mM	2.74ml
KCl	1M	5mM	500µl
Na_2HPO_4 (*$2H_2O$)	120mM	7mM	5.833ml
HEPES		25mM	595.8mg
Aqua dest			**ad 100ml**
adjust to pH7.2			

Digestion buffer

reagent	final concentration	volume / amount
HANKS` medium	100%	100ml
$MgSO_4$ (7*H_2O)	12mM	296mg

Table 1: Common buffer and media			
Neuronal growth medium			
reagent	**stock concentration**	**final concentration**	**volume / amount**
Lonza PNBM (Clonetics cc-3256)			250ml
NSF-1 (Clonetics cc-4459HH)			4ml
L-Glutamine (Clonetics cc-4460HH)			2ml
GA-1000 Gentamicine sulfate (Clonetics cc-4505HH)			200µl

2.1.2 Antibodies

The antibodies used in this thesis are listet in table 2.

Table 2: Antibodies used in this thesis for western blot (WB), immunocytochemistry (ICC), immunohistochemistry (IHC) or immunoprecipitations (IP).							
Antigen	**WB**	**ICC**	**IHC**	**IP**	**Species**	**Productcode**	**Company**
alpha Tubulin	1:2000	1:200	1:400		rabbit	ab52866	Abcam
Arc/Arg3.1	1:10000			1:150	rabbit	156-003	SySy
Arc/Arg3.1			1:2000		rabbit	800/5904 AB pur	
beta Actin	1:5000000				mouse	A5441	Sigma
DsRed		1:1000			rabbit	632496	Clontech
GAD67	1:1000		1:200		mouse	ab26116	Abcam
GAPDH	1:100000				mouse	MAB374	Millipore
GFAP	1:500		1:500		rabbit	G 9269	Sigma
GFP	1:10000	1:10000			chicken	ab13970	Abcam
GluA1	1:2000	1:200	1:500		rabbit	AB1504	Millipore
GluA2	1:2000		1:2000		mouse	BD556341	
GluA3	1:2000		1:200		mouse	MAB5416	Millipore
GluN1	1:3000				mouse	MAB363	Millipore
GPR78/BiP	1:1000	1:500	1:1000		rabbit	ab21685	Abcam
HA		1:1000			mouse	MMS-101R	Covance
HA		1:1000		1:100	rabbit	PRB-101P	Covance
MAP2	1:10000	1:10000	1:4000		chicken	ab5392	Abcam
Myc		1:1000			mouse	MMS-150P	Covance
NaK-ATPase	1:500				mouse	ab7671	Abcam
NeuN			1:500		mouse	MAB337	Chemicon
NSE	1:500				chicken	NB1 0 0 - 1606	Novus
Claudin 11	1:1000		1:200		rabbit	ab53041	Abcam
p230 trans Golgi	1:500		1:200		mouse	611280	BD
PSD95		1:50			mouse	ABR-01204 (clone 6G6-1C9)	Dianova

Table 2: Antibodies used in this thesis for western blot (WB), immunocytochemistry (ICC), immunohistochemistry (IHC) or immunoprecipitations (IP).

Antigen	WB	ICC	IHC	IP	Species	Productcode	Company
PSD95	1:2000				mouse	ABR-01205 (clone 7E3-1B8)	Dianova
Rab5	1:5000	1:2000			rabbit	ab18211	Abcam
Sec23	1:500		1:500		rabbit	ab50672	Abcam
Tmem128	1:400				rabbit	various sera	Eurogentec
Tmem128		1:2000			rabbit	1329AK2	Eurogentec
Tubulin J		1:1000			rabbit	MBR435P	Covance
VAMP2	1:10000				rabbit	104 202	SySy

Anibodies were purchased at the following companies (in alphabetical order): **Abcam** (Abcam plc, 330 Cambridge Science Park, Cambridge, CB4 0FL, UK); **Cell Signalling Technology** (Cell Signaling Technology, Inc., 3 Trask Lane, Danvers, MA 01923, USA); **Covance** (Distributed via HiSS Diagnostics GmbH, Güterhallenstraße 3, 79106 Freiburg i.Br., Germany); **Dianova** (DIANOVA GmbH, Warburgstraße 45, 20354 Hamburg , Germany) 65824 Schwalbach, Germany); **Millipore** (Distributed via Merck Chemicals, Am Kronberger Hang 5, 65824 Schwalbach, Germany); **NEB** (New england Biolabs, Brüningstr. 50 Geb. G 810, 65926 Frankfurt am Main, Germany); **Novus** (Novus Biologicals, Ltd., 12 Cambridge Science Park, Cambridge, CB4 0FQ, United Kingdom); **Santa Cruz** (Santa Cruz BIOTECHNOLOGY Inc., Bergheimer Straße 89-2, 69115 Heidelberg, Germany); **SySy** (Synapic Systems, Rudolf-Wissell-Str. 28, 37079 Göttingen, germany).

2.1.3 Technical equipment

Equipment for DNA handling and analysis

A NanoDrop2000 spectrophotometer (Thermo Scientific) was used for DNA concentration measurements and PerfectBlue chambers (Peqlab) were used for agarose gel electrophoresis. Photoplates exposed to radioactive southern blots were developed in a FLA-3000 (Fujifilm) and a Victor3 Multilabel counter (PerkinElmer) was used for chemiluminescence and fluorescence based plate assays.

Equipment for protein handling and analysis

BCA assays for protein concentration analysis were detected in a SLT Rainbow Scanner (SLT Labinstruments) and SDS-PAGEs were run in Minigel-Twin chambers (Biometra). Westen blots were performed in Trans-cell tank blot chambers (Biorad) and chemiluminescent detection and image acquisition was carried out in an ImageQuant LAS4000mini detector (GE Healthcare). An Ettan IPGphor chamber was used for isoelectric focussing and a DESAGA Desaphor VA300 chamber with a temperature controlled circulating pump for running of second dimension SDS-PA gels. A VT 1200 S microtome with vibrating blade and VibroCheck for optimal positioning of the blade (Leica) was used to prepare brain slices.

Microscopes

Confocal laser scanning microscope:

Inverted Olympus Fluoview 1000 (AR Laser (458nm, 476nm, 488nm, 514nm); GreNE Laser (543nm); HeNe Laser (633nm); AOTF (Acousto-Optical-Tunable-Filter), six channels for computer assisted individuel adjustement of the laserpower of each single Laserline. Spectral scanner with adjustable windows for fluorochromes showing green to dark red fluorescence and for different Green Fluorescent Protein Variants (CFP, GFP, YFP) and DsRed. Three PMTs (epifluorescence, reflection) and one PMT for transmission mode Scanformat up to 2048 x 2048 pixel, 12 bit, scanfield rotatable –5 up to +95 °

Epifluorescence microscope:

Upright Zeiss Axio Imager.M2 with HXP 120C mercury short-arc lamp.

Software

Olympus and Zeiss proprietary software was used for image acquisition and ImageJ was used for image processing and semi-automatic counting of cell nuclei. Figures were assembled in Adobe Illustrator and this thesis was written in Microsoft Word and Adobe InDesign. Graphs were plotted with GraphPad Prism. Molecular cloning was planned and evaluated using the SeqMan, EditSeq and SeqBuilder packeges of DNASTAR Lasergene. Programs used for predictions of transmembrane domains were: HMMTOP (Tusnády and I. Simon, 1998 and 2001), psipred V2.3 (Buchan et al., 2010), TMHMM (Sonnhammer et al., 1998), TMPred (Hofmann and Stoffel, 1993).

2.2 Methods

2.2.1 Animals

All animal breeding, handling and experiments were carried out in accordance with local animal welfare law §6 TierSchG permission „ORG 443" for organ harvests, „G11/020 Aktivitätsregulierte Gene" for kainic acid injections, and „A6/499 Perfusion" for perfusions (under supervision of PD Dr. Guido Hermey or Dr. Claudia Mahlke).

The database software TBase was used for colony management.

For biochemical experiments, animals were sacrificed by cervical dislocation. For immunohistochemical experiments, animals were sacrificed by cardiovascular perfusion with paraformaldehyde.

Primers for genotyping are listed in table 3 (see Results section 3.4.2 for a genomic map with indicated primer positions):

Table 3: Genotyping primers

primer	sequence
Primer gen for	5' - gatccacctgtctctgtggatgct - 3'
Primer gen rev	5' - gggtgtcttgctgttttctg - 3'
Primer cas rev	5' - gtgaggccaagtttgtttcc - 3'

Tail cuts were stored in 96well PCR-microplates at -20°C until genotyping. For tissue lysis, 22µl lysis buffer (table 4) and 3µl ProteinaseK (10mg/ml in a.d.) were added to each well. Plates were incubated at 37°C over night under moderate shaking (up to 350rpm) or at 55°C for 3h. After heat inactivation of the ProteinaseK by boiling at 95°C for 15min, 175µl TE-buffer (pH7.6) were added. 2µl of genomic DNA were used for genotyping PCR reactions.

Table 4: Tail-prep buffer

reagent	stock concentration	final concentration	volume
Tris pH 8.5	2M	100mM	2.5ml
EDTA	0,5M	5mM	0.5ml
SDS	10%	0.2%	1.0ml
NaCl	5 M	200mM	2.0ml
Aqua dest			**ad 50ml**

Preparation of mouse brain lysates

One mouse brain (including cerebellum but without bulbus olfactorius) of each genotype was removed from the brain cavity, weighed and photographed. Each brain was put into a dounce homogenizer together with 4ml homogenization buffer (table 5) and homogenized using 15 strokes of a Potter S tissue homogenizer at 900rpm. The homogenate was centrifuged for 10min at 1000g (3000rpm in a SS-34 rotor) and the supernatant (S1') stored at 4°C. The pellet was solubilized in another 4ml homogenization buffer and the procedure was repeated. The supernatants from both centrifugation steps were pooled and labeled S1 (post nuclear supernatant = PNS). Protein concentrations were measured using the BCA method and samples were adjusted to 1µg/µl protein with 2x protein sample buffer and boiled at 95°C for 5min. Samples were then stored at -80°C until further use.

Table 5: Tissue homogenization buffer

reagent	stock concentration	final concentration	volume
HEPES	100mM	4mM	2ml
Surose	2.0M	0.32M	8ml
Aqua dest			**ad 50ml**
adjust pH to 7.4			

Subcellular fractionation

The starting material for the subcellular fractionation was the S1 supernatant from the initial brain lysates. S1 was centrifuged for 15min at 12000g (10000rpm in a SS-34 rotor). The pellet (P2 = crude synaptic membranes) was solubilized in 200µl homogenization buffer and stored at 4°C. The Supernatant (S2) was transferred to thick walled ultracentrifugation tubes and centrifuged in a Optima L-90k ultracentrifuge (BeckmanCoulter) for 1h at 4°C and 160000g (42000rpm 70ti rotor) [small volumed samples were centrifuged in a table top ultracentrifuge Beckman TL-100 in a TLA55 rotor at 55000 rpm]. The supernatant (S3 = cytosol and small vesicles) was stored at 4°C. The pellet (P3 = microsomes) was solubilized in 200µl homogenization buffer and stored at 4°C. Protein concentrations of all samples were measured using the BCA-method and all samples were adjusted to 1µg/µl with 2x protein sample buffer. Samples were boiled at 95°C for 5min and stored at -80°C until further use.

Perfusion of mouse brains

The perfusion tubing was rinsed with water for several minutes. After that, the entire tubing including the perfusion needle was filled with 0.01% Heparin/PBS and put aside until the mouse was anesthetized. The mouse was injected i.p. with a Ketamine/Xylazine solution at 2.65µl/kg body weight (100mg/ml Ketamine, 20mg/ml Xylazine). After 10 to 15 minutes the depth of the anesthesia was tested using the toe-reflex of the mouse. If the mouse still reacted it was injected a second time with half of the original volume of Ketamine/Xylazine. After another 10 minutes the mouse was fixed onto a styrofoam board with needles through the limbs. The fur from the chest was removed and the chest cavity was opened carefully using forceps and scissors. The heart was mobilized carefully using forceps. The Perfusion needle was inserted into the prominent left ventricle and immobilized on the Styrofoam board. A small cut was made into the right atrium. The animal was then perfused with 10-15ml of Heparin solution. Subsequently the perfusion solution was exchanged for 4% Paraformaldehyde (pH 7.4, the PFA was filtered in order to remove impurities or unsolved PFA that could clogg small arteries). After perfusion with 50ml PFA, the brain of the animal was removed and fixed overnight in 4% PFA.

Seizure induction with kainic acid

Kainic acid (Asc-100 from Ascent) was dissolved in PBS at a concentration of 4mg/ml and stored in aliquots at -20°C. Mice were injected i.p. with 25mg/kg body weight kainic acid. After injection, the mice were kept under low light conditions under constant surveillance. The onset of seizure activity was estimated from behavioural cues (cramping, arching of the back, repetitive behavior, “piano player”). Animals were sacrificed at various time points after start of seizure activity.

Immunohistochemistry

The fixed mouse brain was put on a flat glass surface (which itself is put on ice) with the cerebellar side down (for coronal sections) and slowly covered with melted 2% agarose. As soon as the agarose was cooled and hardened, a cube shaped block with the embedded brain in the middle was cut out of the agarose. The block was put on to a paper towel to dry the bottom surface and then glued onto an object holder belonging to the vibratome. The vibratome is assembled and used according to the manufacturer´s instructions. The brain was sliced in 30µm thick free floating sections, which were collected with a fine brush and stored in 24-well plates filled with PBS / 15µM NaAcide until use. 2-3 sections from different depths in the brain can be comfortably stored in one well.

If heat mediated antigen retrieval (HIER) was necessary for antibody detection, sections were transferred to a 24 well plate with 10mM Tri-Sodiumcitrate dihydrate at pH6.0. This plate was placed in a 80°C water bath for 45 minutes. Sections were then transferred into a new 24 well plate with PBS-Tr (PBS supplemented with 0.01% Triton X-100) and subjected to either DAB or fluorescent staining.

Staining of brain sections with DAB

The sections were washed several times with PBS-Tr and then incubated in 0.3% H_2O_2 (in PBS) for 30min to inactivate endogenous peroxidases. The sections were then washed with PBS-Tr again several times and incubated at RT with blocking solution (PBS +10% Horse serum, +0.2% BSA, +0.3% Triton X-100). Subsequently the blocking solution was replaced with the first antibody in carrier solution (PBS +1% Horse serum, +0.2% BSA, +0.3% Triton X-100) and incubated over night at 4°C. On the next day, slices were washed again with PBS-Tr and incubated with the bridging antibody in carrier solution. Bridging antibodies were biotin conjugated antibodies raised against various species. For the final staining step the ABC-solution (ABC-Kit PK-6100 from Vector) was prepared 30min prior to the staining step. Slices were incubated in ABC-solution for 60min at RT and subsequently washed with PBS-Tr again. Stainings were developed using DAB- and Urea-tablets.

Slices were washed with PBS-Tr and transferred to object glasses and arranged carefully with a fine brush. The object glasses were placed on a 75°C heating plate for several minutes. The object glasses carrying the dried slices were dipped into Xylol briefly and mounted with DPX mountant and a large glass cover slip.

Staining of brain sections with fluorescent markers

The staining procedure is similar to the DAB protocol but omitting the H_2O_2 step and the DAB step. Secondary antibodies were the same fluorescently conjugated antibodies as used for immunocytochemistry. Before mounting, the slices were incubated in a 0.1µg/ml DAPI solution in PBS for 10min at RT.

2.2.2 Molecular biology

If not noted otherwise, steps were carried out at room temperature (RT).

Gateway recombination reactions (Table 6) were used for convenient transfer of coding sequences from a donor vector (pENTR) to e recipient vector (pDEST), which contains inframe tags and eukaryotic selection sequences. Induction of a PCR amplified coding region into pENTR is achieved via a TOPO reaction (see Table 6 for reaction details) and transfer to the expression vector is achieved by a LR reaction.

TOPO-reaction:

Coding sequences of interest were amplified via PCR with 5'Primers adding a Kozak sequence (5'-cacc-3') to the start ATG and 3'Primers ending with a STOP-codon or a mutated STOP-codon. The resulting PCR-product was purified on spin columns (NucleoSpin ExtractII - Macherey-Nagel) and used for a topoisomerase reaction with the Invitrogen Vector pENTR_D_TOPO. The reaction was incubated at room temperature for 20 minutes and then transformed into competent *E.coli* XL1-blue.

LR Reaction:

Recombination ingredients (table 6) were mixed and incubated at RT for 1h. Then, 1µl ProteinaseK was added and the mixture was incubated for 15 minutes at 37°C to digest the LR clonase enzyme. After that the reaction was transformed into competent *E.coli* TOP10.

Table 6: Gateway recombination techniques (Invitrogen)	
components in a TOPO reaction	**components in a LR reaction**
1µl PCR-construct (10ng)	1µl pENTR_D_TOPO including coding sequence of interest (100ng)
0.5µl pENTR_D_TOPO	1µl pDEST (60ng)
0.5µl TOPO-salt solution	1µl LR-ClonaseII
2µl a.d.	2µl TE pH8.0

Plasmid DNA preparation by alkaline lysis with SDS (minipreparation)

Buffers for minipreparations are listed in table 7.

A single bacterial colony was transferred from a LB plate and incubated in 3.5ml LB-medium containing the appropriate antibiotic (Maniatis et al., 1982) at 37°C over night. 2ml of this culture were used to sediment the bacteria at 13000 rpm for 1 minute. After resuspending the pellet in 250µl S1 buffer, 250µl of S2 buffer were added and the content was mixed by inverting. The mixture was incubated for 2 minutes. 250µl of ice-cold S3 buffer were added and the mixture was inverted repeatedly. After centrifugation at 14000g for 10 minutes, 490µl Isopropanol were added to the supernatant. The plasmid DNA was precipitated at 14000g and 4°C for 15 minutes and the resulting DNA pellet was washed using 70% ethanol. The pellet was air dryed and solubilized in 30µl water.

Table 7: Buffers for DNA Mini-prep			
Buffer S1			
reagent	**stock concentration**	**final concentration**	**volume / amount**
TrisHCl pH8.0	1M	50mM	50ml
EDTA pH 8.0	250mM	10mM	4ml
RNAseA		100µg/ml	100mg
Aqua dest			**ad 1000ml**
Buffer S2			
NaOH	2M	200mM	100ml
SDS	10%	1%	100ml
Aqua dest			**ad 1000ml**
Buffer S3			
KAc pH5.5	10M	3M	300ml
Aqua dest			**ad 1000ml**

Preparation of plasmid DNA by alkaline lysis with SDS (midipreparation), Macherey-Nagel kit

All buffers were supplied by the manufacturer. Bacteria were grown in 100ml LB-Medium containing the appropriate antibiotic at 37°C over night and pelleted by centrifugation at 5000 rpm for 15 minutes. The Pellet was solubulized in 8ml S1 buffer. After addition of 8ml S2 buffer, the tubes were inverted several times and incubated for 2 minutes. 8ml S3 buffer were added; samples were mixed and poured on Nucleobond Xtra Midi filter

columns, which were previously equilibrated with 12ml equilibration-buffer. Filter columns were washed one time with 5ml equilibration-buffer and after discarding the filter, columns were washed with 8ml wash-buffer. The plasmid DNA was eluted with 5ml elution-buffer and precipitated using 3.5ml isopropanol. After centrifugation at 5000 rpm for 45 minutes the pellet was solubulized in 200µl TE-Buffer. The Plasmid DNA was transferred into a 1.5ml reaction tube and 1ml 100% Ethanol and 20µl 3M NaAcetat pH5.2 were added. Plasmid DNA was precipitated by centrifugation at 14000g and 4°C for 10 minutes. Pellets were air dried and solubulized in 100µl water. The concentration of nucleic acids was measured with a spectral photometer. The OD260 / OD280 ratio was used to assess the purity. OD260 = 1 corresponds to approximately 50 µg/ml double stranded DNA or 40 µg/ml single stranded RNA.

Digestion, extraction and ligation of DNA

DNA was digested in recommended buffers according to NEB or NBI Fermentas. Digestions were carried out in a final volume of 20µl with 0.5-1µg DNA for 20minutes for FastDigestTM-enzymes and for 2 hours for regular enzymes at 37°C.

For analysis of DNA preparations, restrictions of plasmid DNA, and for isolation of DNA fragments the DNA was separated according to its size in horizontal agarose gels. Depending on the size of the DNA fragment the appropriate amount of agarose (0.5 -2% w/v) was heated to boiling in TAE buffer (table 8) in a microwave oven and mixed with GelRed (3µl per 100ml gel). The loading dye for fragments over 500bp was Bromphenolblue and Xylencyanol for fragments up to 500bp. The electrophoresis was carried out in TAE at 10V/cm for 1 h.

Table 8: TAE buffer 50x

reagent	stock concentration	final concentration	volume / amount
Tris Base pH8.4		2M	242g
Acetic acid		5.71%	57.1ml
EDTA pH8.0	500mM	50mM	100ml
Aqua dest			**ad 1000ml**

DNA extraction was carried out with the NucleoSpin Extract II kit (Macherey-Nagel). DNA fragments were detected under UV – light and excised with a clean scalpel. Gel slices were transferred into a 2ml cup. For each 100mg of gel 200µl of loading buffer were added and the gel fragments were melted in a thermomixer at 55°C and 1200rpm until dissolved completely (5-10 minutes). The sample was loaded onto a NucleoSpin Extract II column, placed in 2ml collection tube, and centrifuged at 11000rpm for 1 minute. The flow-through was discarded and the column was placed back into the collecting tube. 600µl washing-buffer was added followed by centrifugation for 1 minute at 11000rpm. Again the flow-through was discarded and the column was placed back into the collecting tube. The column was dried by centrifugation for 2 minutes at 11000rpm. The column was then placed into a 1.5ml reaction tube and 30µl elution buffer were added. After incubation at RT for 1 minute, DNA was eluted by centrifugation at 11000rpm for 1 minute. For large fragments (> 5-10kb) the elution buffer was pre-warmed (55°C). 50-200ng vector DNA were ligated with 150-600ng insert DNA using 1U T4-DNA-ligase, 2µl ligation buffer and water in final volume of 20µl for 2 hours at room temperature or over night at 4°C.

Transformation of competent bacteria with DNA

Depending on the experimental goal, diferent strains of competent bacteria were used (table 9). 50µl of -80°C cold competent bacteria were thawed on ice for 10 minutes and then carefully mixed with 10µl of ligation reaction. After incubation on ice for 30 minutes, bacteria were heat shocked for 45 seconds at 42°C. 250µl antibiotic free SOC-medium were added and after 45 minutes of incubation at 37°C and 250rpm bacteria were plated on LB-agar plates, containing the appropriate antibiotic.

Table 9: Chemically competent *E.coli* strains

strain	use
XL1-Blue	amplification of plasmid DNA
TOP10 (DH10B)	amplification of plasmid DNA after perfotming LR-gateway reactions. Selection of ccdB negative plasmids
ccdB Survival™ 2 T1R	amplification of pDEST-vectors of the Gateway cloning system
stbl3	amplification of lentiviral plasmids containing long repetitive sequences
GM 2163 (dam^-, dcm^-)	amplification of plasmids for methylation sensitive cloning
BL21 (DE3) pLysS	protein expression

DNA sequence analysis

All plasmid constructs were confirmed by sequence analysis. DNA sequence analysis with the Didesoxymethod (Sanger et al., 1977) was carried out by Eurofins MWG Operon (Martinsried).

Preparation of RNA by Phenol – Chloroform extraction with TRItidyG – reagent

For all RNA containing procedures DEPC treated water was used. 1ml DEPC (Diethylpyrocarbonate) was added to 1 liter millipore water and then autoclaved. DEPC binds covalently to histidine residues of proteins and single stranded nucleic acids. It is used to inactive RNAses. It is inactivated by autoclaving which results in CO_2, H_2O and ethanol.

Primary hippocampal or cortical neurons were grown at various densities in 6cm dishes. Cells were placed on ice and washed two times with ice-cold PBS. Per dish 1ml TRItidyG reagent was added and cells were harvested using a cellscraper. TRItidyG – reagent (ApplyChem) is a mono-phasic solution of Phenol and Guanidinium – Isothiozyanat. The lysate was transferred into a 2ml reaction tube and incubated at RT for 10 minutes. For each milliliter of TRItidyG reagent 200µl Chloroform were added. Cups were vigorously shaken for 15 seconds and then incubated at RT for another 10 minutes. Subsequent centrifugation for 15 minutes at 12000g and 4°C resulted in three phases. The upper aqueous RNA containing phase was transferred into a new 1.5ml cup and 1Vol. isopropanol was added. After incubation at RT for 15 minutes the centrifugation step was repeated. The pellet was washed in 1ml 70% ethanol in DEPC-water and centrifuged again for 10 minutes at 4°C and 7500g. The washing procedure was repeated with 1ml 100% ethanol. The pellet was then dried at 55°C and resolved in 50µl a.d. at 55°C for 10 minutes before storage at -80°C.

For analysis of RNA for Northern-blotting, the RNA was separated according to fragment size in horizontal agarose gels. Agarose was heated in DEPC treated water and poured into a gel slide, which had been incubated with 3% H_2O_2 for 30 minutes. RNA samples as well as 10µl of the RNA size marker were mixed with RNA sample buffer (table 10) and incubated at 50°C for 15 minutes. 1xMOPS buffer was used as running buffer (table 10) and a Bromphenolblue/Xylencyanol mix was used as loading dye. Electrophoresis was carried out at 7.5V/cm for 5 h.

Table 10: RNA gel electrophoresis buffers

MOPS gel running buffer 10x			
reagent	**stock concentration**	**final concentration**	**volume**
MOPS	1M	200mM	200ml
sodium acetate	1M	50mM	50ml
EDTA	250mM	10mM	4ml
Aqua dest (DEPC)			**ad 1000ml**
adjust to pH7.0 with NaOH			

RNA sample buffer 1x			
reagent	**stock concentration**	**final concentration**	**volume**
Formaldehyde (37%)	12.3M	2.214M	9µl
Formamide	100%	30%	15µl
Glycerol	100%	20%	10µl
Ehidium bromide	100%	2%	1µl
RNA loading dye			5µl
Sample RNA	1µg/µl	200ng/µl	10µl

Northern Blotting

The premade northern blots used in this study were obtained from Gentaur (distributed through Zyagen). The two different blots were mouse neuronal tissue panel (Zyagen MN-200) and mouse multiple tissue (MN-MT-1) with 20mg RNA in each lane. For detection of specific RNAs, blots were soaked in 2xSSC and prehybridized at 60°C for 2 hours using preheated Stratagene QuickHyb mix. Radioactively labeled DNA probes were generated using rediprime DNA labeling mix (Amersham). For that purpose 1µg of a DNA fragment was diluted in 45µl a.d. and denatured at 95°C for 5 minutes. The mixture was cooled down on ice for two minutes and then mixed with the labeling mix and 5µl [α32P] dCTP (50µCi). After 30 minutes incubation at 37°C the reaction was stopped by adding 50µl TE-buffer. By centrifuging the mixture through a mini quick-spin DNA column (Roche) labeled DNA was separated from unbound [α32P] nucleotides. 100µl salmon sperm DNA (10mg/ml) was added to the labeled DNA. After denaturing at 95°C for five minutes labeled samples were added to the QuickHyb mix. Hybridization was carried out in a hybridization oven under rotation at 65°C over night. After hybridization the membrane was washed two times at RT for 15 minutes with 2xSSC + 0.1%SDS and one time at 60°C for 30 minutes with 0.2xSSC + 0.1%SDS. Then a film was exposed at -80°C for several hours to days.

Polymerase chain reaction (PCR)

A basic PCR protocol that was used for all PCRs (table 11).

Table 11: Basic PCR protocol

step	temperature	time	repeats	comment
1	95°C	03:00		initital denaturation
2	95°C	00:30	Step 2 to 4 were repeated between 20 and 40 times	denaturation
3	50-72°C	00:30		primer annealing
4	72°C	00:30-03:00		amplification
5	72°C	04:00		terminal amplification
6	8°C	00:00		storage temperature

The primer annealing temperature (3) depends on the GC content and the primer length and was calculated for each primer pair by using the online tool of the primer synthesis company (Eurofins MWG Operon). The length of the amplification (4) step depends on the length of the amplified fragment. The amplification speed of the used polymerases is approximately 1000bp/min.

Each PCR reaction was set up according to table 12.

Table 12: Basic PCR reaction mix

volume	reagent
x µl	Template DNA (various sources: cDNA, Plasmids, genomic DNA)
1µl	Forward Primer 10µM
1µl	Reverse primer 10µM
1µl	dNTPs (10-25mM each)
5µl	10x Reaction buffer provided by polymerase supplier (incl. $MgCl_2$)
x µl	Polymerase
2.5µl	DMSO (optional for templates with high GC-content)
ad 50µl	**Aqua dest (genotyping PCRs were performed in a volume of 25µl)**

Different sources of template material with different concentrations of DNA were used. Standard amounts were 0.5µl Plasmid DNA (1µg/µl), 1-2µl genomic DNA, 0.5µl cDNA (1µg/µl). Different types of polymerases were used depending on the desired fragment: Analytic PCRs were performed with 0.3-1µl DreamTaq DNA Polymerase (5U/µl - Thermo Scientific), preparative PCRs were performed with Pwo DNA Polymerase (1U/µl - Rapidozym), and PCR reactions for the cloning of coding sequences from cDNA libraries were performed with High-Fidelity PCR Enzyme Mix (5U/µl - Thermo Scientific).

Reverse Transcriptase PCR (RT – PCR)

For semi quantitative mRNA analysis the SuperScriptIII RT-PCR system from Invitrogen was used to generate complementary DNA (cDNA). 3µg RNA, 1µl Oligo(dT)20 Primer (50µM) and 1µl dNTPs (10mM each) were mixed in a PCR-reaction tube (200µl). DEPC treated water was added to a final volume of 10µl. The RNA was denatured at 65°C for 5 minutes and cooled down on ice for 2 minutes to allow Primer annealing. For cDNA synthesis the following substances were added: 4µl 5xReaction buffer, 2µl 100mM DTT, 1µl RNAseOut (40U/µl) and 1µl SuperScriptIII RT (200U/µl). cDNA was synthesized at 50°C for 1 hour and after that

the reverse transcriptase was denatured at 70°C for 15 minutes. Then 1µl RNAseH (2 U/µl) were added to digest the RNA template at 37°C for 20 minutes. The cDNA was stored at -20°C. For quantitative PCR analysis 1/20 of the the concentration of cDNA was measured using the spectral photometer NanoDrop and diluted to a final concentration of 50ng/µl.

2.2.3 Biochemistry

Tandem-Affinity-Purification

All steps were carried out on ice or at 4°C if not stated otherwise, buffers are summarized in table 13.

Ten to fifteen mice from each group (wild type or transgenic for either N-TAP-Arc/Arg3.1 or C-TAP-Arc/Arg3.1) were sacrificed and the brains removed. The brains were put into a dounce homogenizer together with 5ml lysis buffer and homogenized using 15 strokes of a Potter S tissue homogenizer at 900rpm. The douncer was cleared with another 5ml lysis buffer and the combined homogenates were incubated under rotation for 1h and subsequently centrifuged for 20min at 12000g (SS34 – Rotor) to sediment nuclei and cell debris. 100µl cleared lysate was taken as sample. 500µl IgG-Beads (GE Healthcare) were washed 5x with lysis-buffer and transferred to a 15ml centrifugation tube. The cleared lysate was incubated with the beads over night under rotation. Beads were pelleted at low centrifugation speed and the supernatant was taken as a sample. Beads were washed 3x with lysis buffer. The beads were then transferred to a 1.5ml microcentrifugation tube and washed 3x with TEV-buffer. The Beads were resuspended in 1ml TEV-buffer and 10µl were taken as a sample. 100U AcTEV (MoBiTec) was added to each tube and rotated at room temperature for 7h. Beads were pelleted and 20µl of the supernatant were taken as a sample. The beads were taken as a sample, resuspended in 1ml TEV-buffer. 500µl Calmodulin beads (GE Healthcare) were washed 5x with calmodulin binding buffer and mixed with the supernatant after TEV-cleavage in a 15ml centrifuge tube and volume was adjusted to 4ml with calmodulin binding buffer. After adding 15µl 2M $CaCl_2$ the mixture was incubated under rotation over night at 4°C.

The beads were pelleted and the supernatant was kept as a sample. The beads were washed 6x with calmodulin binding buffer. Proteins were eluted from the beads 10x by adding 100µl calmodulin elution buffer (prewarmed to 37°C) and rotating at room temperature for 5 minutes. The empty beads were kept as a sample, resuspended in calmodulin elution buffer. The Eluates were kept as samples.

For two dimensional gel electrophoresis protein concentrations of final TAP eluates H1 from wild type and TAP-mice were measured using the 2DE-Quant kit (GE Healthcare) and 20µg of each sample were precipitated with acetone and rehydrated with 50µl IPG-Rehydration solution. Samples were stored at -80°C until use.

Table 13: TAP buffers

Lysis buffer

reagent	stock concentration	final concentration	volume / amount
HEPES-KOH pH7.5	1M	50mM	25ml
EDTA pH 8.0	500mM	1mM	1ml
KCl	1M	100mM	50ml
NP-40/Igepal	20%	0.5%	12.5ml
Aqua dest			**ad 500ml**

TEV protease buffer

reagent	stock concentration	final concentration	volume / amount
Tris pH8.0	1M	50mM	25ml
NaCl	5M	150mM	30ml
EDTA pH 8.0	500mM	0.5mM	500µl
DTT	1M	1mM	500µl
NP-40/Igepal	20%	0.1%	2.5ml
Aqua dest			**ad 500ml**

Calmodulin binding buffer

reagent	stock concentration	final concentration	volume / amount
Tris pH8.0	1M	10mM	5ml
2-Mercaptoethanol	14.2M	10mM	3521µl
NaCl	5M	150mM	30ml
MgOAc	200mM	1mM	2.5ml
Imidazol	1M	1mM	500µl
$CaCl_2$	1M	2mM	1ml
NP-40/Igepal	20%	0.1%	2.5ml
Aqua dest			**ad 500ml**

Elution buffer

reagent	stock concentration	final concentration	volume / amount
Tris pH8.0	1M	10mM	500µl
2-Mercaptoethanol	14.2M	10mM	352µl
NaCl	5M	150mM	3ml
MgOAc	200mM	1mM	250µl
Imidazol	1M	1mM	50µl
NP-40/Igepal	20%	0.1%	250µl
EGTA	500mM	2mM	200µl
Aqua dest			**ad 50ml**

Immunoprecipitation from secondary cell lines

500000 HeLa cells were seeded in a 6cm plastic cell culture dish. On the next day, cells were transiently transfected with the two tagged proteins whose interaction was to be tested, using Lipofectmine2000. 24-48h later the co-immunoprecipitation was carried out.

15µl magnetic ProteinA-Sepharose beads (Invitrogen) were washed two times with wash-buffer and then resuspended in 500µl wash-buffer (table 14). 2µg specific antibody or unspecific IgGs of the same species were added to the beads and incubated for 1h at room temperature under rotation. At the end of the incubation period the beads are washed three times with lysis buffer to remove unbound antibodies. In the meantime the transiently transfected HeLa cells were removed from the culture dishes with cell scrapers and washed two times with PBS. Cells were then resuspended in 200µl lysis buffer and vigorously pipetted (while avoiding the formation of foam). The cells were placed on ice for 30 minutes with pipetting every 10 minutes. The lysate was centrifuged at 130000 rpm and 4°C for 10 minutes to sediment nuclei and debris. 5% of the lysate was mixed with protein loading buffer and stored as the input sample. The rest was distributed equally between the beads bound with antibodies and IgGs. After incubation at room temperature for 2h the beads were sedimented, the supernatant was discarded and the beads were washed three times with wash-buffer. The washed beads were resuspended in protein sample buffer and heated to 95°C for 5 minutes. All samples were subjected to SDS-PAGE and western blotting. Antibodies against both tags present in the cells were used to check for immunoprecipitation and co-immunoprecipitation.

Table 14: CoIP-buffers

Lysis buffer

reagent	stock concentration	final concentration	volume / amount
TrisHCl pH 7.4	1M	50mM	5ml
EDTA pH 8.0	250mM	1mM	400µl
NaCl	5M	150mM	3ml
Triton X-100	20%	1%	5ml
Aqua dest			**ad 100ml**

Wash buffer

reagent	stock concentration	final concentration	volume / amount
TrisHCl pH 7.4	1M	50mM	25ml
EDTA pH 8.0	250mM	5mM	10ml
NaCl	5M	300mM	30ml
Triton X-100	20%	0.2%	5ml
Aqua dest			**ad 500ml**

One dimensional sodium dodecyl sulfate – poly acrylamide gel electrophoresis (1D SDS – PAGE)

Protein separation was carried out in a vertical two step gel system (Minigel-Twin Biometra). Seperating gels were cast first and overlaid with 2-Propanol until polymerization. Propanol was washed off with water and stacking gels were cast and combs inserted. For an overview of SDS-PAGE components, see table 15.

Table 15: SDS-PAGE components

Separating gels				
component	**8% gel**	**10% gel**	**12% gel**	**15% gel**
Acrylamid (29:1)	2ml	2.5ml	3ml	3.8ml
H_2O	3.6ml	3.1ml	2.6ml	1.8ml
4x lower Tris	1.9ml	1.9ml	1.9ml	1.9ml
APS	37.5µl	37.5µl	37.5µl	37.5µl
TEMED	7µl	7µl	7µl	7µl
4x lower Tris consists of 0.5M Tris at pH8.8 and 0.4% SDS				

Stacking gel	
component	**4% gel**
Acrylamid (29:1)	350µl
H_2O	1.4ml
4x upper Tris	585µl
APS	34µl
TEMED	4µl
4x upper Tris consists of 0.5M Tris at pH6.8 and 0.4% SDS	

10x running buffer		
reagent	**final concentration**	**volume / amount**
Tris Base	255mM	30.88g
Glycin	862mM	144.2g
SDS	1%	10g
Aqua dest		**ad 1000ml**

Western-blot

Western blots were carried out at 4°C using the Mini PROTEAN TransBlot system from BioRad according to the manufacturer's instructions with home made transfer buffer (table 16) either for 2h at 110V or over night at 80mA. After blotting and before blocking, membranes were subjected to PonceauS staining (10x Ponceau: 1% PonceauS in 10% acetic acid) to visualize prominent protein bands. The Membranes were cut horizontally with a scalpel at specific heights and the individual membrane strips were then blocked with 5% non-fat milk in PBS/0.1% Tween-20 (PBS-T) at RT for 60min. After washing with PBS-T, the membranes were incubated with specific primary antibodies over night at 4°C and, after additional washing, with peroxidase conjugated secondary antibodies for 2h at RT. Specific bands were visualized with Pierce Super Signal ECL solution and image acquisition was carried out with the LAS4000Mini system from GE Healthcare (formerly Fuji). Quantitative analysis of digital western blots images was performed using the ImageJ variant Fiji normalization to the housekeeping gene Glyceraldehyde 3-phosphate dehydrogenase (GAPDH). For protein quantification, each sample was run as triplicates on SDS-PAGE and normalized

band densities were averaged. Averages from three different animal pairs (wild type and Tmem128 knockout) were then tested for significant differences in protein expression. Outliers were identified as valiues that lay beyond two times the standard deviation from GAPDH average. Outliers were excluded from the quantification.

Table 16: Transfer buffer		
reagent	**final concentration**	**volume / amount**
Tris Base	25mM	15.14g
Glycin	192mM	72.07g
MetOH	10% (v/v)	500ml
Aqua dest		**ad 5000ml**

Stripping of western-blot membranes

If necessary, blots were washed with PBS-T after the first imaging, incubated with stripping buffer (table 17) at 50°C under rotation in a hybridization oven and again subjected to the staining procedure including blocking.

Table 17: Western blot stripping buffer			
reagent	**stock concentration**	**final concentration**	**volume**
TrisHCl pH 6.8	1M	62.5mM	31.25ml
SDS	10%	2%	100ml
2-Mercaptoethanol	14.2M	100mM	3521µl
Aqua dest			**ad 500ml**

Two dimensional sodium dodecyl sulfate – poly acrylamide gel electrophoresis (2DE)

First dimension: Isoelectric focussing (IEF)

The IEF gel strips with immobilized pH-gradients (IPG strips - 18cm with pH3-10 Amersham Biosciences) were stored at -80°C until use. Final TAP-eluate samples were thawed on ice and mixed with 290µl IPG-rehydration solution. The samples were pipetted into ceramic IPG-strip holder with a 1000µl pipette. Air bubbles were burst with a fine canula. Then the IPG strips were taken from the freezer and carefully placed with the gel-side down onto the samples. IPG strips were overlayed with 1.5ml oil (Dry Strip Cover Fluid - Amersham Biosciences). Ceramic strip holders were covered with individual lids and placed onto the gold contacts of the Ettan IPGphor chamber and aligned at the appropriate 18cm line. The focussing program (table 18) was carried out over night.

Table 18: Isoelectric focussing program	
13h	30V
1h	100V
1h	200V
2h	Gradient to 1000V
1h	Gradient to 8000V
4h	8000V

After finishing the first dimension, strips were removed with fine forceps and placed onto whatman paper with the gel side up, to remove excess oil. The strips were then transferred to glass tubes filled with equilibration solution 1 (table 19). The glass tubes were closed and gently stirred on a shaking platform (IPG strips should at all times be covered with fluid). After 15 minutes the strips were transferred into glass tubes containing equilibration solution 2 for another 15 minutes. After that the strips are stored at -80°C until used for the second dimension run.

Table 19: Equilibration solutions (15ml aliquots stored at -20°C)

Equilibration solution 1			
reagent	**stock concentration**	**final concentration**	**volume / amount**
Urea		6M	90g
Glycerin	100%	30% (v/v)	75ml
SDS		2% (w/v)	5g
Tris-HCl pH8.8	50mM	3M	4.175ml
Bromphenolblue	1%	0.002%	500µl
DTT		64mM	2.5g
Aqua dest			**ad 250ml**

Equilibration solution 2			
reagent	**stock concentration**	**final concentration**	**volume / amount**
Urea		6M	90g
Glycerin	100%	30% (v/v)	75ml
SDS		2% (w/v)	5g
Tris-HCl pH8.8	50mM	3M	4.175ml
Bromphenolblue	1%	0.002%	500µl
Iodacetamid		135mM	6.25g
Aqua dest			**ad 250ml**

Second dimension:SDS-PAGE

Solutions and buffers for second dimension SDS-PAGE are summarized in table 20.

Table 20: Solutions and buffers for 2DE

15% SDS-Polycrylamid solution (large scale mastermix)		
reagent	**final concentration**	**volume / amount**
Tris Base	375mM	110.408g
Tris HCl	375mM	45.436g
SDS	0.1% (w/v)	3.2g
Aqua dest		**ad 1400ml**
Acrylamid	15%	498g
Bis-acrylamid	0.2%	6.64g
Aqua dest		**ad 1660ml**
Incubate for 1h with 2.5% Amberlite (41.5g) then filtrate to remove Amberlite. Fill a 5l suction bottle with exactly 1600ml acrylamid solution, 1400ml SDS solution and a rotating magnet. Degas under negative pressure for 30 minutes. Add 960µl TEMED. Filtrate through fiber glass filter and store 67.5ml aliquots at -20°C.		

Table 20: Solutions and buffers for 2DE

Persulfate solution		
reagent	**final concentration**	**volume / amount**
Persulfate	1.25%	3.2g
Aqua dest		**ad 250ml**
Store persulfate solution in 10ml aliquots at -20°C.		

levelling solution		
reagent		**volume / amount**
Tris Base		17.25g
Tris HCl		7.1g
SDS		0.5g
Aqua dest		**ad 500ml**
Store in 10ml aliquots at -20°C.		

5.5x SDS runnig buffer		
reagent	**final concentration**	**volume / amount**
Tris Base	25mM	33.3g
Tris HCl	192mM	158.4g
SDS	0.1%	11g
Aqua dest		**ad 2000ml**

Two large glass plates for each gel were cleaned with 99.9% EtOH to remove acrylamid and silicone residues from previous gel runs. On the long edges of each glass plate silicon was applied with a small sponge the width of the plastic gel spacers. The spacers were then placed onto the silicone layer of one plate and the second plate placed on top of that. Spacers need to be precisely aligned with all edges. The long edges of the glass plates were fixed with the appropriate clamps (very tight without breaking the glass plates) and placed onto the gel stand above the openings of the tubing. Both syringes and the tubing of the gel stand were filled air free with 40% glycerin and the gel stand was arranged with a water balance to be level.

Per gel, one aliquot of acrylamid solution and one aliquot of persulfate solution were thawed at room temperature. Solutions were mixed (Persulfate final concentration 0.08%) and speedily poured between the two glass plates. A layer of 1.5ml glycerin was carfully pushed beneath ech gel with the prepared syringes. The acrylamid should pour over the edges of the galss plates. The top opening of the glass plates was loosely covered with parafilm (no stretching and sealing required). After one hour the gels were taken from the gel stand and the glycerin removed with whatman paper. The gels were reversed and placed onto the gel stand again. The empty space between the glass plates (where the glycerin was) was fille with levelling solution and again covered with parafilm. Gels were allowed to polymerate over night. 5l of distilled water were cooled to 4°C.

On the morning of the next day the gel chamber was filled with 2l 5.5x running buffer and 4l distilled water. Then the 5l pre-cooled water was added (EK 1x running bufer). The thermostat of the circulating pump was set to 17°C. The chamber was balanced on one corner and the circulating pump was started. Two IPG strips with completed first dimension

run were taken from the -80°C freezer and placed into glass tubes filled with 1x running buffer from the gel chamber. The space between the glass plates of the second dimension gels was filled with running buffer and one IPG strip placed carefully there. The same was done with the other strip and gel. The running buffer was removed from the space with whatman paper and replaced with Agarose /bromphenol blue (~40°C). When the agarose had cooled and hardened after a few minutes, the gels were placed with the agarose side down onto the anode (seperate part of the gel chamber) and fixed in place with clamps. The circualting pump was stopped, the chamber put level and 1.6l of cooled 1x running buffer removed from the chamber. The Anode with the gels was placed in the chamber, any air bubbles beneath the gels were removed (with a long cell culture scraper) and he anode was filled with the 1.6l running buffer. The Pump was started again and the power supply for the running chamber was also started (table 21).

At the end of the gel run, the glass plates were carfully removed and the gels (marked at one or two corners) were placed in the fixation solution for silver staining.

Table 21: 2D running conditions for two gels	
15 minutes	65mA at 150-160V
5-6 hours	85mA at 210-260V (at the start of the run)
	85mA at 750-900V (at the end of the run)

Coomassie staining

Gels were gently shaken in the staining solution (table 22) for 45 minutes. The Solution can be stored at room temperature and reused. Gels were then shaken in decolorization solution for several hours with repeated exchange of decolotization solution until bands were clearly visible. The decolorization solution can be destained by filtering through active charcoal. Gels were stored at RT in storage solution until they were scanned or dried.

Table 22: Coomassie solutions		
staining	**decolorization**	**storage**
500ml MetOH	50ml MetOH	
100ml acetic acid	125ml acetic acid	70ml acetic acid
0.1% (w/v) Coomassie brilliant Blue R-250		
ad 1000ml aqua dest	**ad 1000ml aqua dest**	**ad 1000ml aqua dest**

Silver staining

For each step of the silver staining procedure a new set of disposable gloves was used and all incubation steps were carried out in clean glass trays with lids under gentle agitation. Only chemicals of the highest purity were used for the different solutions (table 23), which were all prepared freshly for each staining procedure.

Gels were carefully placed in the glass trays and incubated with 1l fixation solution per gel over night at 4°C. Gels were washed once with 99.9% EtOH for 10 minutes and twice with 50% EtOH for 25 minutes each. The gels turn opaque and shrink when placed in the EtOH solutions but this process reverts over time during the next staining steps. The gels were

incubated with sensitization solution for 2 minutes and immediately washed three times with water for 20 seconds each. The Gels were then incubated in staining solution for 20 minutes in darkness and after that again washed three times with water for 20 seconds each. Gels were finally incubated in developer solution for an appropriate amount of time until staining intensity was satisfying (typically 2-15 minutes, depending on the amount of loaded protein) and placed in the stop solution to terminate the colorization reaction.

Table 23: Silver staining solutions

fixation	sensitization	staining
500ml EtOH	0.2g Sodium thiosulfate * $5H_2O$	2g silver nitrate
100ml acetic acid		750µl Formaldehyde (37%)
500µl Formaldehyde (37%)		
ad 1000ml aqua dest	**ad 1000ml aqua dest**	**ad 1000ml aqua dest**

developer	stop
60g Sodium carbonate	18.612g EDTA (Titriplex)
500µl Formaldehyde (37%)	200mg Thimerosal (not suitable for subsequent mass spectrometry)
4mg Sodium thiosulfate * $5H_2O$	
ad 1000ml aqua dest	**ad 1000ml aqua dest**

Recombinant expression of proteins in *E.coli* with the GST gene fusion system

A 25ml primary culture of *E.coli*, transformed with a GST – fusion construct (pGEX 4T – Vector from GE Healthcare or pDEST24 from invitrogen), was incubated over night at 37°C and 250rpm. On the next day 20ml were added to 1 liter LB-medium. The culture was incubated until an optic density (OD) of 0.4 to 0.6 at 600nm was reached. Then 1ml 1M Isopropyl-β-D-thiogalactopyranosid (IPTG) was added to induce the expression of the GST-fusion protein. The culture was incubated under constant shaking for another 4 hours. Then the bacteria were distributed to centrifuge cups and sedimented at 4°C and 5000g for 15 minutes. The supernatant was discarded and the pellets were carefully solubilized in 10ml ice cold 1xPBS and thereby pooled. The samples were transferred to 50ml reaction tubes and one tip of a spatula of lysozyme was added. The samples were incubated at 4°C for 30 minutes and carefully inverted every 10 minutes. Subsequent sonification (3x10 seconds at 30% output power) and addition of 2ml 20% Triton-X-100 completed the cell lysis. The lysate was transferred into centrifugation cups for an SS-34 rotor and cell debris was sedimented at 4°C and 9500g for 15 minutes. Meanwhile 700µl glutathione-sepharose beads were washed three times with ice cold 1xPBS in a 50ml reaction tube. The cleared lysate was transferred into 50ml reaction tubes also containing the glutathione-sepharose beads and rotated at 4°C over night or even better for another day. The beads were then sedimented at 500g for 5 minutes and transferred into a 1.5ml microcentrifuge cup. The beads were washed three times with ice cold 1xPBS and the proteins were eluted. For that, 700µl freshly prepared ice cold GST-elution buffer (50mM Tris-HCl at pH8.0, 10mM reduced glutathione) were added to

the beads and rotated at RT for 5 minutes. The beads were again sedimented at 500g for 5 minutes and the supernatant containing the GST-fusion protein was transferred into a new 1.5ml microcentrifuge cup. The elution procedure was repeated three times.

The beads can be stored in PBS/ethanol at 4°C and reused for a purification of the same protein.

2.2.4 Cell culture

Targeted embryonic stem cells

ES cell clones ordered a the KOMP konsortium were delivered on dry ice and stored at -80°C immediately upon arrival. All further handling of ES cels was carried out by PD Dr. I. Hermans-Borgmeyer and Sarah Homann.

Isolation of primary cells from mouse brain

For the generation cell cultures from either primary hippocampal or cortical neurons or glia cells, either wild type C57Bl/6J or Tmem128 knockout female mice were used. The pregnant mice were sacrificed 16-17.5 days after breeding to wild type or Tmem128 knockout males in accordance with animal welfare laws. Embryos were removed from the mothers and sacrificed by decapitation. Brains were removed using microscissors and forceps and stored on ice in HANKS‘ medium supplemented with 20% FCS. Under a binocular microscope hippocampi and cortices were isolated from the embryonal brains and stored in HANKS‘ +FCS. All further steps were carried out under a laminar flow hood. Brain samples were washed two times with HANKS‘ with sedimentation by gravity flow. 2ml digestion buffer supplemented with 2mg Papain and 1mg DNAse (3kU in 0.15M NaCl) were added and brain samples were incubated in this buffer for 30 minutes at 37°C and 5% CO_2. Brain samples were subsequently washed again two times with HANKS‘ and then resuspended in 2ml dissociation buffer supplemented with DNAse. Cells were separated from each other by triturating the brain samples 20 times with a Pasteur pipette and again 20 times with a fire polished Pasteur pipette with a narrow opening. The cells were then resuspended in 10ml HANKS‘ + 20% FCS and sedimented for 10 minutes at 100g. The cell pellet was resuspended in growth medium and counted using a Neubauer cell counting chamber. Neurons were seeded at a density of 40000 -80000 cells per cm^2 (low density for hippocampal cultures and high density for cortical cultures) on glass cover slips and at a density of 120000 cells per cm^2 on 6cm- plastic dishes. Glass cover slips and plastic dishes were previously coated over night at 37°C and 5% CO_2 with 0,5mg/ml poly-L-Lysin and washed three times with water. Cells were then left to grow undisturbed for several days in vitro (DIV) in a humidity controlled incubator at 37°C and 5% CO_2. Transfection with Lipofectamine was carried out at DIV 4-7 and infection with viral constructs was carried out between DIV3 and 14. Cells were prepared for microscopy or biochemical experiments at various DIVs.

For cultivation of glia cells, all leftover cells from the tissue-prep were seeded onto poly-L-Lysin covered 10cm dishes and cultured with DMEM +20% FCS in a humidity controlled incubator at 37°C and 5% CO_2.

Induction of activity in cultured neurons with KCl

For activity induction, 2.5M KCl solution (in water) was mixed with prewarmed growth medium [EK 50mM] and equilibrated at 37°C and 5% CO_2 for up to 14 hours (at least one hour). Growth medium on the neurons was then replaced (the old medium was stored) with the KCl-medium. After 10 minutes, the KCl medium was replaced with the old medium and cells were incubated at 37°C and 5% CO_2 until cell lysis at various time points.

Culturing of secondary eukaryotic cell lines

All operations were carried out under a laminar flow hood (clean bench) and cells were cultured in a gas incubator under 5% CO_2 and 95% humidity at 37°C.

Cell lines used for this work:

SH – SY5Y is a clonal subline of the neuroepithelioma cell line SK-N-SH that had been established in 1970 from the bone marrow biopsy of a 4-year-old girl with metastatic neuroblastoma (Biedler et al., 1973).

HEK – 293 cells (Human Embryonic Kidney) were established from a human primary embryonal kidney transformed by adenovirus type 5 (Ad 5) (Graham et al., 1977).

HEK – 293T cells (Human Embryonic Kidney) are a highly transfectable derivative of HEK 293, containing the temperature sensitive mutant of SV-40 large T-antigen (express SV-40 large T at 33°C, but not at 40°C). Classified as risk group 1 according to the German Central Commission for Biological Safety (ZKBS) (Pear et al., 1993).

HeLa cells were established from the epitheloid cervix carcinoma of a 31-year-old black woman in 1951; later the diagnosis was changed to adenocarcinoma; first aneuploid, continuously cultured human cell line (Gey et al., 1952).

N2a Neuro-2a cells were established by R.J. Klebe and F.H. Ruddle from a spontaneous tumor of a strain A albino mouse in 1969 (Olmsted et al., 1970).

Passaging of cells

Cells were cultured in small culture flasks (25cm^2) 90% DMEM (Dulbecco´s modified eagle medium) and 10% FCS (fetal calf serum). Cells were split every 3-4 days. They were washed with PBS, incubated with 500µl filter sterilized trypsin solution (10mg/ml trypsin in Ca^{2+}/ Mg^{2+} free PBS) for 3 minutes at 37°C, then washed from the flask surface with 5ml medium and transferred into a 15ml reaction tube. After sedimentation at 1200g for 2 minutes the supernatant was discarded and the cell pellet was resuspended in 5ml medium. 250µl of the cell suspension was mixed with 5ml fresh medium and cultured.

Freezing of cells

Cells were harvested from a medium culture flask (75cm^2) and resuspended in 2ml complete medium mixed with 2ml freshly prepared 2x cryoprotectant medium (table 24). The cell suspension was pipetted into four cryo vials and slowly frozen in a Styrofoam box at -80°C. One week later the vials were transferred into the vapor phase in a liquid nitrogen tank.

Table 24: 2x cryoprotectant medium	
reagent	**final concentration**
sterile Dimethyl sulfoxide (DMSO)	20%
sterile fetal calf serum	40%
Dilbeccos' modified eagle medium (DMEM)	40%

Thawing of cells

Cells in cryoprotectant medium were thawed by adding prewarmed complete medium. After sedimenting them at 1000g for 2 minutes the supernatant was discarded and the cell pellet was resuspended in 5ml complete medium. Cells were transferred into a small culture flask and incubated in a cell culture incubator.

Transfection of primary and secondary cells

Transfection of secondary cell lines with FuGENE 6 reagent

One day before transfection 150000 cells per well were seeded into a 6well plate.

For transfection 3µg DNA was pipetted into a 1.5ml microcentrifuge cup with 200µl serum free DMEM. In another cup 9µl FuGENE6 reagent (Roche) was slowly pipetted into 200µl serum free DMEM and incubated at RT for 5 minutes. This mixture was carefully pipetted drop by drop into the DNA and mixed by snapping the cup. After incubation at RT for 20 minutes the sample was pipetted onto the cells in 2ml serum free DMEM, which had previously been washed two times with serum free DMEM. After 5 hours of incubation at 37°C 200µl serum and 1ml DMEM (+10% serum) were added.

For generation of stably transfected cell lines, cells were harvested and resuspended in 40ml complete medium containing 250µg/ml Zeocine or 10µg/ml Blasticidine two days after transfection. The cell suspension was distributed onto two 96-well plates with 200µl cell suspension per well. 10-14 days after the transfer plates were screened under a microscope for clonal colonies. Cells containing a fluorescent construct were also screened under a fluorescence microscope. Cells containing a non-fluorescent construct were screened by Western-blotting and immunocytochemistry with construct specific antibodies.

Transfection of secondary cell lines with Lipofectamin2000 reagent

One day before transfection 150000 cells per well were seeded into a 6well plate.

For transfection 4µg DNA was pipetted into a 1.5ml microcentrifuge cup containing 250µl pre warmed OptiMEM. In another cup 10µl Lipofectamin2000 reagent (Invitrogen) was slowly pipetted into 250µl pre warmed OptiMEM and incubated at RT for 5 minutes. This mixture was carefully pipetted drop by drop into the DNA and mixed by snapping the cup. After incubation at RT for 20 minutes the sample was pipetted onto the cells.

Transfection of primary neurons with LipofectaminLTX reagent

An appropriate number of wells in a 24-well plate was filled with 500µl OptiMEM (Invitrogen) and equilibrated over night at 37°C and 5% CO_2. Cover slips with neurons were removed from their culture dishes and placed in the 24-wells and incubated at 37°C and 5% CO_2 for 1h before adding of the transfection mix. The transfection mix was prepared by adding

2µg of plasmid-DNA (1µg for double transfections) and 2µl of PlusReagent (Invitrogen) to 100µl OptiMEM (37°C) in a 1.5ml cup and 2µl LipofectaminLTX to 100µl OptiMEM (37°C) in another 1.5ml cup. After incubation at RT for 5min, the Lipofectamin-mix was carefully added to the DNA-mix and mixed by snapping the tube. The transfection mix was incubated at RT for 20min and then added to the neurons (100µl transfection mix per cover slip - constructs were always transfected as duplicates). After incubation for at 37°C and 5% CO_2 30min, cover slips were transferred to their original culture dishes. At DIV14 to DIV21 cells were fixed and immunostained.

Infection of primary neurons and secondary cells with lentiviruses

4 million 293-T cells were seeded onto 6cm plastic dishes in DMEM. On the next day, cells were carefully washed with pre-warmed DMEM and incubated with 3ml DMEM at 37°C until transfection. Transfection was carried out with Lipofectamine2000. 4µg Plasmid DNA together with a 10µl Master mix of helper plasmids (2.4µg pLP1, 1.2µg pLP2 and 0.8µg pLP-VSVG diluted in OptiMEM (curtesy of P. Osten) were used. 6h after transfection DMEM was replaced with prewarmed neuronal growth medium. 24-48h after transfection medium was harvested, passed through a 0.22µm PES syringe filter and 100µl aliquots in thin-walled PCR tubes were flash frozen in liquid nitrogen. Virus aliquots were stored at -80°C. For transfection of primary neurons, two cover slips with neurons were transferred to a 3cm culture dish, containing 2.5ml prewarmed neuronal culture medium. An aliquot of virus was thawed at RT and an appropriate amount of virus (has to be determined for each batch of virus - but usually between 25 and 100µl) was added to the culture dish. Cells were incubated for at least 7 days before fixation and counterstaining.

Immunocytochemistry

Saponin method

Cells were grown on small glass cover slips (12mm diameter) which were transferred to 24-well plates for the staining procedure. Cells were washed 2 times with PBS and incubated in paraformaldehyde (4% w/v in PBS, + 4% w/v sucrose) for 10-12 minutes. Then PFA was exchanged against PBS and subsequently PBS was exchanged with PBS + 0.05% Saponin (PBS-S) and the cells were permeabilized at 4°C for 30 minutes or up to 12 hours. After the permeabilization-step a "humid chamber" was prepared on a table (a parafilm surface surrounded by wet tissues and covered by a light proof box). The antibody solution consisted of PBS-S, 10% FCS and an appropriate amount of antibody. Per cover slip 30µl of the solution were pipetted on the parafilm. The cover slips were lifted with a needle hook and then transferred with forceps onto the antibody drop with the cell side down. After 2 hours incubation in the dark "humid chamber" at RT the cover slips were transferred back into the 24-well plate and washed 3 times with PBS-S with 5 minutes each. The secondary antibody solution was prepared like the first solution and again 30µl per cover slip were pipetted on the parafilm. The cover slips were again incubated with the cell side down for 2 hours and then again washed 3 times with PBS-S. They were then washed two times with water to remove salt residues. A drop of mounting medium (80% Immu-Mount mixed with

20% ProlongGold anti fade with DAPI) per cover slip was placed on a glass microscope slide and the cover slips were placed cell side down on the mounting medium. The slides were stored at 4°C in the dark.

Digitonin method

Cells were grown on small glass cover slips (12mm diameter) which were transferred to 24-well plates for the staining procedure. The 24-well plate was put on ice and the cells were washed 2 times with PBS and incubated with 25µg/ml Digitonin in KHM-buffer (in mM: 110 KOAc, 20 HEPES, 2 MgOAc, pH7.4). The cells were washed again with PBS and then fixed and stained as described for the saponin-method, with the important exception, that no detergent was used during staining and washing. Only PBS.

3 Results

3.1 Approaches to identify novel Arc/Arg3.1 interaction partners

In order to better understand the role of Arc/Arg3.1 in the formation and maintenance of long-term memories, we set out to identify and characterize novel protein interaction partners. As outlined in the introduction, Arc/Arg3.1 is involved in several intracellular sorting processes in postsynaptic spines. We were therefore especially interested in protein interaction partners that could link Arc/Arg3.1 to these kind of processes. To achieve this goal we used a technique that was suited for the identification of native protein complexes from mouse brain (TAP) and a high throughput screen for the specific identification of membrane associated interaction partners (Split-Ubiquitin-Approach).

3.1.1 Tandem Affinity Purification did not reveal novel Arc/Arg3.1 interaction partners

One approach that we used to identify novel interaction partners of Arc/Arg3.1 was the purification of interacting proteins by Tandem Affinity Purification (TAP) (Puig et al. 2001; Bailey et al. 2012). For this approach we used a transgenic mouse line that expresses a TAP-Tag-Arc/Arg3.1 fusion protein under the control of the forebrain specific Thy.1 promoter. This transgene inserted randomly in the genome and the transgenic mice still express the wild

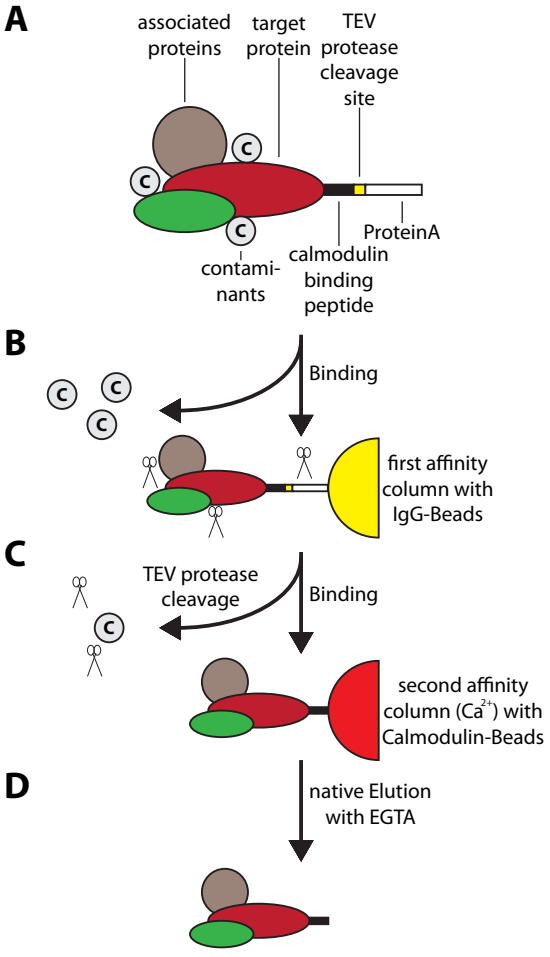

Figure 4: Schematic representation of the TAP procedure.

(A) Protein complexes of the TAP-tagged protein of interest and its interaction partners are carefully released from cells or tissues. (B) In the first step of purification the protein complex is precipitated on a column of IgG coated sepharose beads via the interaction with the ProteinA-moiety of the TAP-tag. After carefully washing the complex and removing many unspecific binding partners, the complex is released by the addition of TEV-protease which cleaves the TAP-tag between the ProteinA moiety and the Calmodulin Binding Peptide (CBP) moiety. (C) The released protein complex is bound to a column of calmodulin coated sepharose beads in the presence of Ca^{2+} and excessive washing ensures the removal of more unspecific binding partners and the TEV-protease. (D) The purified native protein complex consisting of the protein of interest and its binding partners is released by chelating the Ca^{2+} with EGTA. The released complex can be further analyzed. Modified after Puig et al., Methods (2001).

type Arc/Arg3.1 protein. TAP is designed for the purification of protein complexes consisting of the TAP-tagged protein of interest and its interaction partners in two subsequent affinity purification steps, with each purification step being carried out under mild conditions. This ensures enrichment and purification of the proteins of interest without disturbance of the native complexes. The TAP approach thus allows the isolation of intact and specific protein complexes. Various combinations of tags have been established for TAP (Grant 2010; Bailey et al. 2012). The TAP tag we used in this study consisted of a ProteinA moiety followed by a TEV-protease cleavage site and a calmodulin binding domain (CBD) attached to either the N-Terminus (N-TAP) or C-Terminus (C-TAP) of Arc/Arg3.1 (figure 4A). For a TAP experiment 10 to 15 mice of each experimental group were sacrificed, the brains removed and subsequently homogenized. In the first step of the TAP procedure, protein lysates are separated on a column of IgG coated sepharose beads (figure 4B) and the link between the two affinity tags is then separated by enzymatic cleavage using TEV protease (figure 4C), thereby circumventing the problem of a harsh elution. In the presence of Ca^{2+} the second

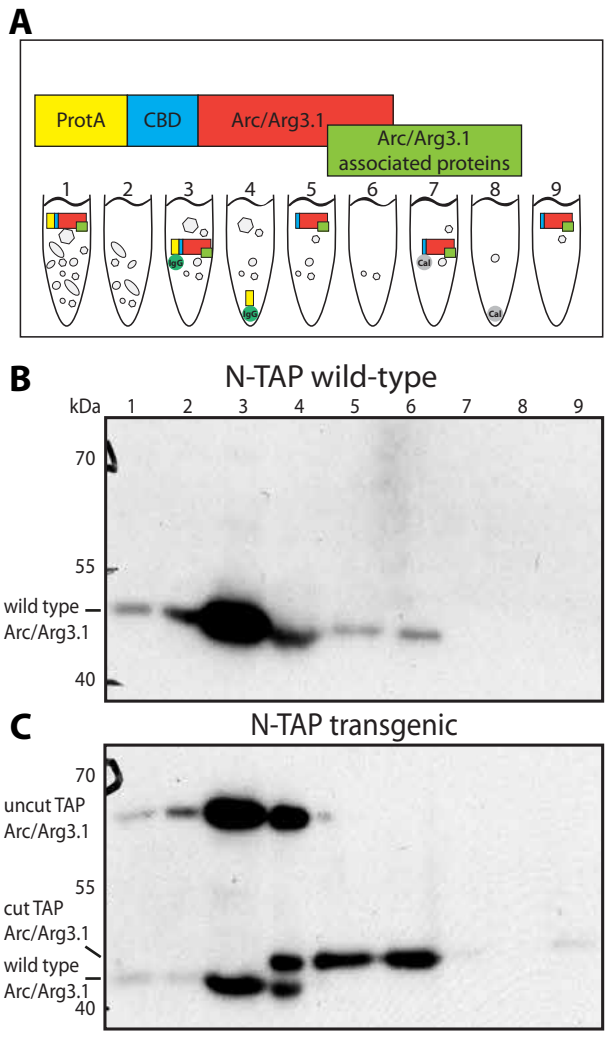

Figure 5: Representative results from a TAP procedure from wildtype and transgenic littermates from the N-TAP-Arc/Arg3.1 line.

(A) Schematic representation of the samples aquired during the Tandem affinity purification procedure. Under ideal conditions, the protein of interest and its interaction partners should only be present in samples 1, 3, 5, 7 and 9. (B) and (C) Representative western blots probed with an antibody against Arc/Arg3.1. (B) In the wild type samples only bands at the molecular weight of wild type Arc/Arg3.1 are detectable (lanes 1-6). (C) Various bands can be detected in the transgenic animals at the molecular weight of wild type Arc/Arg3.1 (~45kDa, lanes 1-4) and at the molecular weight of the TAP-tagged Arc/Arg3.1 before (~65kDa, lanes 1-4) and after digestion with TEV-protease (~49kDa, lanes 4-9).

1	**Lysate of mouse brains**
2	**Supernatant of lysate after IgG precipitation**
3	**IgG precipitate**
4	**IgG sepharose after TEV-cleavage**
5	**Supernatant after TEV-cleavage**
6	**Supernatant after calmodulin precipitation**
7	**Calmodulin precipitate**
8	**Calmodulin beads after EDTA-elution**
9	**Supernatant after EDTA-elution**

part of the TAP tag then binds to a column of calmodulin coated beads (figure 4C) from which the complex is then eluted with the Ca^{2+} chelating agent EGTA (figure 4D). Multiple wash steps under mild conditions are carried out during the entire procedure.

Samples were taken at each step of the purification process and analyzed by western blotting to assess the effectiveness of the TAP-procedure (figure 5). During the TAP procedure nine samples were taken from wild type and TAP-Arc/Arg3.1 lysates. Each sample either contains the TAP-Arc/Arg3.1 (odd sample numbers in figure 5A) or should not contain it any more due to specific precipitation (even sample numbers in figure 5A). Unfortunately the western blot analysis was not as unambiguous as in theory. Despite intensive effort to improve elution

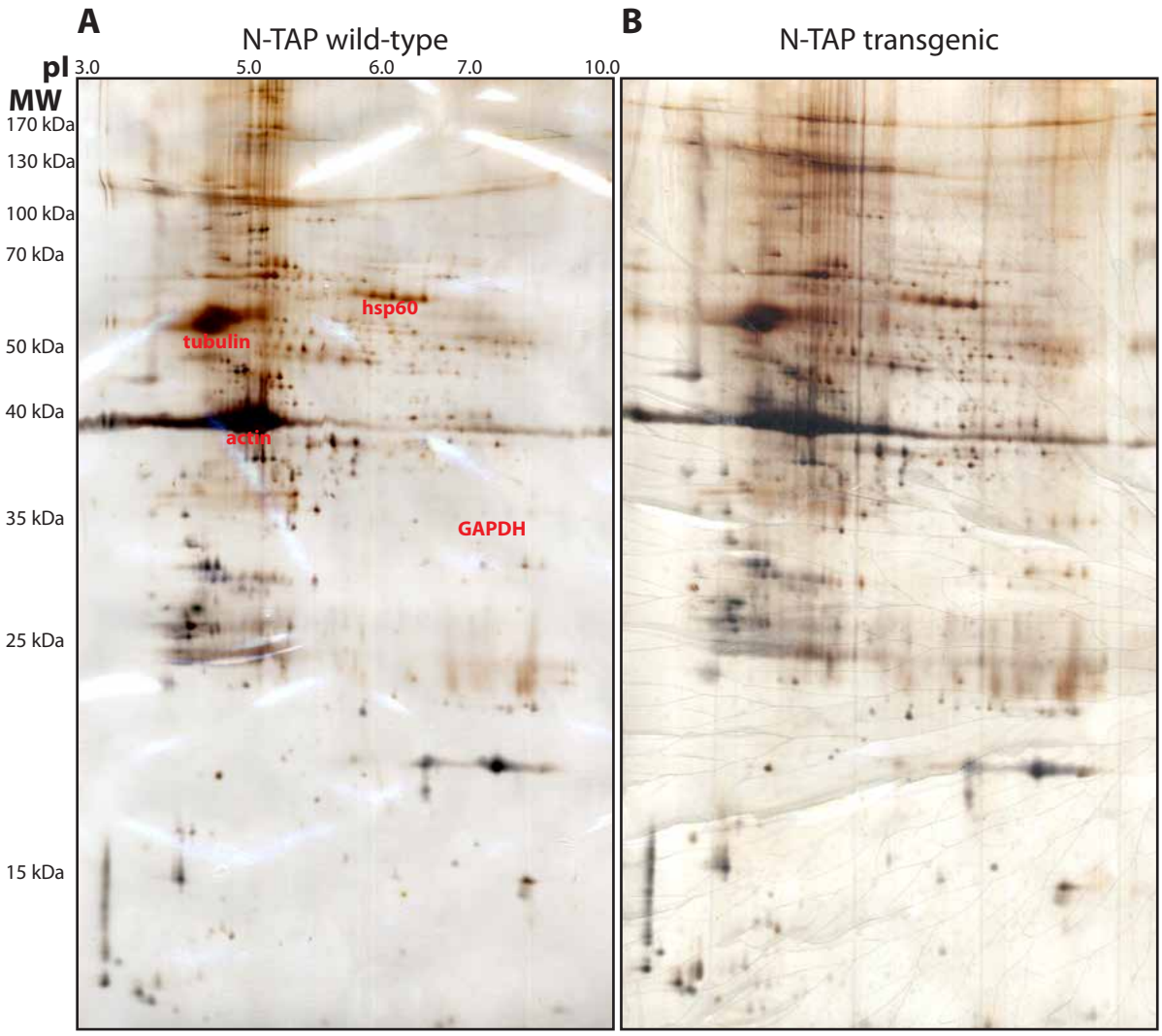

Figure 6: Eluates from from wildtype and transgenic littermates from the N-TAP-Arc/Arg3.1 line analyzed by 2DE gel electrophoresis.

Representative silver stained gels after 2-dimensional gel electrophoresis of protein complexes isolated from wild type animals and N-TAP-Arc/Arg3.1 transgenic animals using tandem affinity purification. Gels were vacuum sealed in cellophane and scanned on a flatbed scanner. No consistent differences in protein spot composition could be detected between wild type and transgenic animals over several TAP experiments. Spot positions of prominent house-keeping proteins are marked in red.

from the sepharose columns, large amounts of TAP-Arc/Arg3.1 were still detectable on the IgG-beads even after elution (figure 5C lane 4). On the other hand only small amounts of the size-reduced TAP-Arc/Arg3.1 after the TEV protease cleavage bound to the calmodulin column (figure 5C lane 7) and the majority of protein stayed in the supernatant (figure 5C lane 6). This resulted in only little sample being eluted from the last column (figure 5C lane 9). In wild type as well in TAP-Arc/Arg3.1 samples, native Arc/Arg3.1 could be detected in the initial samples (figure 5B lanes 1-6 and figure 5C lanes 1-4) before it was eventually washed off.

We separated the final eluate (figure 5C lane 9) using 2 dimensional gel electrophoresis (2DE) and visualized proteins by silver staining (figure 6). The analysis of TAP-eluates by 2DE varied strongly in quality and consistency and no systematic differences in spot patterns or intensity could be detected between eluates from wild type versus TAP-Arc/Arg3.1 mice. To circumvent this problem and eventually identify clearer differences between the samples, we subjected the final eluate to standard SDS-PAGE analysis with subsequent silver staining. Prominent bands differing between TAP and control animals appeared only in one experiment. We excised these bands (figure 7) and analyzed them using mass spectrometry. Peptide analysis revealed only keratin, a common contaminant.

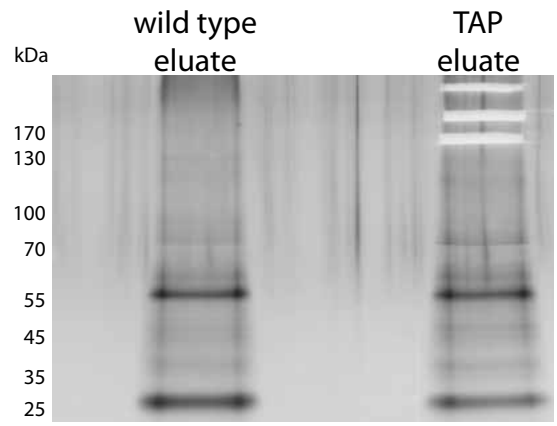

Figure 7: Eluates from N-TAP-Arc/Arg3.1 and wild type animals analyzed by SDS-PAGE.

Representative silver stained gels after gel electrophoresis of protein complexes isolated from wild type animals and N-TAP-Arc/Arg3.1 animals using tandem affinity purification. Only three weak bands were detected in the eluate of the transgenic animals that were not visible in the eluate of the wild type animals. Bands were excised and subjected to mass spectrometry. The analysis identified keratin.

Because Arc/Arg3.1 interacting proteins are likely to be diverse and sparse, endogenous Arc/Arg3.1 could potentially interfere with the TAP- procedure. TAP-Arc/Arg3.1 animals were therefore crossed with Arc/Arg3.1 knockout animals. This did not lead to increased protein amounts isolated during the TAP procedure and identifiable bands in Coomassie or silver stained gels of the final eluates.

3.1.2 The Split-Ubiquitin screen identified several potential interaction partners for Arc/Arg3.1

A second avenue to identify Arc/Arg3.1 interaction partners employed the Split-Ubiquitin-Approach (figure 8), a modified Yeast-TwoHybrid screen (Johnsson and Vershavsky, 1994; Snyder et al., 2010). This approach is based on the fact that the evolutionarily conserved small protein Ubiquitin can be split in two independent polypeptides at amino acid 34, generating the N-terminal ubiquitin fragment N_{UB} and the C-terminal ubiquitin fragment C_{UB}. N_{UB} and C_{UB} will spontaneously reassemble in cells to form a non-covalently bound but stable pseudoubiquitin (figure 8D).

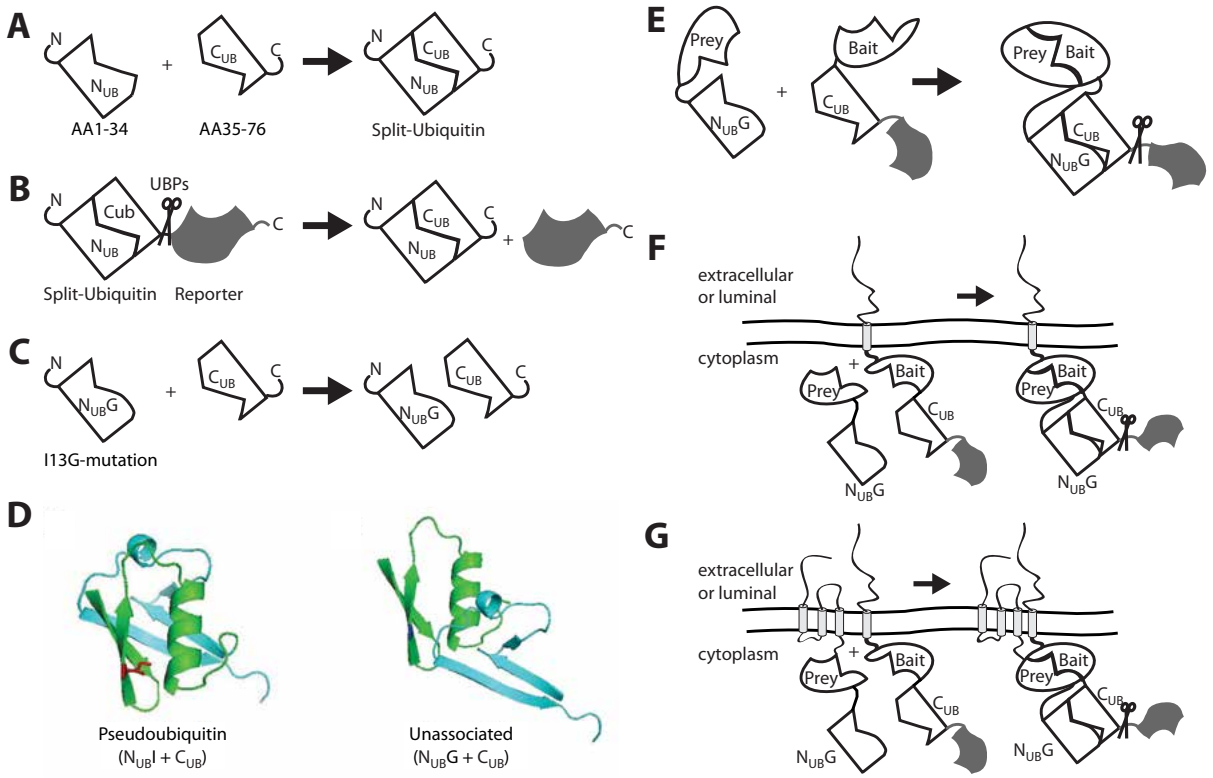

Figure 8: Schematic representation of the principle underlying the split ubiquitin screen.

(A) Expression of the N-terminal 34 (N_{UB}) and C-terminal 42 (C_{UB}) amino acids of ubiquitin in cells leads to a spontaneous reassembling and reconstitution of pseudoubiquitin. (B) Ubiquitin specific proteases (UBPs) recognize the complete protein and cleave off any C-terminally fused proteins, such as reporter proteins. (C) Introduction of a point mutation (Isoleucin 13 to Glycin) to N_{UB} generates $N_{UB}G$, which shows a dramatically reduced affinity to C_{UB}. (D) Secondary structure of reassembled pseudoubiquitin and unassembled NubG and C_{UB}. (E) Fusion of two interacting proteins to the N-termini of $N_{UB}G$ and C_{UB} forces them into close proximity and thereby increases the probability of the formation of pseudoubiquitin and subsequent release of a reporter by UBPs. Once the reporter is released, it translocates to the nucleus and promotes transcription of survival relevant genes. This setup can be used to screen a library of potential interaction partners (preys) for a protein of interest (bait). (F) If the prey is not a transmembrane protein itself, it can be anchored to the plasma membrane as a fusion protein with a Type I transmembrane protein. Interaction partners that are localized near the membrane or are transmembrane proteins themselves (G) can be identified this way. (A-C) and (E-G) modified after Hermey et al. (2010) and (D) modified after Snider et al. (2010).

And to prevent the spontaneous reassembling, a point mutation is introduced in N_{UB} (Isoleucin 16 to Glycin) generating $N_{UB}G$. $N_{UB}G$ and C_{UB} will only reassemble if brought into close proximity to one another. For the purpose of a screen, $N_{UB}G$ and C_{UB} are fused to a bait protein and a library of pray proteins. $N_{UB}G$ and C_{UB} reconstitute the full ubiquitin only upon interaction of bait and prey proteins. The reassembled ubiquitin is recognized by ubiquitin specific proteases (USPs), localized in the nucleus and cytoplasm of al eucaryotic cells. USPs cleave off any C-terminal attachments, usually another ubiquitin but in this case a transcription factor consisting of the bacterial LexA-DNA binding domain and the *Herpes simplex* VP16 transactivator domain. The transcription factor serves as the reporter for positive interactions by translocating to the nucleus and promoting yeast survival on nutrient deficient medium. Thereby only yeast cells that express interacting proteins will survive and form colonies. Positive colonies are lysed and sequenced to identify the interacting prey-protein expressed by that colony. The bait protein, if it is not an integral membrane protein, can be fused to the transmembrane domain of another protein in order to screen preferentially for membrane near protein-protein interactions (figure 8F and G). This has been done in our case by fusing Arc/Arg3.1 to the transmembrane domain of the yeast protein Ost4.

The screen for the identification of Arc/Arg3.1 interaction partners was planned and coordinated in cooperation with the Paris based company Hybrigenics and the actual yeast experiments were carried out in the laboratories of Hybrigenics. Figure 9 details the screen setup and protein constructs used in the screen. An adult mouse brain library was screened and an estimated number of 45 million interactions were tested. 190 yeast colonies were picked and sequenced. The 182 successfully cloned interaction partners coded for 13 different proteins, nine transmembrane and four soluble proteins. I categorized these 13

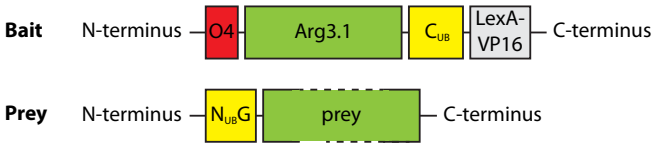

O4	Ost4 transmembrane anchor
Arg3.1	rat Arc/Arg3.1 amino acids 2-396 (without start-Met) - hybrigenics code for this bait: hgx2113v2_pB107
C_{UB}	amino acids 35-76 of ubiquitin
LexA-VP16	reporter casette
$N_{UB}G$	amino acids 1-34 of ubiquitin with an I16G point mutation
prey	mouse adult whole brain library (dT-primed with 10^6-10^7 independent clones)

Figure 9: Constructs used for the Split-Ubiquitin-screen.

The Bait construct consisted of the transmembrane anchor of the yeast type I transmembrane protein Ost4, followed by Arc/Arg3.1, C_{UB} and the LexA/VP16 reporter cassette. The Library with the potential interaction partners consisted of prey proteins derived by dT-priming of adult mouse whole brain cDNA fused to the C-Terminus of $N_{UB}G$. The yeast strain was NMY32-DeltaGal4 and the selection media were DO-trp-leu-his and DO-trp-leu-his + 20mM 3-Aminotriazol (3-AT).

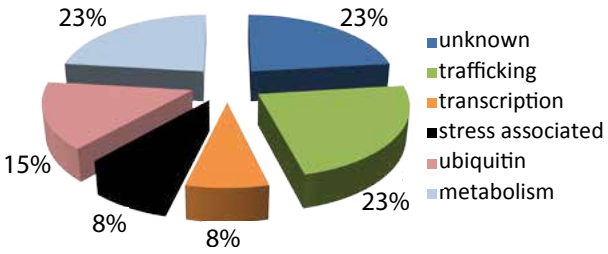

Figure 10: Categories of potential interaction partners of Arc/Arg3.1 identified in the Split-Ubiquitin-screen.

Identified prey proteins were categorized according to their described functions or homologies to known proteins in cases of unknown preys. 23% of the identified proteins are categorized as being involved in intracellular trafficking processes or having homologies to proteins with trafficking function.

potential interaction partners according to their described cellular functions or (in case the proteins were so far undescribed) their homology to other proteins (figure 10). As Arc/Arg3.1 is implicated in the surface expression of AMPA type glutamate receptors as well as the correct trafficking of the Familial Alzheimer's Disease risk gene Presenilin1, the category "trafficking", in which 23% of the identified proteins were grouped, was of special interest to us. Proteins in this category had either known or predicted functions in intracellular sorting or endosomal trafficking. Of the 13 potential interaction partners for Arc/Arg3.1 identified in the screen, I eliminated seven as potential false positives by educated guessing (e.g. extracellular proteins or proteins connected to ubiquitin signalling). Six proteins from different categories were picked as targets of interest: Four so far uncharacterized transmembrane proteins (RIP5, Gpsn2, Tmem128 and Yipf6), and two cytoplasmic proteins (CKB and SelK). RIP5, Tmem128 and Yipf6 were from the "trafficking" category, CKB and SelK from "metabolism", and Gpsn2 was of unknown function.

3.2 Validation of RIP5 and Tmem128 as novel interaction partners of Arc/Arg3.1

Before further characterizing the potential interaction partners I attempted to validate their interaction with Arc/Arg3.1 in biochemical and cell biological assays.

3.2.1 Co-immunoprecipitations

I performed co-immunopreciptitations from lysates of transiently transfected HeLa-cells, overexpressing tagged versions of Arc/Arg3.1 and the individual potential interaction partners. In several independent experiments the interaction between Arc/Arg3.1 and CKB, SelK, Gpsn2 and Yipf6 could not be confirmed (data not shown). The published interaction partner Dynamin2 was used as a positive control and could be confirmed in this assay (figure 11A). Two weak but consistent interactions with RIP5 and Tmem128 were reproduced in several independent experiments (figure 11B). Another interesting finding was that RIP5 and Tmem128 reproducably coimmunoprecipitated with each other (figure 11C).

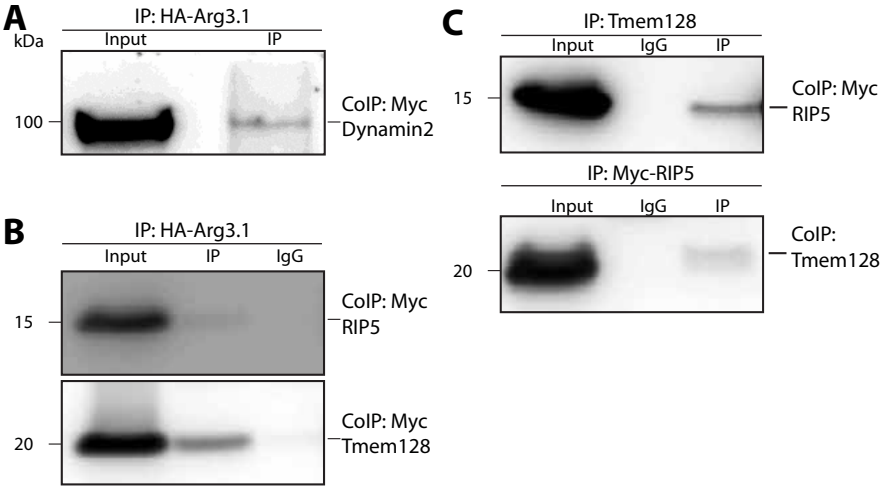

Figure 11: Co-immunoprecipitations of Arc/Arg3.1 and interacting proteins:

(A-B) HA-tagged Arc/Arg3.1 was precipitated from HeLa-cell lysate and Myc-tagged interaction partners were detected by western blot analysis. (A) The interaction with the previously described interaction partner Dynamin2 was confirmed. (B) There is a weak, but consistent, band in the IP lane and no band in the IgG lane for RIP5, indicating a direct interaction of Arc/Arg3.1 and RIP5. Similarly, there is a band in the IP lane and no band in the IgG lane for Tmem128, indicating a direct interaction of Arc/Arg3.1 and Tmem128. (C) When Tmem12 was precipitated, Myc-tagged RIP5 was co-immunoprecipitated. This was also true for the reverse experiment.

3.2.2 Mammalian-Two-Hybrid system

To further confirm the interaction of Arc/Arg3.1 with RIP5 and Tmem128, I used the Mammalian-Two-Hybrid system, a luciferase based cell assay. For this purpose, potentially interacting proteins are cloned in vectors encoding either a DNA-binding domain (Gal4) or a DNA polymerase activating domain (VP16). Both resulting fusion proteins are then expressed in the neuronal mouse cell line N2a together with a vector encoding firefly luciferase as a Gal4-dependent reporter gene and an EGFP containing vector for normalization. When the two fusion proteins come in close proximity to each other, the transcription of the luciferase reporter gene is initiated and the released chemiluminescence indicates protein-protein interaction.

Only the N-terminal domains of RIP5 and Tmem128, which are predicted to face the cytoplasm of the cell (figure 13), were used in this screen because in this approach the investigated proteins have to localize to the nucleus. I observed a direct interaction between the N-teminus of Tmem128 and Arc/Arg3.1 but not between the N-terminus of RIP5 and Arc/Arg3.1 (figure 12). The interaction between Arc/Arg3.1 and the known interaction partner Dynamin2 could also not be confirmed in this assay.

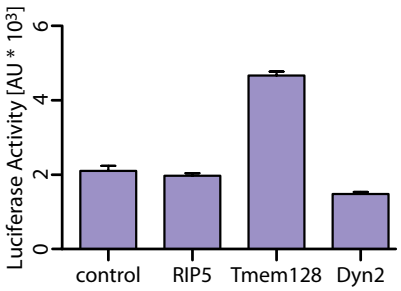

Figure 12: Results of the mammalian-2-hybrid analysis.

Full length Arc/Arg3.1 interacts with the N-terminal domain of Tmem128 but not with the N-terminal domain of RIP5. Dynamin2 also shows no interaction with Arc/Arg3.1 in this experimental setting. Vectors encoding only the transcription factor domains were used as controls.

3.3 Characterization of RIP5 and Tmem128

After having confirmed Tmem128 and, to a lesser degree, RIP5 as interaction partners of Arc/Arg3.1, I set out to investigate these so far completely uncharacterized proteins.

3.3.1 RIP5 and Tmem128 are proteins with multiple transmembrane domains

The National Center for Biotechnology Information (NCBI) lists the proteins under the names "Rab5 interacting protein (RIP5)" and "Transmembrane protein128 (Tmem128)". Based upon homology RIP5 is counted among Rab5 interacting proteins with no experimental evidence for this interaction. RIP5 consists of 135 amino acids, has a predicted molecular weight of about 15kDa and is conserved among eukaryotes, with 40% amino acid identity from rice (*Oryza sativa*) to mouse (*Mus musculus domesticus*) and 71% amino acid identity from zebrafish (*Danio rerio*) to human (*Homo sapiens*) and over 95% identity among higher vertebrates.

Tmem128 contains no conserved protein domains and shows no homologies to other mouse proteins when the entire sequence is analyzed. When only parts of the protein are compared to the mouse proteome, weak homologies to members of the Rab family of small GTPases, to members of the KIF family of molecular motors and to members of the SLC6A subfamily

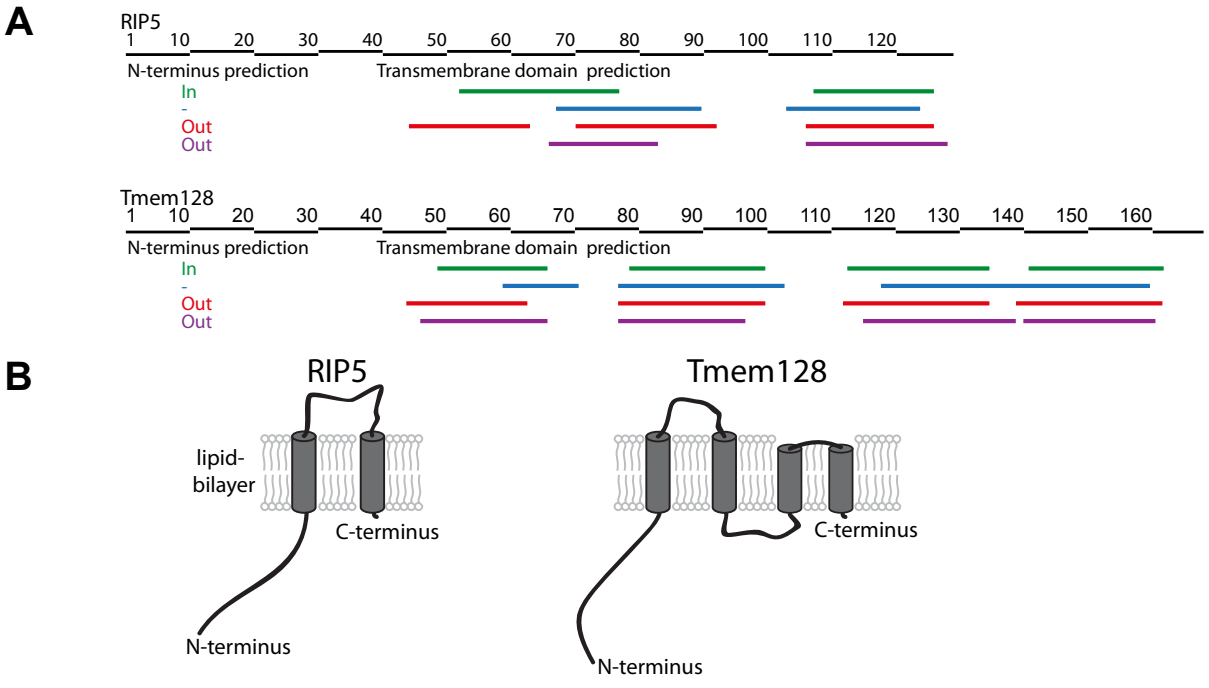

Figure 13: Amino acid composition and transmembrane domain predictions for RIP5 and Tmem128.

(A) RIP5 and Tmem128 are smal proteins of 135 and 165 amino acids respectively. The number and position of transmembrane domains are predicted diferently by different web based bioinformatic programs (green: HMMTOP; blue: psipred; red: TMHMM; purple: TMPred). The orientation of the N-termini (either intracelular or extracellular) are ambigous. (B) Likely secondary structures of RIP5 and Tmem128 within a lipid bilayer.

of transmembrane amino acid transporters are seen. Tmem128 consists of 165 amino acids, has a predicted molecular weight of about 20kDa and is highly conserved among vertebrates, with the N-terminus showing higher variability between lower and higher vertebrates than the transmembrane regions.

I used different web-based bioinformatic tools for an hydrophobicity analysis of the amino acid sequences of both proteins. All but one program predicted two transmembrane domains for RIP5 and all programs predicted four transmembrane domains for Tmem128 (figure 13A). And although the resulting topologies within the membrane are clear for both proteins (figure 13B), the direction in which they are located whithin the membrane is not consistent between the programs. With some programs predicting the N-termini to be intracellular and some programs predicting them to be extracellular. Both Proteins contain short C-termini and moderately long N-termini (45-65 amino acids for RIP5 and 46-68 amino acids for Tmem128), depending on the position of the transmembrane domains.

3.3.2 RIP5 and Tmem128 are localized to the endoplasmic reticulum of secondary cell lines and cultured primary neurons

For general characterization of both proteins, I generated GFP-fusion proteins using standard molecular cloning techniques. Expression of these tagged versions of RIP5 and Tmem128 in the secondary cell lines Hek293 and HeLa revealed a defined subcellular localization (figure 14A and C). Coexpression with fluorescent subcellular markers and counterstaining with

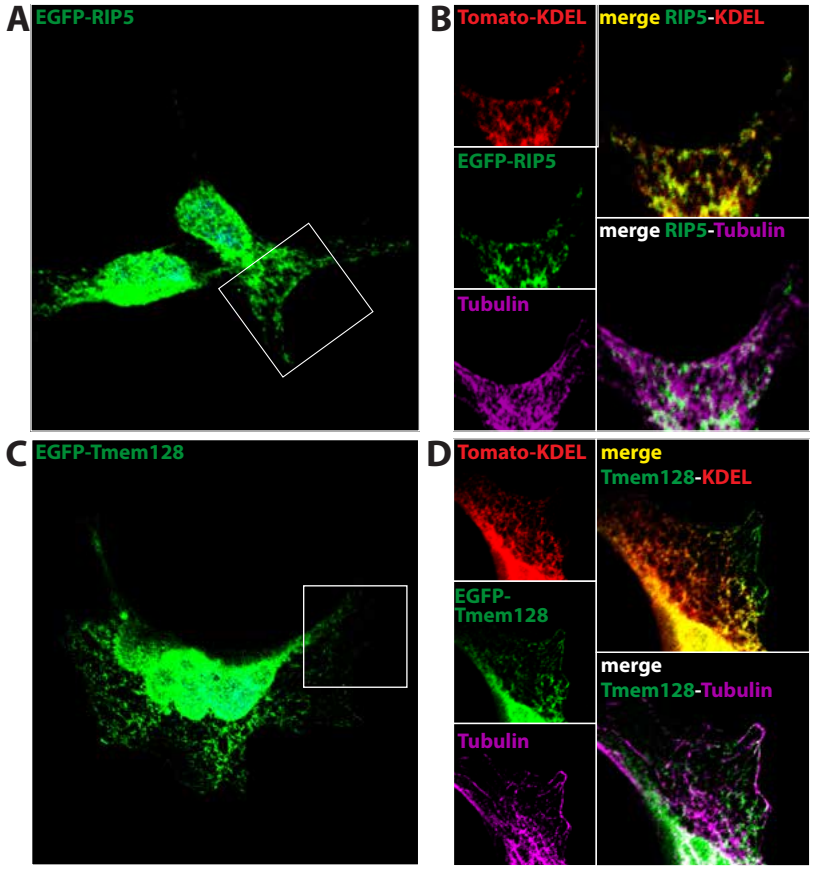

Figure 14: Subcellular localization of RIP5 and Tmem128 in HeLa cells.

Expression of EGFP-tagged RIP5 (A-B) and Tmem128 (C-D) in HeLa cells and colocalization with different marker proteins. Insets were acquired with a higher magnification objective to demonstrate extensive colocalization of EGFP-RIP5 and EGFP-Tmem128 with the ER-marker tdTomato-KDEL but only little colocalization with an antibody against alphaTubulin. All images were obtained using a confocal laser scanning microscope.

antibodies revealed a strong colocalization of RIP5 with an endoplasmic reticulum (ER)-marker (a flourophor framed by an ER localization and retention signal) but not with the intracellular tubulin network, which shows a similar subcellular distribution (figure 14B). Tmem128 also shows colocalization with the ER but also with the tubulin network at the cell periphery (figure 14C and D).

Expression of EGFP tagged RIP5 and Tmem128 in cultured hippocampal neurons showed partial colocalization with the ER marker as well (figure 15 and 16), especially in peripheral dendrites (15E). The observed colocalization of RIP5 and Tmem128 with the ER and with Arc/Arg3.1 was independent of the type of fluorescent protein or tag that was used and its position at the N- or C-terminus of RIP5 and Tmem128. Also, there are a number of classical ER-retention motifs present in the amino acid sequence of RIP5 and Tmem128. The most common is a double or triple Arginine motif in the cytoplasmic tail of an ER-resident transmembrane protein. Both RIP5 (amino acids 5-6) and Tmem128 (amino acids 11-13) possess such a signal in their N-temini. I have mutated both signals to alanins, but I could see no difference in the ER localization. Similarly, I have mutated the double Lysine (amino

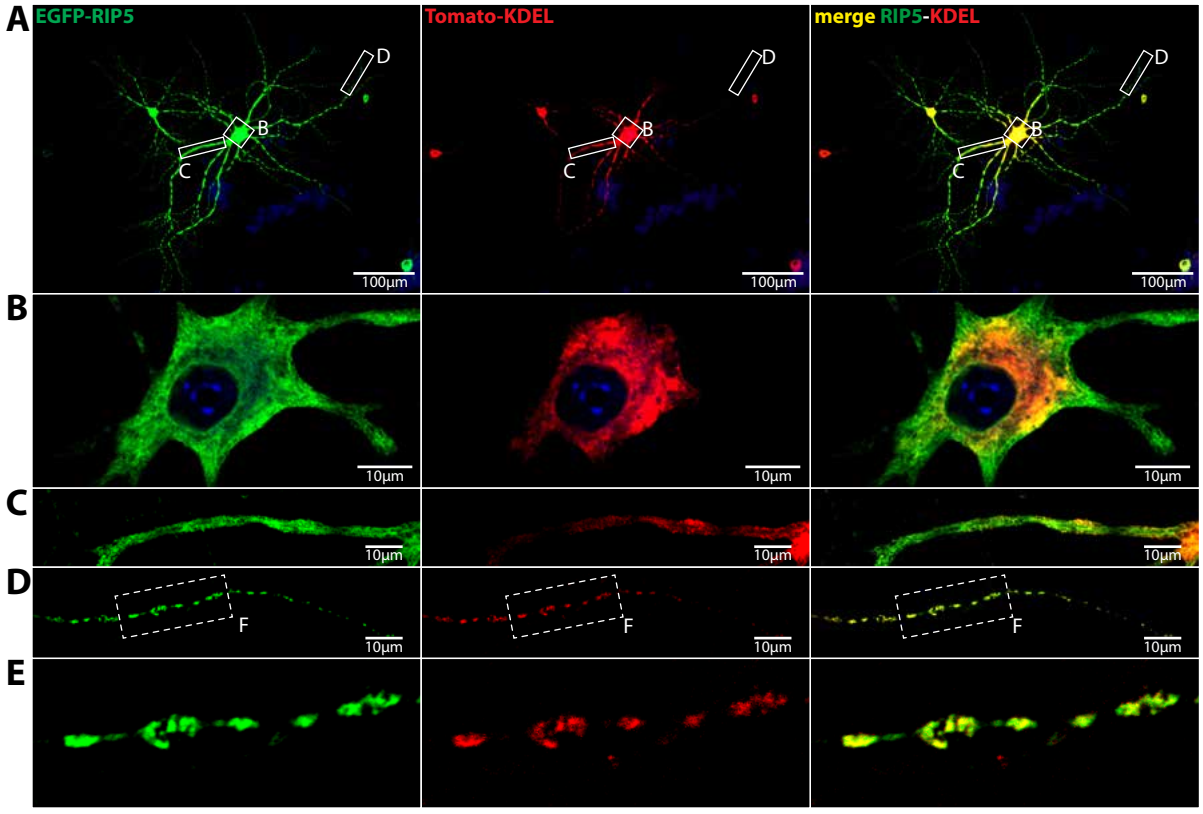

Figure 15: Tmem128 is localized to the neuronal endoplasmic reticulum.

Partial colocalization of EGFP-Tmem128 with a genetically encoded ER-marker in DIV14 cultured hippocampal neurons. (A) was obtained with a 20x objective. The image was overexposed in order to visualize the extensive dendritic and axonal branching and the localization of overexpressed EGFP-Tmem128 and Tomato-KDEL in all neurites. (B-D) are single optical planes of confocal images obtained with a 60x objective. An inset of (D) is magnified in (E).

acids 38-39) present in the N-teminus of Tmem128, just before the beginning of the first transmembrane domain. But again I could see no difference in the localization of EGFP-tagged Tmem128-KA (all data not shown).

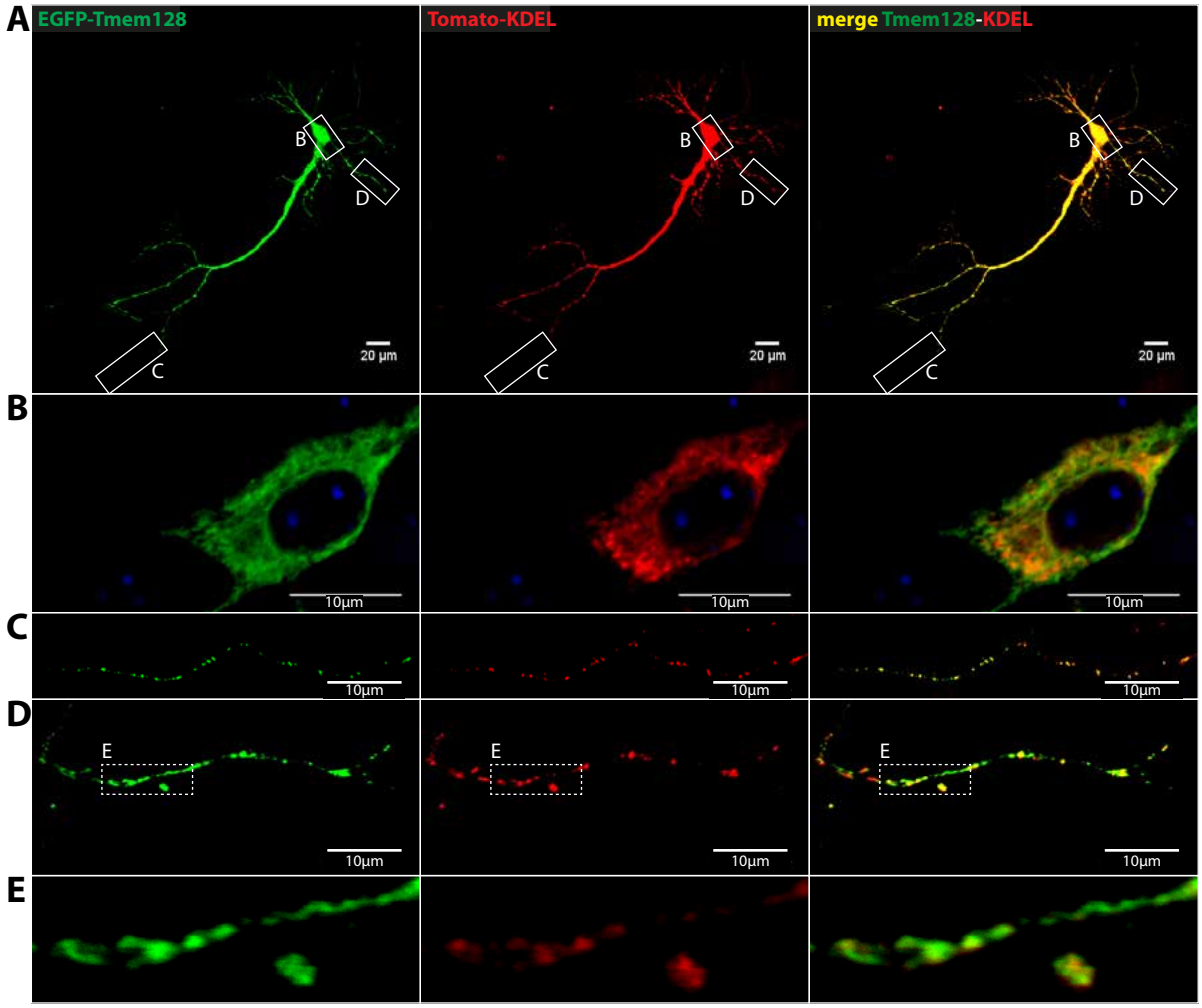

Figure 16: Tmem128 is localized to the neuronal endoplasmic reticulum.

Partial colocalization of EGFP-Tmem128 with a genetically encoded ER-marker in DIV14 cultured hippocampal neurons. (A) was obtained with a 20x objective. The image was overexposed in order to visualize the extensive dendritic and axonal branching and the localization of overexpressed EGFP-Tmem128 and Tomato-KDEL in all neurites. (B-D) are single optical planes of confocal images obtained with a 60x objective. An inset of (D) is magnified in (E).

When expressed in neurons, RIP5 and Tmem128 were localized to the soma and throughout all neurites. Expression of EGFP-RIP5 as well as EGFP-Tmem128 together with a tdTomato labeled Arc/Arg3.1 in neurons lead to extensive colocalization in the soma and neurites of neurons (figure17 and 18). While Arc/Arg3.1 is expressed in a large number of dendritic spines, RIP5 and Tmem128 label only a subset of dendritic spines (figure 17F and 18G).

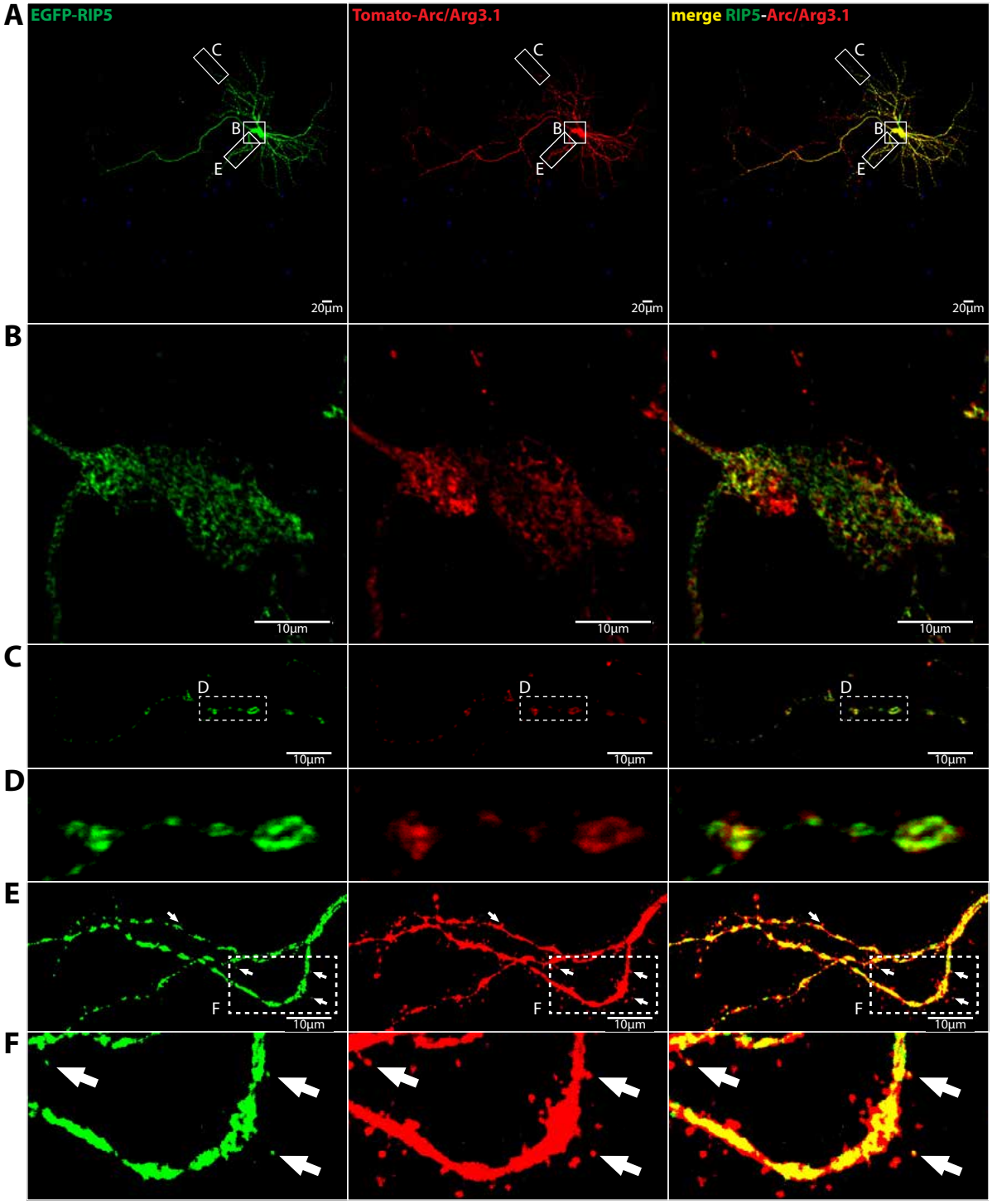

Figure 17: RIP5 and Arc/Arg3.1 colocalize in cultured hippocampal neurons.

Colocalization of EGFP-RIP5 and Tomato-Arc/Arg3.1 in cultured hippocampal neurons at DIV17. (A) was obtained with a 20x objective in a single optical plane and was overexposed in order to visualize the extensive dendritic and axonal branching and the localization of overexpressed EGFP-Tmem128 and Arc/Arg3.1-Tomato in all neurites. (B), (C) and (E) are single optical planes of confocal images obtained with a 60x objective. (D) and (F) are magnifications of (C) and (E). (C and D) partial colocalization of RIP5 and Arc/Arg3.1 in a proximal dendrite. (E and F) overexposed confocal image of a dendritic branch with many spines. Arc/Arg3.1 is localized to a large number of spines and RIP5 is present in a subset of spines (arrows).

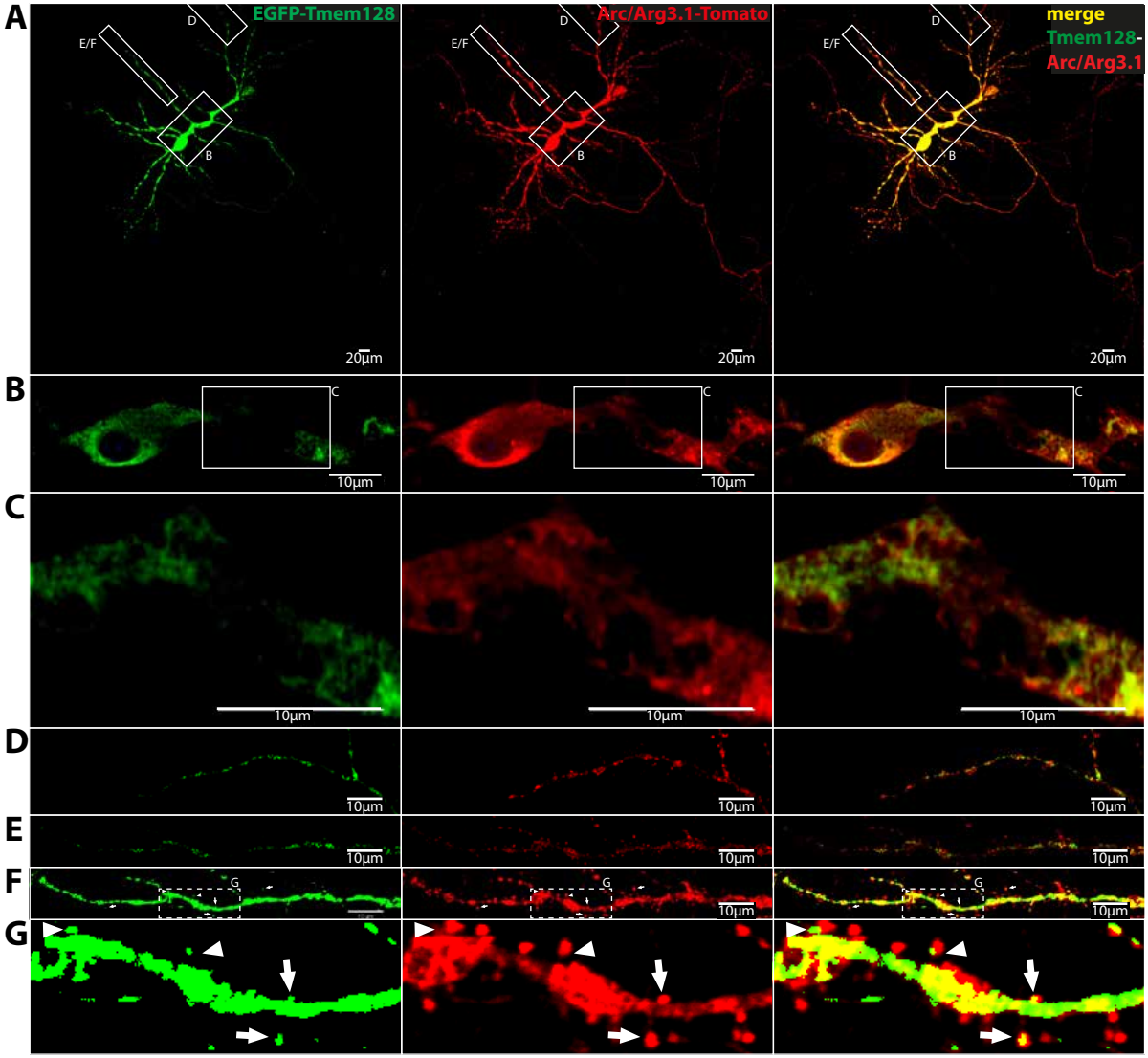

Figure 18: Tmem128 and Arc/Arg3.1 colocalize in cultured hippocampal neurons.

Colocalization of EGFP-Tmem128 and Tomato-Arc/Arg3.1 in cultured hippocampal neurons at DIV17. (A) is a maximum intensity projection of a stack obtained with a 20x objective and was overexposed in order to visualize the extensive dendritic and axonal branching and the localization of overexpressed EGFP-Tmem128 and Arc/Arg3.1-Tomato in all neurites. (B), (D), (E) and (F) are single optical planes of confocal images obtained with a 60x objective. (C) and (G) are magnifications of (B) and (F). (B-E) partial colocalization of Tmem128 and Arc/Arg3.1 in the soma and proximal dendrites. (E and F) overexposed confocal image of a dendritic branch with many spines. Arc/Arg3.1 is localized to a large number of spines and Tmem128 is present in a subset of spine necks (arrowheads) and spine heads (arrows).

3.3.3 RIP5 and Tmem128 face the cytoplasm with their N-termini

As discussed above, the topology of N- and C-termini of RIP5 and Tmem128 was inconsistent among various bioinformatic predictions (figure 13). In order to analyze the orientation of RIP5 and Tmem128 within the membrane of the ER I used a Digitonin based immunocytochemical assay. Digitonin is a non-ionic detergent that solubilizes the cholesterol in cell membranes and preferentially permeabilizes the plasma membrane (figure 19A) (Plutner et al., 1992; Aridor et al., 2004). Full permeabilization was achieved using Saponin, which also is a non-ionic detergent that solubilizes membranes independent of cholesterol and therefore also

permeabilizes internal membranes of the cell. Digitonin can thus be used to determine the topology of transmembrane proteins in intracellular membranes: Only epitopes that face the cytoplasmic side can be detected with antibodies after Digitonin permeabilization (figure 19B and C). I therfore generated versions of RIP5 and Tmem128 containing two different tags: A double Myc-tag, introduced into the loops between the first two transmembrane domains of RIP5 and Tmem128 (position 2 in figure 19B and C), and a quadruple HA-tag attached to he N-terminus of both proteins (position 1 in figure 19B and C). The cytoplasmic protein betaTubulin and the ER resident protein Protein Disulfide Isomerase (PDI) were used as controls for selective permeabilization of the plasma membrane (figure 20). With this setup, N-terminal tags on RIP5 and Tmem128 could be detected independent of the detergent used for permeabilization, indicating that both proteins face the cytoplasm with their N-termini. The tags introduced between the first and second transmembrane domains of RIP5 and Tmem128 could only be detected upon full permeabilization, indicating that they face the lumen of the ER, as is expected with th N-termini facing the cytoplasm. Thus, the structures of RIP5 and Tmem128 can be described as follows: RIP5 contains two transmembrane domains and the N- and C-termini face the cytoplasm. Tmem128 on the other hand contains four transmembrane domains and both termini face the cytoplasm. Whether the second luminal loop of Tmem128 fully enters the lumen of the ER or whether it never leaves the lipid bilayer and represents a reentrant loop, as is suggested by its short length and amino acid composition, cannot ultimately be determined using this method.

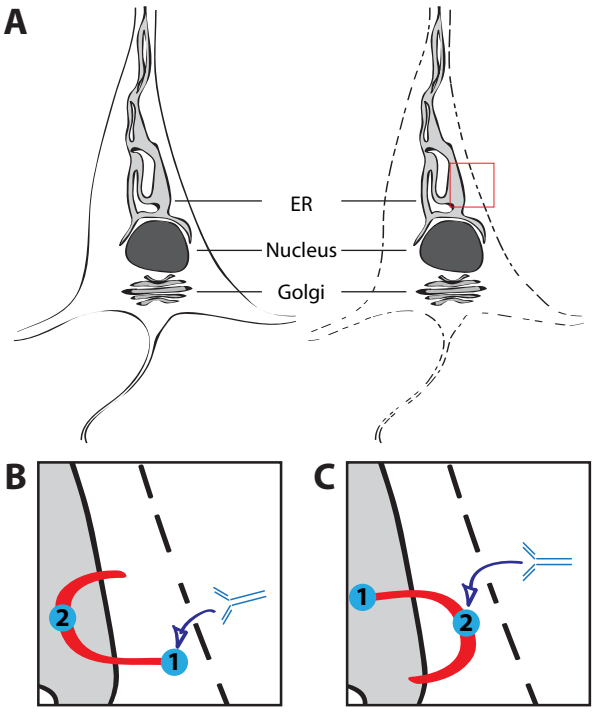

Figure 19: Principle of Digitonin based immunocytochemistry.

(A) Using the non-ionic detergent Digitonin instead of the usual Saponin leads to a selective permeabilization of the plasma membrane, while leaving intracellular membranes mostly intact. (B-C) When using digitonin as a detergent, only tags that face the cytoplasm can be detected either at the terminal ends of the protein of interest (1) or when inserted between two transmembrane domains (2). Thereby the topology of transmembrane proteins can be determined.

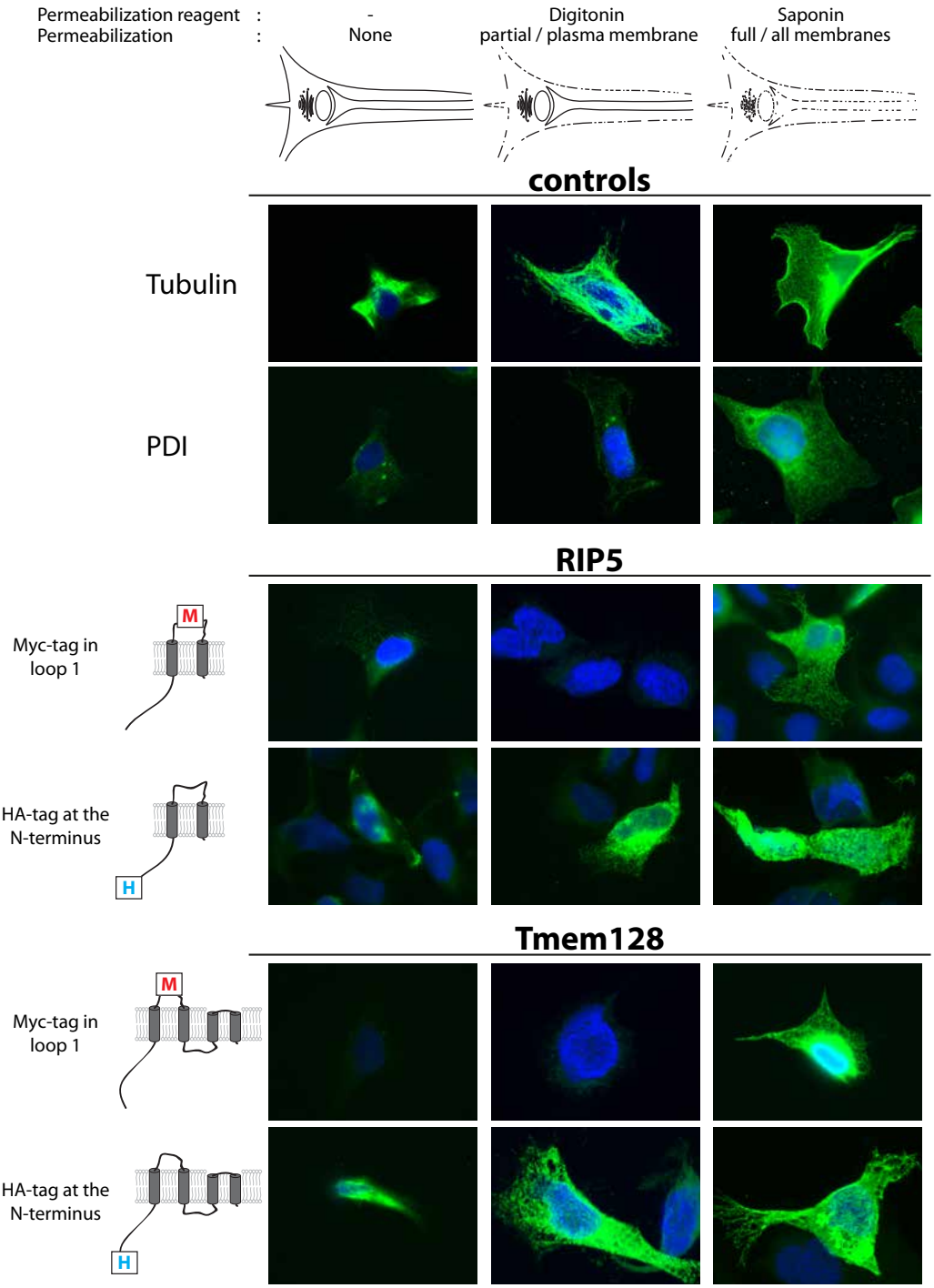

Figure 20: Results from Digitonin Experiment.

HeLa cells transiently transfected with RIP5 and Tmem128 constructs tagged at different positions were fixed with PFA and either not permeabilized, or permeabilized with Digitonin or Saponin. Antibodies against betaTubulin and the ER-resident protein PDI were used as controls for the selective permeabilization of the plasma membrane by Digitonin. N-terminally HA tagged versions of RIP5 and Tmem128 could be detectet with partial, as well as full permeabilization. Myc tags introduced into the loops between the first and second transmembrane domains of RIP5 and Tmem128 could only be detected upon full permeabilization. Nuclei were stained with DAPI and are shown in blue.

3.3.4 RIP5 and Tmem128 are expressed at an early developmental stage and in various tissues and brain regions

After having established the interaction of Arc/Arg3.1 with RIP5 and Tmem128 and the subcellular localization as well as the membrane topology of both proteins, we next analyzed their expression pattern with radioactive in situ hybridizations on coronal sections of mouse brain (figure 21A and C) and on whole embryonic sections (figure 21B and D). On brain sections, the strongest RIP5 signals were detected in the hippocampal formation and the cerebellum. The strongest Tmem128 signals were detected in the hippocampal formation.

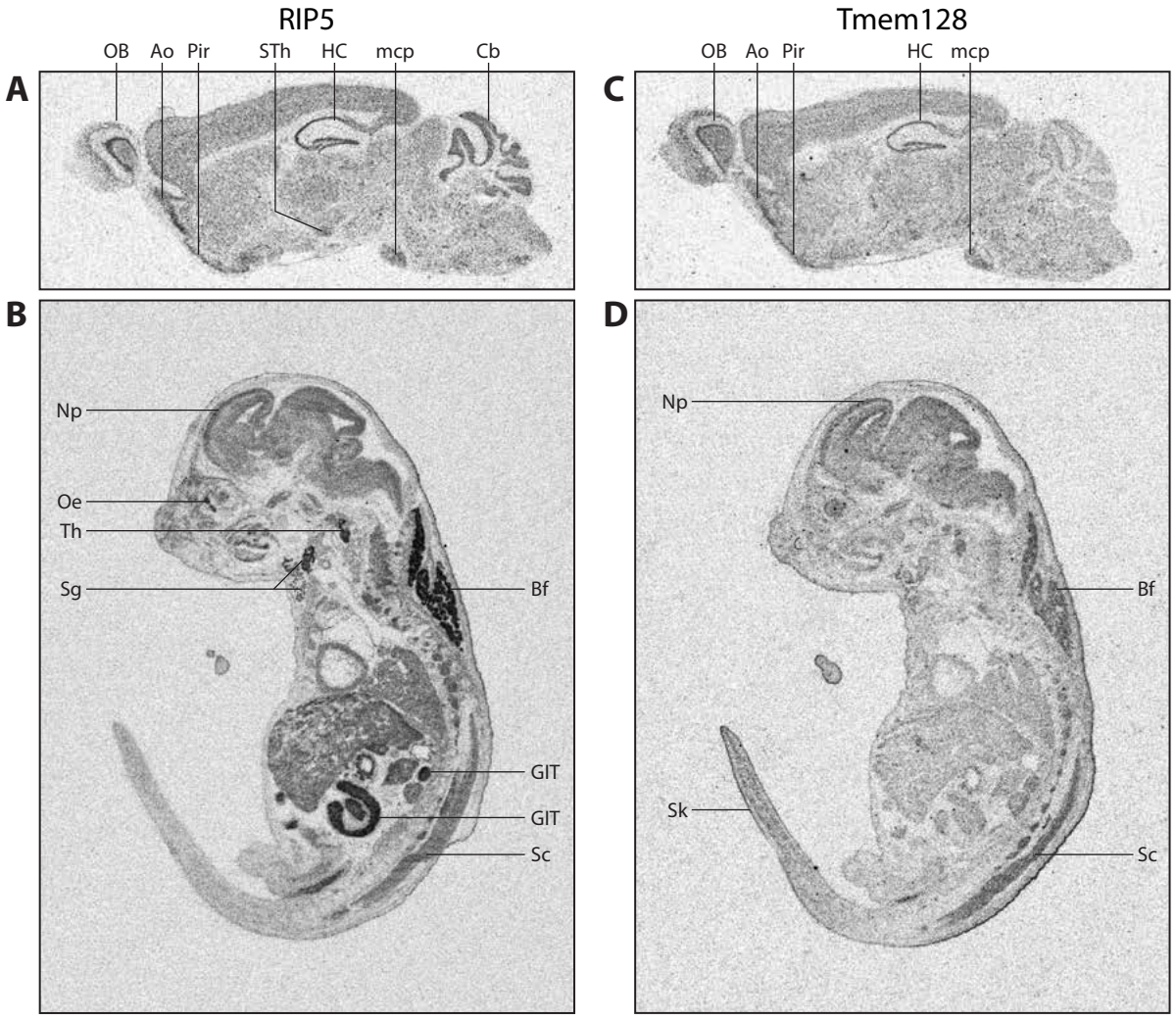

Figure 21: RIP5 and Tmem128 are expressed at low levels in several tissues.

Adult mouse brain and E16.5 embryonic sections were analyzed for RIP5 and Tmem128 expression via radioactive in situ hybridization. Radioactive probes corresponded to RIP5 ORF plus 5' and 3' UTRs and to Tmem128 ORF. (A-B) RIP5 is expressed in the adult mouse brain in the hippocampal formation and the cerebellum and at lower levels in several other brain regions and embryonic tissues. (C-D) Tmem128 is expressed in the adult mouse brain in the hippocampal formation and at lower levels in several other brain regions and embryonic tissues.

Ao = Anterior olfactory nucleus; Bf = deposits of brown (multilocular) fat; Cb = Cerebellum; Cx = Cortex; GIT = Gastrointestinal tract; HC = Hippocampus; mcp = middle cerebellar peduncle; Np = Neopallial cortex; OB = Olfactory Bulb; Oe = Olfactory epithelium; Pir = Piriform cortex; Sc = Spinal chord; Sg = submandibular gland; Sk = Skin; STh = Subthalamic nucleus; Th = Thyroid gland

Both transcripts were also detected at lower levels in other brain regions. On E16.5 mouse embryonic sections, both RIP5 and Tmem128 are expressed in a variety of tissues. Most notably, in addition to neural tissue, RIP5 is also expressed in glandular tissues like the thyroid gland as well as in the gastrointestinal tract (figure 21B) while Tmem128 is expressed in embryonic skin (figure 21D) in addition to neural tissue.

We further analyzed the expression of both genes with radioactively labled northern blots. We used commercially available membranes that were pre-blotted with equal amounts of RNA from either different tissues or different subregions of mouse brain (Gentaur). RIP5 was detected as a single splice variant in all analyzed tissues and brain regions (figure 22A and B arrowheads). Compared to the Actin levels, which were probed as loading control, RIP5 expression levels varied between tissues and highest levels were detectable in liver and kidney. Expression levels in different brain regions on the other hand were of similar strength in all analyzed regions. Tmem128 was detected in two different splice variants in all analyzed tissues (figure 22C arrows) and compared to actin, expression levels varied

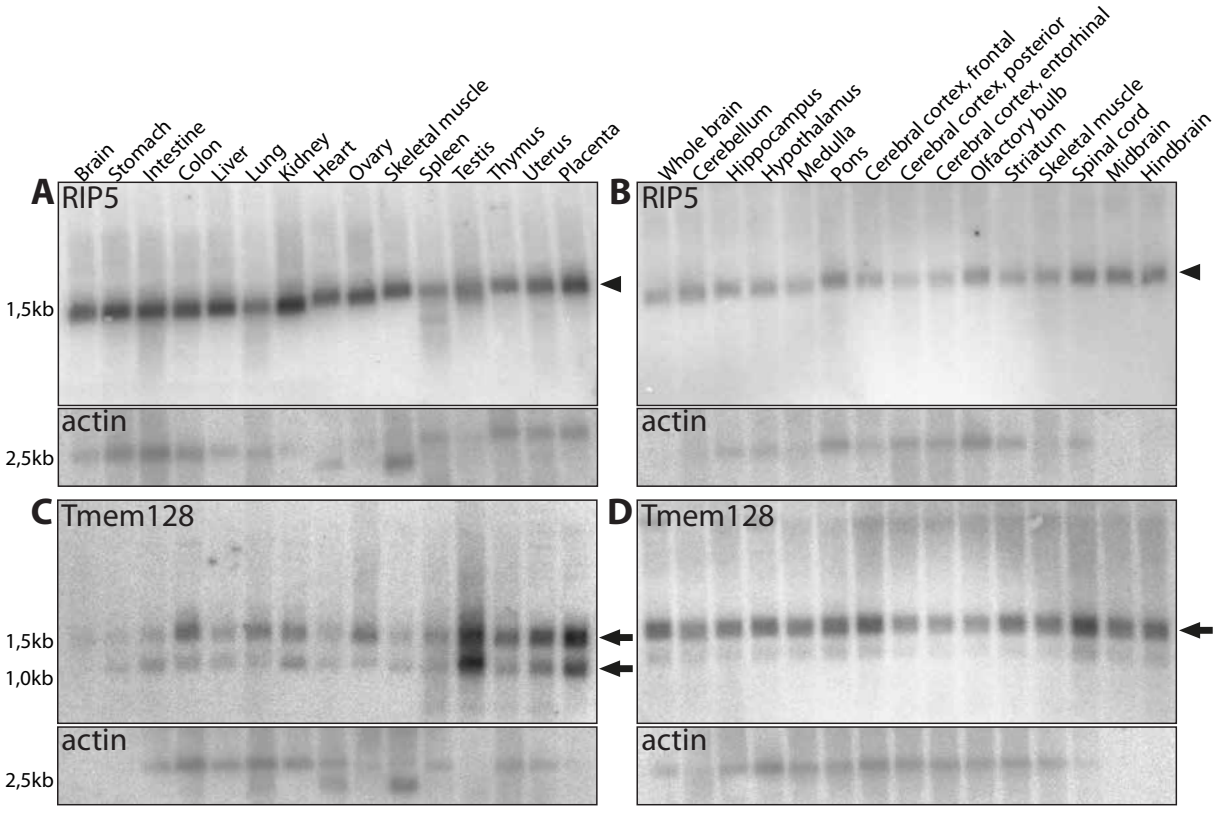

Figure 22: Northern blot analysis of RIP5 and Tmem128 expression levels.

(A, B) Detection of RIP5 mRNA in RNA from different tissues (A) and brain regions (B). A single band was detected at about 1.5kb (arrowheads), expression levels are comparable between different tissues and brain regions. (C, D) Detection of Tmem128 mRNA in RNA from different tissues (C) and brain regions (D). Two distinct bands of 1kb and 1.5kb size were detected at varying levels in diferent tissues (B, arrows), while the higher molecular weight band is predominant in all analyzed brain regions (D, arrow). X-ray films were exposed to the radioactive blots for 11.5 days. To control for blotted RNA amounts, blots were hybridized with a probe against actin.

strongly with a diferent pattern as RIP5. The highest expression levels were detected in testes and uterus. In all analyzed brain regions the longer splice variant, running at the higher molecular weight, was the predominant transcript (figure 22D arrow) and the shorter splice variant was barely detected at all.

3.3.5 RIP5 and Tmem128 mRNAs are not dynamically regulated during differentiation of cultured neurons

Genomic information from publicly available databases (NCBI and ENSEMBLE) was used to determine the gene structure of RIP5 and Tmem128 (figure 23A). RIP5 consists of 5 exons, four of which are protein coding, and most likely gives rise to only one mRNA (figure 23A and B). Tmem128 on the other hand consists of 4 protein coding exons and two exons encoding the 3' untranslated region. These terminal exons are mutually exclusive. Thus the

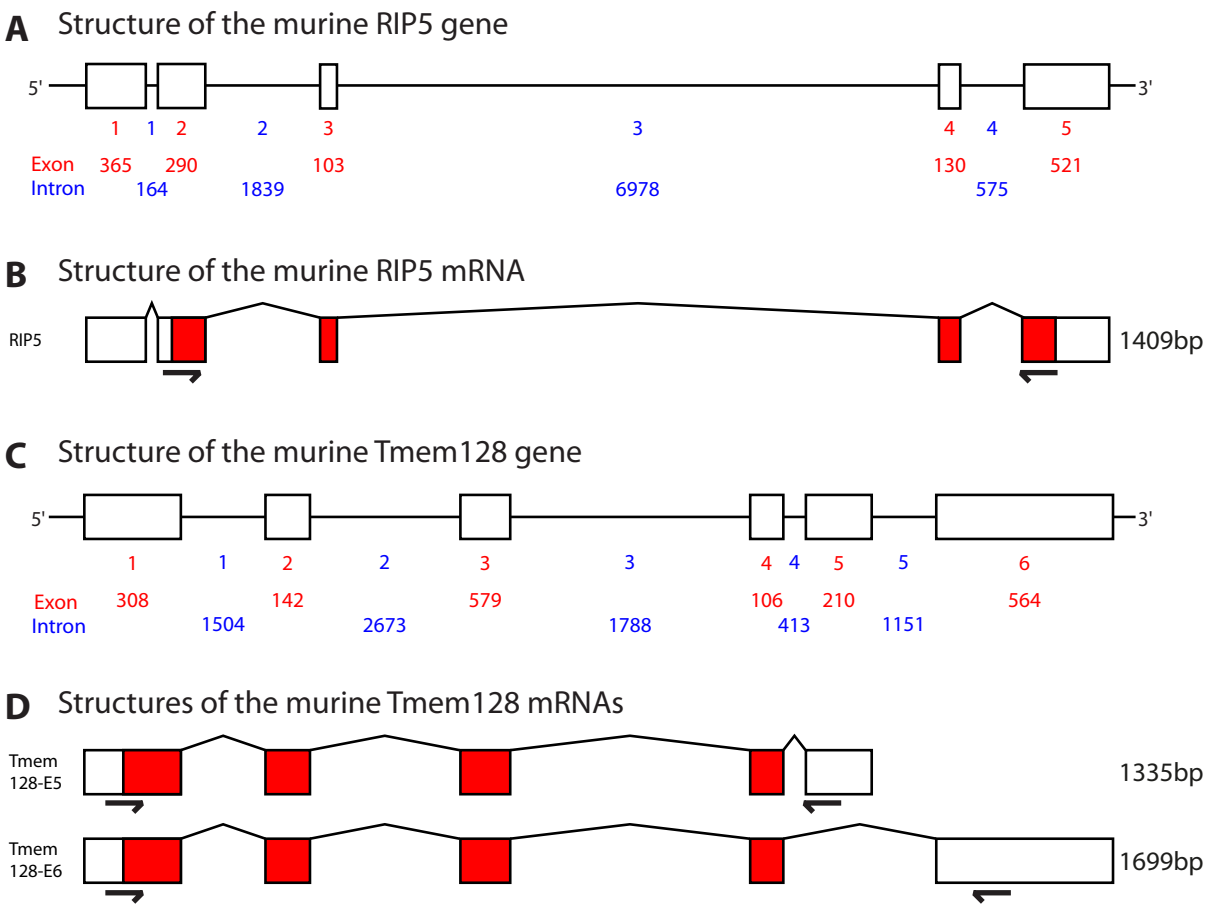

Figure 23: Genomic structure of RIP5 and Tmem128.

(A and C) Schematic representation of the murine gene loci of RIP5 (A) and Tmem128 (C) with exons depicted as boxes and introns depicted as lines. Exons and introns are numbered and sizes are given in base pairs. (B and D) Schematic representation of the spliced mRNA for RIP5 (B) and both possible mRNAs for Tmem128 (D) with red boxes indicating open reading frames. The two splice variants of Tmem128 differ only in their 3' untranslated regions. Arrows mark the priming sites used to detect the different transcripts in neuronal cDNA.

two different mRNAs contain the same coding region but different 3'UTRs (figure 23C and D). One splice variant contains Exon 5 as the 3‘UTR (henceforth referred to as Tmem128-E5) and one contains Exon 6 (henceforth referred to as Tmem128-E6).

Both splice variants contain AAUAAA polyadenylation sigals (figure 24A, arrows) and thus are likely to present real mRNAs. The longer splice variant Tmem128-E6 also contains an ATTTA (figure 24A, asterisk) motif, associated with rapid and regulated RNA turnover (Chen and Shyu, 1995). The situation in the human Tmem128 gene is not as clear, however. According to the NCBI database, only one exon coding for a 3‘UTR is present and it shows homology to the murine Tmem128-E6, including the conserved polyadenylation signals (figure 24B, arrows). The human splice variant even contains three ATTTA motifs (figure 24B, asterisks). But also in the preceding intron 5 an AATAAA polyadenylation signal can be found (figure 24B, arrow), possibly indicating the position of a so far unidentified human Tmem128 exon (figure 24B, dashed box) that corresponds to the murine exon5.

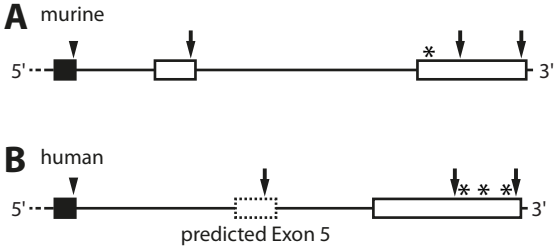

Figure 24: Comparison of murine and human Tmem128 3‘UTRs.

The last protein coding exon (black box) of murine (A) and human (B) Tmem128 are shown, containing the STOP codon (arrowhead). In addition, the exons coding for the 3‘UTRs (white boxes) are depicted. The murine gene contains two confirmed exons 3‘ of the last coding exon (A, solid white boxes), while the human Tmem128 gene contains only one known 3‘UTR exon (B, solid white box) and one putative exon (dashed white box) coding for an aditional 3‘UTR exon. All three known and one predicted 3‘UTR exons contain consensus polyadenylation signals (arrows). The longer, presumably activity regulated, exons contain motifs associated with rapid mRNA turnover (asterisks). The depicted genomic elements are drawn to scale and span roughly 2,4 kb.

mRNA was isolated from primary hippocampal neurons, cultured for 14 days after isolation from mouse brain (14 days *in vitro* - DIV14), and cDNA was generated using a reverse transcriptase. This cDNA was then used as a template for subsequent PCR reactions. The position of the primers that were used to amplify the different fragments are marked in figure 23B and D (arrows). All three transcripts could be detected in the cDNA. Tmem128-E5 and Tmem128-E6 were present in comparable amounts of transcripts (estimated from cycle numbers needed to detect a band), whereas RIP5 was present in larger amounts (figure 25).

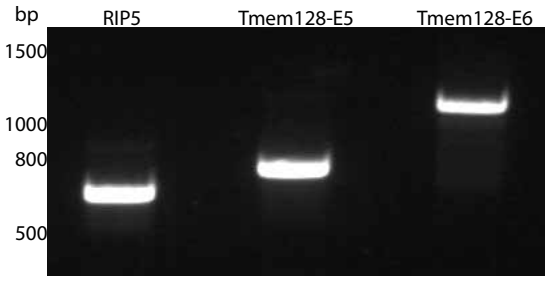

Figure 25: RIP5 and Tmem128 are expressed in cultured neurons.

Semiquantitative reverse transcription PCRs on cDNA isolated from DIV14 cultures of primary hippocampal neurons. Detection of RIP5, Tmem128-E5, and Tmem128-E6. All three predicted mRNAs can be detected.

In order to assess expression levels of RIP5 and Tmem128 during neuronal differentiation, cDNA was generated from mRNA isolated from primary hippocampal neurons that were cultured for different lengths of time (DIV0 to DIV10 and DIV14). All three splice variants of RIP5 and Tmem128 were present in all analyzed samples (figure 26). RIP5 and Tmem128-E5 did not change much in expression relative to the house keeping gene Hypoxanthine-guanine phosphoribosyltranferase (HPRT) from DIV0 (day of isolation of neurons from embryonic mouse brains) to DIV14 (generally accepted to represent "adult" neurons). In comparison, obvious differential expression could be detected for Arc/Arg3.1 which is strongly expressed at DIV0, possibly due to unspecific activation of neurons during the isolation, then detectable from DIV7 on and only at DIV14 again expressed at strong levels. Tmem128-E6 varies in its expression levels at different time points.

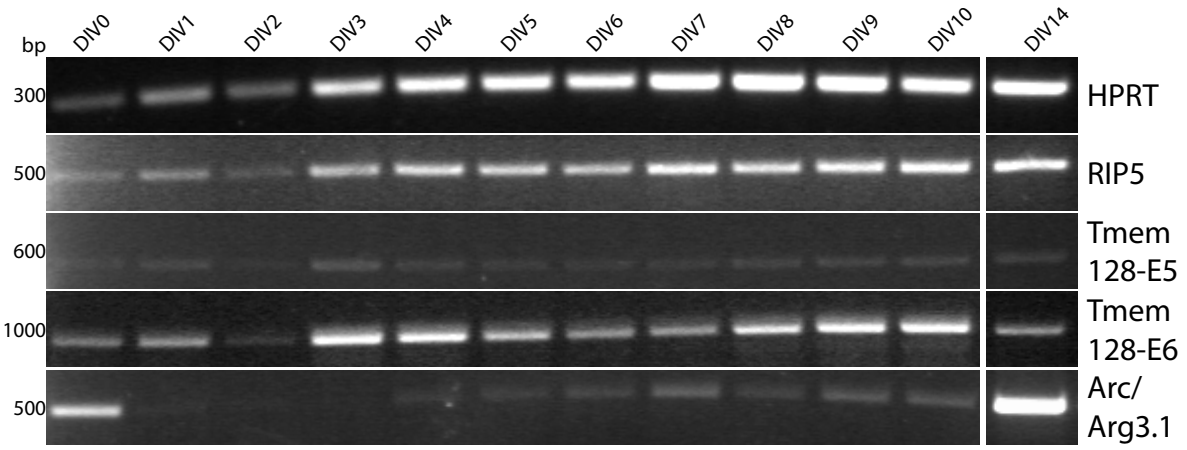

Figure 26: Transcription of RIP5 and Tmem128 in neuronal differentiation.

Semiquantitative reverse transcription PCRs on cDNA isolated from cultures of primary cortical neurons at different developmental stages. The housekeeping gene Hypoxanthine-guanine phosphoribosyltranferase (HPRT) was used as a loading control and shows no obvious regulation by neuronal differentiation. Neither did RIP5 and Tmem128-E5. Arc/Arg3.1 shows strong regulation by neuronal differentiation and is expressed strongest in adult cultures while expression levels of Tmem128-E6 vary during differentiation.

3.3.6 Expression of Tmem128-E6 is induced following synaptic activity in different experimental settings

In a microarray screen performed in our institute (Hermey et al.), differences in the activity regulated transcriptome of the murine hippocampus after kainic acid induced seizures were investigated. In this screen, Tmem128 expression was found to be induced by synaptic activity by about 50% after 4h. Though this induction is relatively modest compared to strongly induced genes like Arc/Arg3.1 or Homer1a, we assessed Tmem128 gene induction after neuronal activity using another paradigm. Cortical as well as hippocampal neurons were cultured to DIV14 and then stimulated with 50mM KCl to induce synaptic activity. At different time points after stimulation mRNA was harvested and transcribed into cDNA, which was then used as template for semiquantitative RT-PCR to determine the relative amounts

of the amplified sequences in each sample. Arc/Arg3.1 was used as a control to confirm that neuronal stimulation had occurred and the housekeeping gene HPRT was used as a non-inducible loading control. We observed an induction of Tmem128-E6 with a similar time-to-peak as Arc/Arg3.1, although overall induction was at a lower level. No such induction was observed for RIP5 and Tmem128-E5 (figure 27).

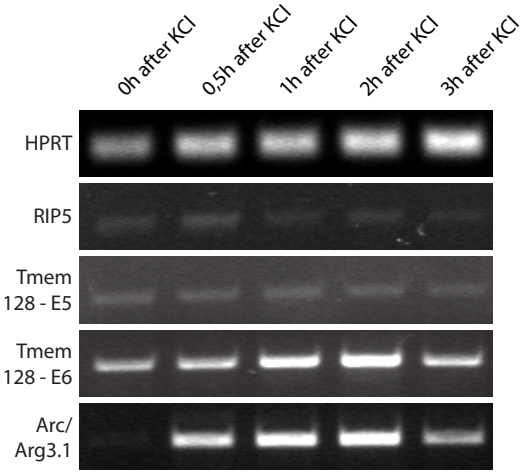

Figure 27: Induction of Tmem128-E6 transcription in cultured neurons by depolarization.

Semiquantitative reverse transcription PCRs on cDNA isolated from adult cultures of primary hippocampal neurons. At DIV14 neuronal activity was induced with KCl. Arc/Arg3.1 serves as a positive control for induction and the house keeping gene Hypoxanthine-guanine phosphoribosyltranferase (HPRT) serves as a negative control for non-induced genes. RIP5 and Tmem128-E5 are equally un-induced while Tmem128-E6 is induced in culture with peak expression at 2h after stimulation.

In order to investigate whether this induction is also seen in an *in vivo* context after strong and concerted network activation, 8 mice in two experimental cohorts were injected with kainic acid and sacrificed at various time points after the onset of the seizure. Frozen sections were hybridized with a probe corresponding to the 3'UTR of Tmem128-E6. A modest but clear induction could be seen in the dentate gyrus 4h after seizure and in CA3/CA1 8h after seizure (figure 28). This Pattern was observed in mice from both groups.

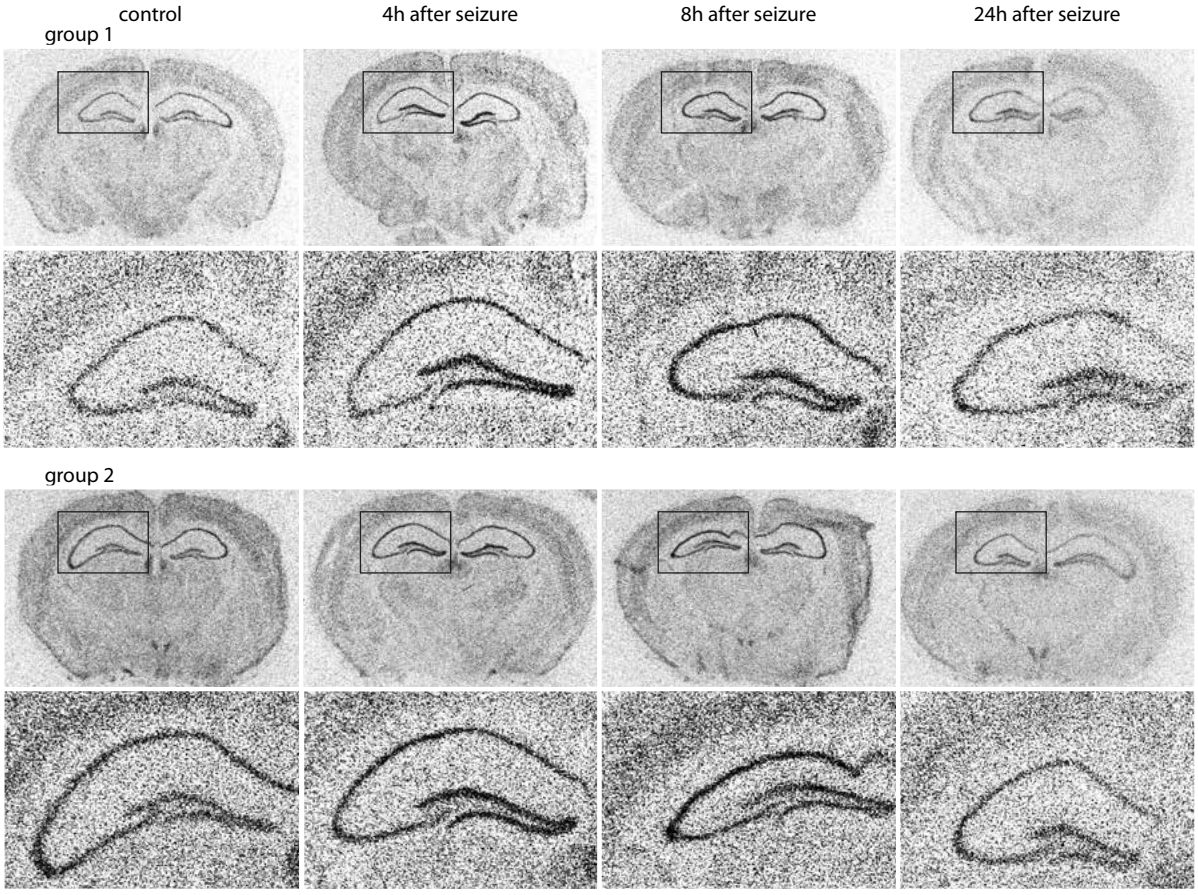

Figure 28: Induction of Tmem128-E6 transcription in mouse brain after kainic acid induced seizures.

Radioactive in situ hybridization probing for Tmem128-E6. After induction of seizures in two groups of mice by i.p. injection of kainic acid, an increase of Tmem128-E6 mRNA-levels can be detected in mouse hippocampi after 4h and 8h.

3.4 Developing tools to study uncharacterized proteins

Since both RIP5 and Tmem128 are so far uncharacterized proteins, no specific tools for the study of both proteins are commercially available. We set out to solve this problem by generating antibodies against both proteins and by generating a conditional knockout mouse line for Tmem128.

3.4.1 Generation of an antibody

N-terminal fusion proteins of GST and the intracellular N-termini of RIP5 and Tmem128 were used as antigens in order to raise antibodies against both proteins in rabbits. For the type of immunization that we performed, only soluble parts of the proteins can be used. The largest soluble parts of RIP5 and Tmem128 are their intracellular N-termini, but since the predicted lengths of these N-termini vary among the hydrophobicity based predictions, we decided to use the smallest common denominator, i.e. the N-terminal 45 and 46 amino acids for RIP5 and Tmem128, respectively. For an immunization with peptides of this size, it is generally recommended to attach the immunogen to a carrier protein. We chose GST (Glutathion-S-Transferase) as a carrier, because it enabled us to purify the proteins before immunization. The preferred position for a GST-tag in our situation would have been the C-terminus of the immunogenic peptides, because it would recapitulate the physiological condition for both proteins with a free N-terminus that could potentially fold similar to the physiological situation in cells. Unfortunately, C-terminal GST fusion proteins are not very stable and rarely used. Only one commercially available plasmid (pDEST24 by Invitrogen) leads to a C-terminal fusion of GST. We used this plasmid and tested expression of RIP5-Nterminus-GST as well as Tmem128-N-terminus-GST for the generation of the immunogenic proteins and later again for the affinity purification of the antibodies (see bachelor thesis by Navid Memarnia), but the expression levels of these constructs in *E.coli* were far too low for the generation of immunogenic proteins. In contrast, the expression of N-terminal fusion proteins was very successful and so we decided to use these proteins for the immunization. The two purified fusion proteins were used for immunization of two rabbits each (rabbits 1327 and 1328 for RIP5 and rabbits 1329 and 1330 for Tmem128) and table 25 depicts the schedule for antibody production with boosts (injections of antigen) and bleeds (harvest of serum).

Table 25: Schedule for an antibody generation protocol at Eurogentec with dates for the immunization of rabbits and the harvest of antisera.

Immunisation and boosts (400µg per injection)	**day 1**	**day 15**	**day 29**		**day 57**	**day 85**		**day 110**	
Bleeds	**day 1** (Preimmune)			**day 38** (small bleed 2ml)			**day 101** (large bleed 20ml)		**day 137** (final bleed 40ml)

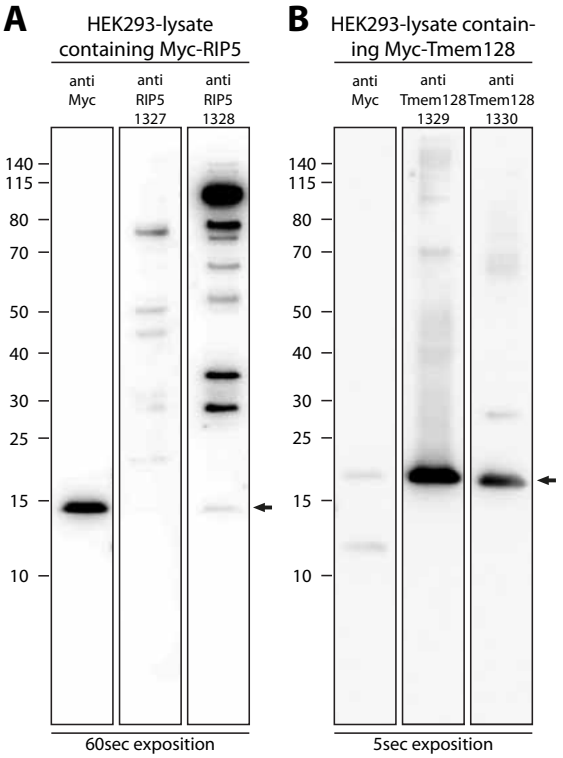

Figure 29: Western blot analysis of final bleed antisera against RIP5 and Tmem128 on lysates of transfected Hek293 cells.

Detection of Myc-RIP5 and Myc-Tmem128 in lysates of transiently transfected Hek293 cells with western blot. Each lane was probed with a different antibody. (A) Myc-RIP5 is clearly detected at ~15kDa with an antiMyc antibody but the final bleed of rabbit 1327 shows no clear signal. Serum 1328 shows an extremely weak signal compared to unspecific bands (arrow). (B) Both final bleed antisera against Tmem128 show a clear signal at the expected molecular weight of ~20kDa (arrow) and only few unspecific bands.

I analyzed samples of each bleed in an immunocytochemical approach on Hek293 cells expressing EGFP-tagged versions of RIP5 and Tmem128 and in western blot on lysates of Hek293 cells overexpressing variants of RIP5 and Tmem128 containing a double-Myc tag inserted between the first two transmembrane domains and thereby leaving the N-termini of both proteins free for antibody detection. On lysates of cells, vastly overexpressing RIP5, only a weak signal was observed in western blot analysis (figure 29 A, arrow) and I could not detect a specific signal colocalizing with EGFP-RIP5 in cells using this antiserum (figure

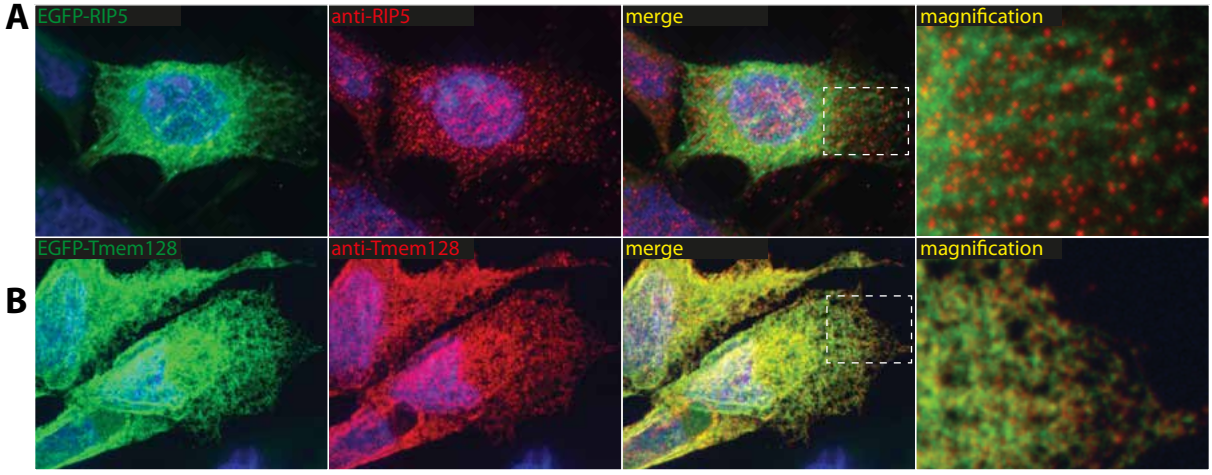

Figure 30: Immunocytochemical analysis of final bleed antisera against RIP5 and Tmem128 on transfected HeLa cells.

Representative fluorescent images taken from transiently transfected HeLa cells, stained with final bleed sera raised against RIP5 (A) and Tmem128 (B). The merge and magnification show the clear colocalisation of the EGFP and antibody signals for Tmem128 but no colocalisation of specific signals for RIP5.

30 A, merge and magnification). Therefore I conclude that the immunization of rabbits against RIP5 failed to generate specific antibodies. And even though the antibodies raised against Tmem128 showed much stronger signals on western blots (figure 29 B, arrow) and generated a signal that strongly colocalized with fluorescently labeled Tmem128 (figure 30 B, merge and magnification), a more sensitive antibody would be preferable for experiments with low amounts of antigens under physiological conditions. Therefore the topic of the bachelor thesis of Mr. Navid Memarnia was the affinity purification of the most promising batch of serum (final bleed) of both antibodies on columns of the antigenic proteins and the analysis of the purification procedure using different biochemical and cell biological assays. This resulted in a marked increase in specificity of anti-Tmem128 antibodies, though unfortunately no improvement could be detected for anti-RIP5 antibodies (see bachelor thesis Memarnia). Due to a lack of tools for the analysis of RIP5, all further investigations focused only on Tmem128.

3.4.2 Generation of a Tmem128 knockout mouse line

For the generation of a knockout mouse line for Tmem128, three different cell clones of mouse embryonic stem cells (ES cells), were ordered from the international Knockout Mouse Project KOMP (KOMP-internal project number KO-1847, Targeting Project CSD36445). These cells were derived from the C57Bl/6N strain and targeted with a promoter-driven knockout first construct directed against Tmem128. The vector construct that was inserted into these ES cells by electroporation, integrated into the wild type Tmem128 gene locus by homologous recombination (figure 31A), and thereby generated a knockout (figure 31B). The targeting construct replaces the wild type gene from 5070bp 5‘ of exon1 to 4205bp 3‘ of exon3. The newly inserted DNA contains several elements including a splice acceptor site (En2 SA) which forces the cell to splice exon1 of Tmem128 to the targeting cassette and thereby generating a nonsense construct, as well as a lacZ coding element for the analysis of Tmem128 promoter activity. The cassette also contains a neomycin resistance gene for selection of correctly inserted ES cells as well as two FRT recognition sites for the FLP recombinase. Exon2 is flanked by loxP sites, thus generating a floxed version of exon2, i.e. a version of exon2 that is flanked on both sides by loxP recognition sites for the Cre recombinase. The cassette therefore contains the possibility for a conditional knockout allele by breeding to a mouse line expressing the FLP recombinase. The resulting gene locus (figure 31C) differs from the wild type locus only in the two recognition sites for the Cre recombinase flanking exon2. Since both loxP sites are located to intronic regions of the Tmem128 gene, the gene is spliced correctly and the wild type protein is expressed. By subsequent breeding to a mouse line that carries the Cre recombinase under a tissue or developmentally specific promoter, exon2 of Tmem128 is excised (figure 31D) and a conditional knockout is generated. Since the resulting protein only contains the sequence

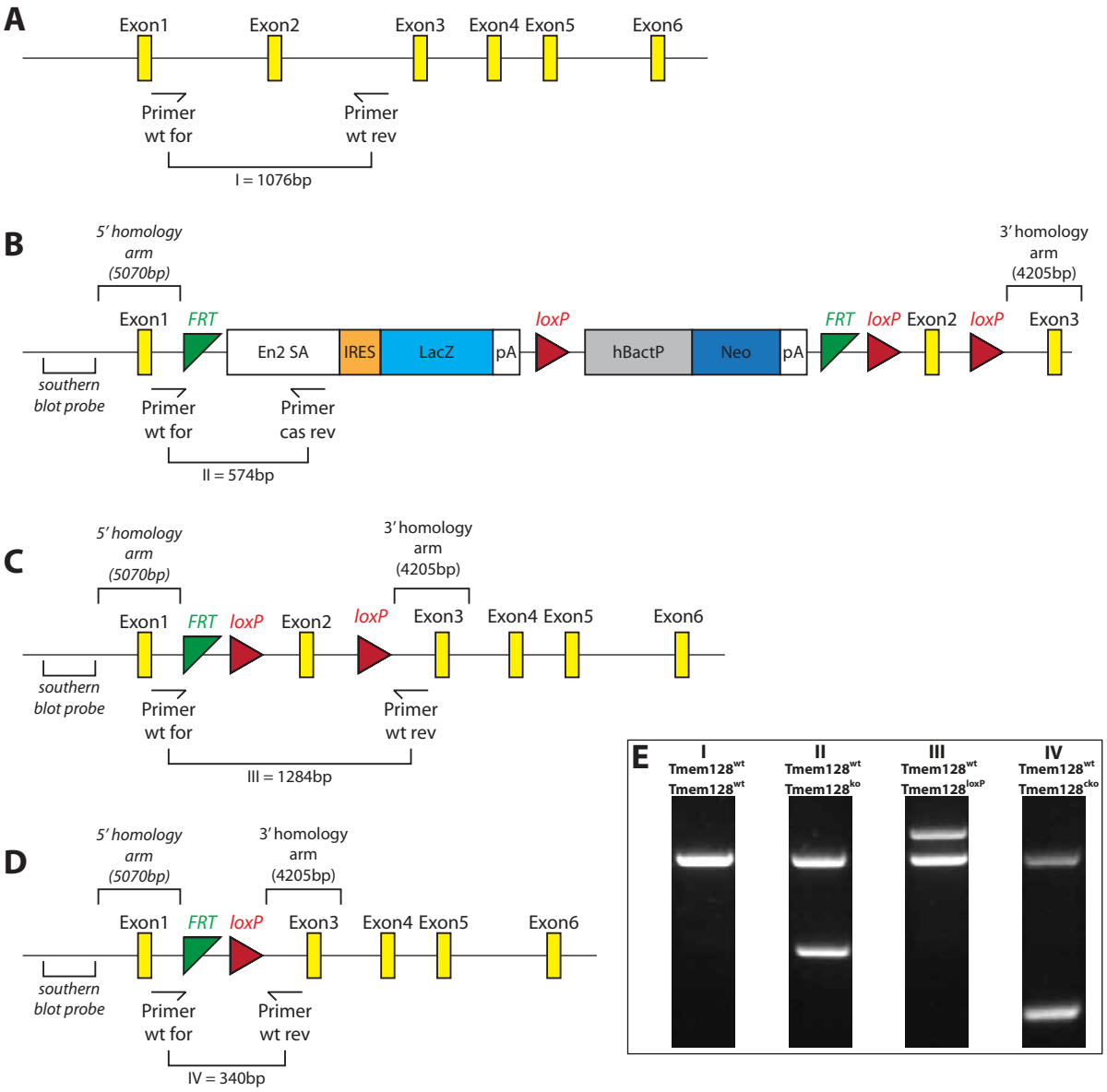

Figure 31: Schematic representation of the Tmem128 gene locus in the wildtype and knockout conditions.

(A) Wild type gene locus. (B) Constitutive knockout situation with the targeting cassette inserted between Exon1 and Exon3. The knockout is achieved by forcing the cell to splice the En2 splice acceptor site to Exon1 and thereby generating a nonsense transcript which is degraded. (C) After crossing the constitutive knockout mice with animals expressing the FLP recombinase, the sequence flanked by FRT is removed and Exon2 remains flanked by loxP sites, thereby generating a conditional knockout animal. The excision of Exon2, and the subsequent generation of a conditional knockout transcript (D), is now only dependent on the presence of the Cre recombinase. Positions of genotyping primers and resulting fragments are indicated in (A-D). (E) representative agarose gel for a homozygous wild type animal (I) and heterozygous transgenic animals (II-IV).

FRT: Recognition site for the Flip recombinase; En2SA: Splice acceptor site of the murine Engrailed2 exon 2; IRES: Internal ribosome entry site; LacZ: E.coli *gene coding for beta-galactosidase; SV40 polyadenylation signal; loxP: Recognition site for the Cre recombinase; hBactP: human beta-Actin Promotor.*

coded for by exon1 and a frameshift sequence from intron2, it is expected to be degraded rapidly. Figure 31 also depicts the positions of the primers used for the genotyping PCRs and representative PCR results (figure 31E).

Three targeted ES-cell clones (clones A04, D05 and E04) were thawed and expanded. Clone D05 did not expand successfully and was not used further. Southern blot analysis from genomic DNA of clones A04 and E04 showed successful insertion of the targeting construct into the correct genomic environment (figure 32A and B). Mice of three different genotypes that resulted from blastocyst injection of these ES cell clones, were also genotyped correctly by southern blot (figure 32C). The probe used for southern blot analysis corresponded to a sequence immediately upstream of the 5'-homology arm of the targeting construct (figure 32B) and the detected double bands in the ES-cells and the heterozygous animal indicate that the construct was inserted only once into the correct genetic environment.

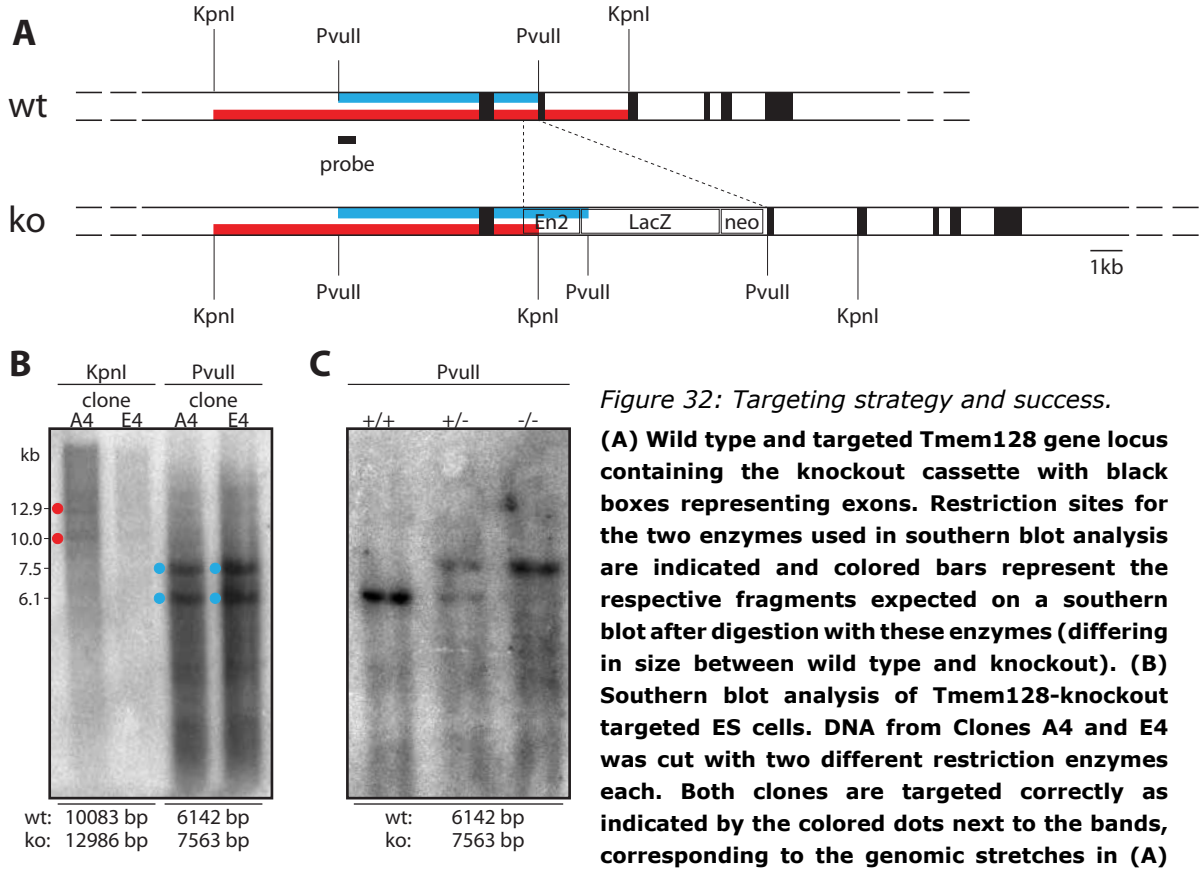

Figure 32: Targeting strategy and success.

(A) Wild type and targeted Tmem128 gene locus containing the knockout cassette with black boxes representing exons. Restriction sites for the two enzymes used in southern blot analysis are indicated and colored bars represent the respective fragments expected on a southern blot after digestion with these enzymes (differing in size between wild type and knockout). (B) Southern blot analysis of Tmem128-knockout targeted ES cells. DNA from Clones A4 and E4 was cut with two different restriction enzymes each. Both clones are targeted correctly as indicated by the colored dots next to the bands, corresponding to the genomic stretches in (A) that are cut out by the restriction enzymes. (C) Southern blot analysis of three mice of the F3 generation of Tmem128 knockout mice.

Resulting chimeric litters (figure 33) were mated with wild type C57Bl/6J mice and the litters of these matings were checked for the targeting cassette via genotyping PCR. Litters of one chimeric animal (derived from clone E04) were genotyped positively for the Tmem128 knockout-cassette, which means that germline transmission of the transgenic construct was achieved in this animal. These heterozygous constitutive knockout animals with inserted targeting cassette (Tmem128wt/Tmem128ko) were used for different further matings (figure 34). Heterozygous mating pairs were used to breed homozygous constitutive

Figure 33: Successful targeting and germline transmission of the mutated Tmem128 locus.

Representative photograph of chimeric animals with different degrees of ES-cell integration indicated by the amount of black fur color.

knockout animals Tmem128ko/Tmem128ko (figure 34A) in order to check overall viability, fertility and gross morphological phenotype. Homozygous knockout animals were used for terminated matings to generate embryos for primary neuronal cell culture. Heterozygous animals were mated with animals heterozygous for the recombinase FLP1 ("flip-deleter-mice") in order to excise a large part of the targeting cassette and thereby generate heterozygous conditional knockout animals (Tmem128wt/Tmem128flox) animals where exon2 is flanked by loxP sites (recognition sites for the Cre recombinase) (figure 34B). Heterozygous conditional knockout animals were then mated with animals ubiquitously expressing the Cre recombinase (Cre-deleter) in order to excise exon2 and thereby generating heterozygous ubiquitous Tmem128 knockout animals (Tmem128wt/Tmem128cko) (figure 34C).

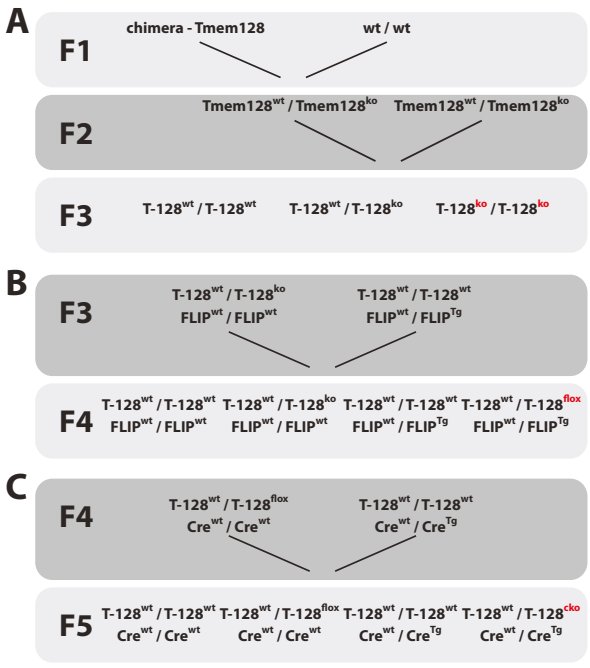

Figure 34: Breeding of Tmem128 knockout animals.

Overview of the mating strategy employed for breeding of the Tmem128 knckout mouse line. (A) Strategy to breed constitutive knockout animals (Tmem128^{ko}/Tmem128^{ko}). (B-C) Strategies to breed (B) floxed animals (Tmem128^{flox}/Tmem128^{flox}) or (C) conditional knockout animals (Tmem128^{cko}/ Tmem128^{cko}).

The distribution of genotypes in the F3 generation of constitutive knockout animals (figure 34A) was in accordance with Mendel's laws of inheritance (figure 35) but the overall breeding efficiency was rather low. Homozygous animals of the F3 generation (Tmem128ko/Tmem128ko) represent the first generation of constitutive knockout mice. These animals were used for the initial characterization of the Tmem128-knockout phenotype.

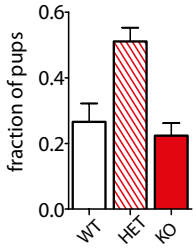

Figure 35: Offspring in the F3 generation of Tmem218 constitutive knockout animals.

The distribution of genotypes in the F3 generation is in accordance with Mendelian laws of inheritance. n=155

3.5 Characterization of Tmem128 knockout mice

3.5.1 Tmem128 knockout animals develop normally

In a first set of analyses the knockout animals were compared to wild-type animals based on weight gain during development and appearance in adulthood. Male and female pups develop differently, but no difference can be seen between the genotypes (figure 36A). It is not possible to differentiate knockout from wild-type animals on first glance (figure 36B). They are completely normal in appearance and overall behavior.

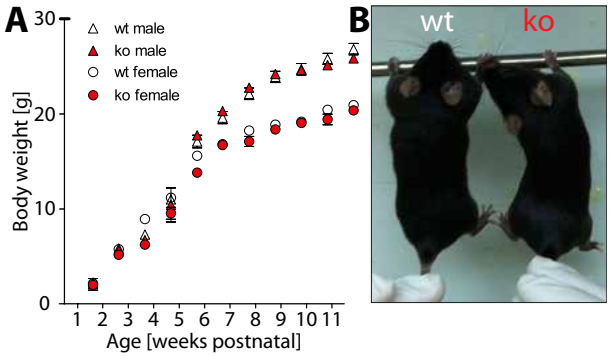

Figure 36: Development and appearance of Tmem128 knockout mice compared to wild type littermates.

(A) Weight gain during pup development of wild types and knockouts of the F3 generation of Tmem128 knockout mice separated by gender. (B) Representative photograph of constitutive knockout and a wild type littermate.

Although the antibody generated by us (3.4.1) detects a large number of bands on western blot of whole brain lysates, I could use brain lysates of Tmem128 knockout animals to identify the correct band (figure 37A). I could thus show on the one hand that the antibody detects native Tmem128 and that the knockout was successful on the protein level. I did not find differences in Tmem128 protein levels between male and female wild type animals and when I analyzed only that part of the western blot membrane, where Tmem128 is expected, the band detected in heterozygous animals is much weaker compared to wild type, indicating that there is no dosis compensation (figure 37B).

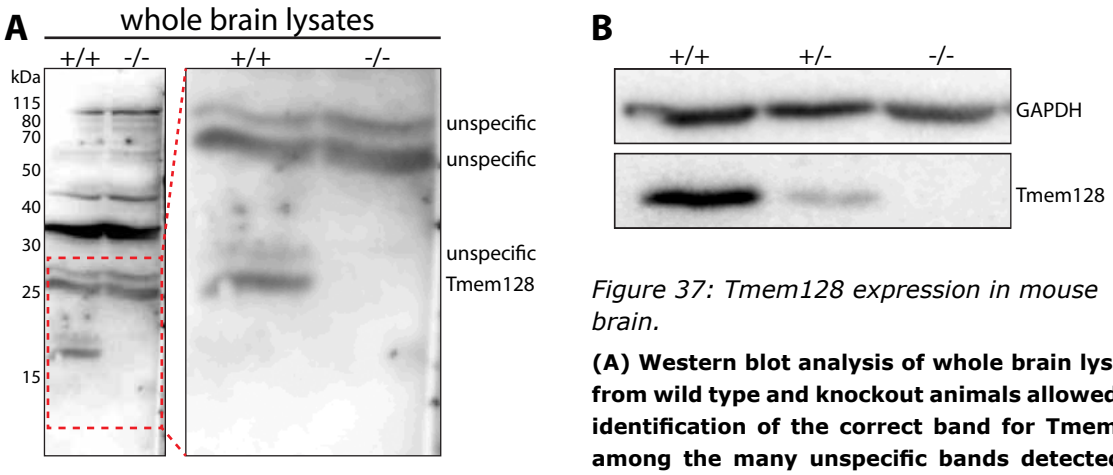

Figure 37: Tmem128 expression in mouse brain.

(A) Western blot analysis of whole brain lysates from wild type and knockout animals allowed the identification of the correct band for Tmem128 among the many unspecific bands detected by the antibody. (B) Comparison of wild type, heterozygous and knockout animals showing the lack of dosis compensation. GAPDH was used as loading control.

3.5.2 Tmem128 knockout animals show no abberations in brain morphology

For an analysis of macroscopic and microscopic brain morphology in Tmem128 knockout animals, PFA fixed brains were measured (figure 38A and B). I observed no macroscopic differences in size or structure and the brain weight of unfixed brains was not significantly different between genotypes (figure 38C).

For a microscopic analysis I subjected the brains to DAPI staining and immunohistochemical staining. I did not observe obvious differences in the distribution of DAPI stained nuclei in regions of special interest like the retrosplenial cortex (figure 39A - representative for the entire cortex) and the hippocampus (figure 39B). For a detailed quantification of nuclei in the cortex, images were processed: After selection of a region of interest (ROI) (figure 39C), a threshold for intensity values was set (figure 39D) and a watershed algorithm was used to isolate individual nuclei or groups of nuclei (figure 39E). The identified signals were then counted automatically. Again, I could not see significant differences in analyzed nuclei number in the retrosplenial cortex (figure 39F). Since the knockout of an ER transmembrane protein could potentially alter the morphology of the ER (e.g. the subcellular distribution, the branching or the curvature of ER tubules), the ER resident protein GPR78/BiP was stained to investigate ER morphology and distribution in the cortex and hippocampus of Tmem128 knockout mice. The overall distribution of ER in the cortex (figure 40A), as well as areas

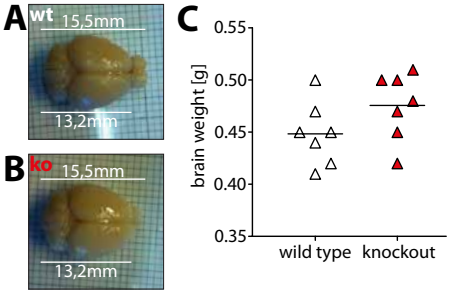

Figure 38: Morphological comparison of brains.

Representative photographs of PFA fixed brains from wild type (A) and knockout (B) littermate animals display no obvious morphological or size differences. (C) Brain weights are not significantly different between animals of different genotypes.

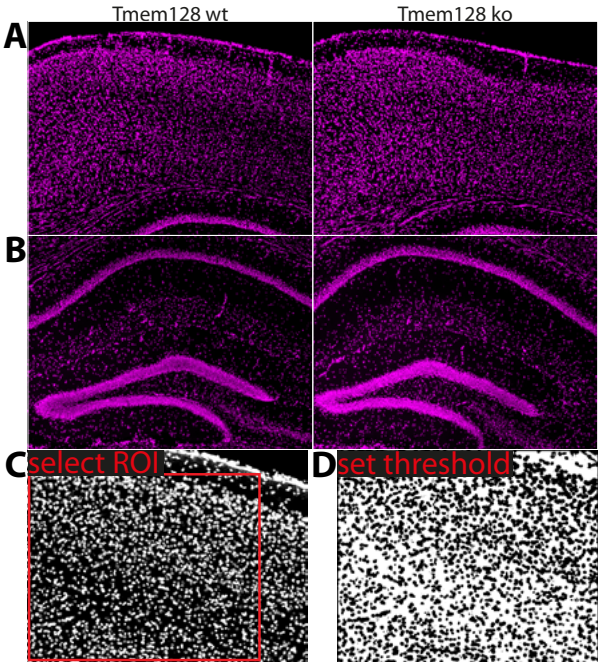

Figure 39: Analysis of cell density.

40µm thick PFA-fixed coronal sections showing either the cortex (A) or the hippocampus (dentate gyrus and CA1) (B) from wild type and knockout animals. (C)-(E) Image procesing for automated nuclei counting. Images were cropped to a cortical area of defined size (C), thresholded (D) and subjected to a watershed algorithm (E). (F) Nuclei per mm² of cortical tissue were quantified in 12 sections of each genotype in two pairs of animals. One representative example is shown.

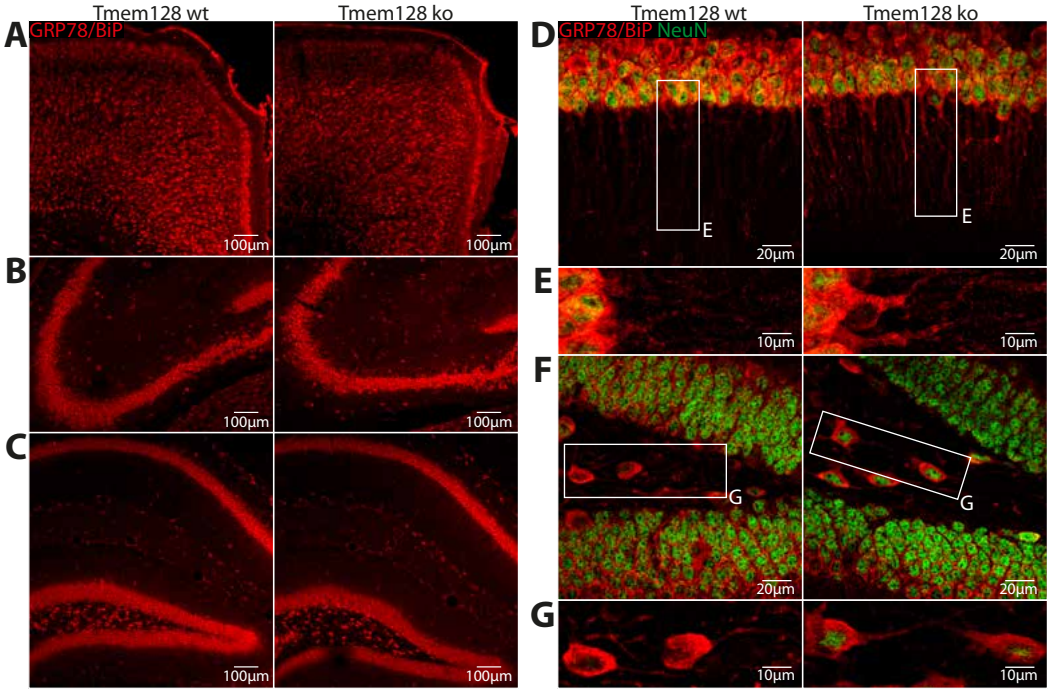

Figure 40: Microscopic analysis of the endoplasmic reticulum marker GRP78/BiP.

The morphology of the ER, as revealed by the ER resident protein GRP78/BiP (red), is not different in neurons of Tmem128 knockout animals compared to wild type. Panels show representative examples of cortex (A), CA3 (B) or DG/CA1 (C). Cellular distribution of neuronal ER (BiP-stained) is shown for CA1 (D-E) and dentate gyrus (F-G).

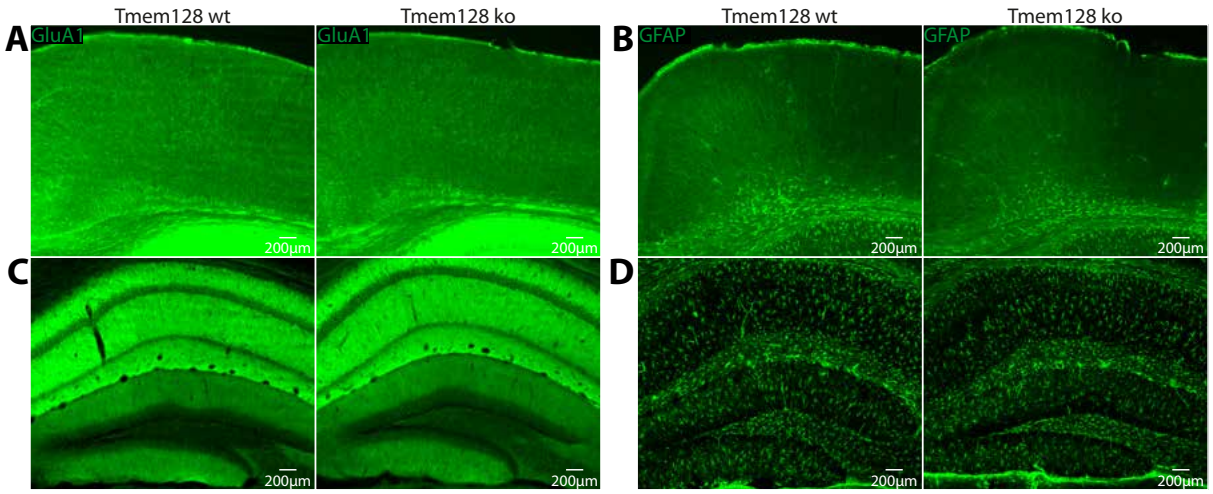

Figure 41: Antibody staining for neuronal and glial markers.

Representative antibody stainings of PFA-fixed coronal sections showing cortex (A, B) and parts of the hippocampal formation (C, D) from wild type and knockout animals. Neither GluA1 (A, C), a marker for pyramidal cells, nor GFAP (B, D), a marker for astrocytes, show any obvious differences.

CA3 (figure 40B) and dentate Gyrus/CA1 (figure 40C) is comparable between wild type and knockout animals. Higher magnifications of CA1 (figure 40D-E) and dendate gyrus (figure 40F-G) did not reveal differences in ER morphology on the cellular level.

To investigate the distribution of two major cell populations of the brain, additional stainings were performed. AMPA-type glutamate receptor subunit A1 (GluA1) was stained to visualize neurons in the cortex and hippocampus (figure 41A and C) and glial fibrillary acidic protein (GFAP) was stained to visualize astrocytes (figure 41B and D). Differences in signal intensity are due to staining efficacy but on a detailed level no differences between wild-type and knockout brains are visible. Thus in all analyzed paradigms the brain morphology of wild type and Tmem128 knockout animals is very similar.

3.5.3 Neurons cultured from wild type and Tmem128 knockout animals develop similarly

In order to investigate the development and morphology of wild type as well as Tmem128 knockout neurons, I used primary hippocampal and cortical cultures. Neurons from knockout mice grew and developed indistinguishable from wild type neurons. Staining with the antibody that was generated by us (3.4.1), showed a punctate staining in Map2 positive wild type neurons (figure 42A-E), that was strongly reduced in neurons cultured from knockout animals (figure 42F-J). Comparable to the unspecific bands detected by this antibody in western blot analysis of mouse brain lysates, it also generates an unspecific background signal on neuronal cultures. This background signal is strongest in the somatic region of the neuron (figure 42G) but is only weakly detectable in dendrites of Tmem128 knockout neurons (figure 42H-J). In wild type neurons on the other hand, the antibody generated a punctate signal in neuronal somata (figure 42B) as well as in proximal and distal neurites

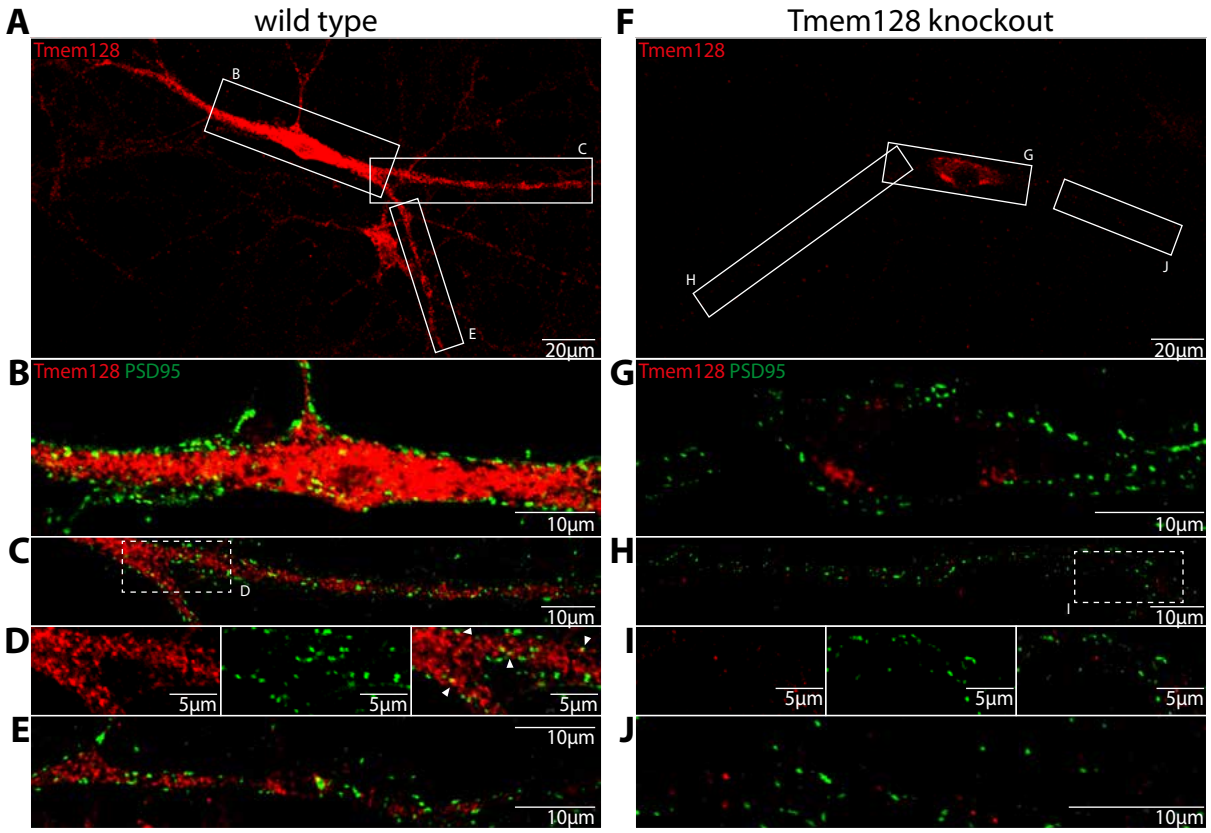

Figure 42: Endogenous Tmem128 in cultured hippocampal neurons.

Wild type (A-E) and Tmem128 (F-J) knockout hippocampal neurons were cultured for 14 days in vitro and stained for Tmem128 (red) and PSD95 (green). Neurons were selected for a MAP2 positive signal (not shown). All images except A and F are confocal images in one optical plane. A and F are maximum intensity projections to visualize Tmem128 staining in the entire cell. The antibody against Tmem128 shows a strong punctate signal in wild type neurons (A-E) that is largely absent in neurons cultured from Tmem128 nockout animals (F-J). Colocalization between Tmem128 and PSD95 can be seen on the soma and on dendrites in wild type neurons (D, arrows).

(figure 42C-E). Staining against the postsynaptic density protein PSD95 revealed an apparently normal distribution of synapses on the somata and dendrites of neurons of both genotypes. Interestingly, the endogenous Tmem128 signal colocalized with PSD95 puncta in the somatic region, as well as on dendrites (figure 42D arrowheads in the merge image) and no colocalization between PSD95 and the background signal generated by the Tmem128 antibody could be seen in Tmem128 knockout animals (figure 42I).

3.5.4 Tmem128 knockout animals display no alterations in protein expression or subcellular distribution

We were interested in the expression of Tmem128 in the juvenile and adult mouse brain and its influence on the expression or subcellular localization of other neuronal and non-neuronal proteins. I therefore generated brain lysates from developing mouse pups as well as adult mice and analyzed Tmem128 expression by western blot, using knockout mice as negative controls to identify the correct band stained by our self-made antibody. In the developing mouse brain, Tmem128 can be detected from post natal day 6 (P6), the earliest analyzed

time point (figure 43A) and its expression declines until adulthood. Expression levels in adult animals were observed to be variable (data not shown). In the adult mouse brain Tmem128 was detected in homogenates from cortex, hippocampus and cerebellum (figure 43B). It is expressed in hippocampus on a slightly higher level than in cortex or cerebellum. Since Tmem128 is expressed in all three investigated brain regions, I performed all further experiments on whole brain homogenates, including the cerebellum.

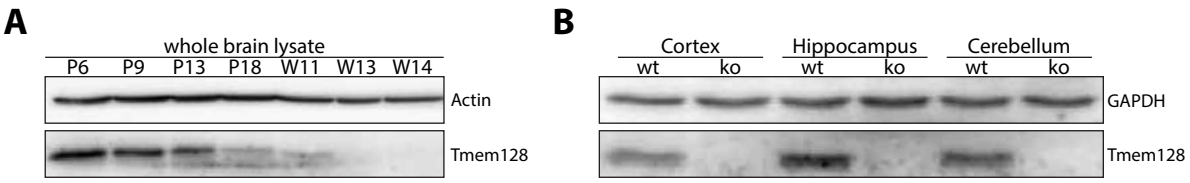

Figure 43: Tmem128 expression in mouse brain.

Western blot analysis of Tmem128 expression during brain development and in different brain regions. (A) Tmem128 expression is high in young animals and declines during adolescence. (B) Tmem128 is expressed at different levels in cortex, hippocampus and cerebellum of adult mice.

P = Post natal day, W = Post natal week; 20µg protein loaded per lane

I compared the expression levels of several proteins, normalized to the house keeping gene GAPDH (Glyceraldehyde 3-phosphate dehydrogenase), between wild type and Tmem128 knockout animals and could not detect significant differences in expression levels for a number of neuron specific proteins or for the ER resident protein GPR78/BiP (figure 44).

To visualize the distribution of Tmem128 within different subcellular compartments and to test for eventual differences in the subcellular distribution of other proteins, I used a subcellular fractionation protocol that gives rise to four different fractions: Post nuclear supernatant (whole brain homogenate without nuclei and large cell debris), crude synaptic membranes (including pre- and postsynaptic membranes), microsomes (including dendritic and axonal membranes, the ER and the Golgi apparatus), and cytosol (including small vesicles). In all analyzed animals, Tmem128 was enriched in the microsomal fraction together with the ER marker GPR78/BiP and the ER-exit site marker Sec23. In most animals it was also present in the cytosolic/vesicle fraction

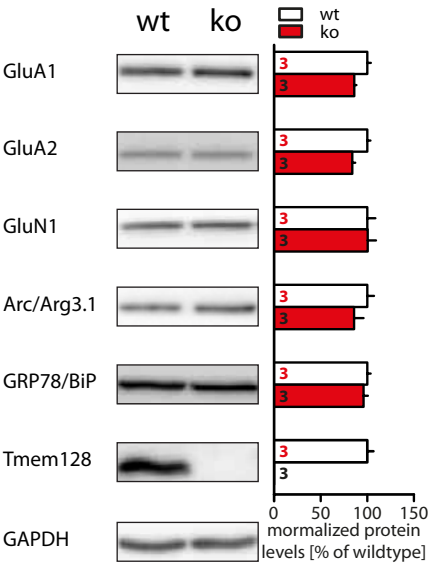

Figure 44: Biochemical analysis of protein expression in whole brain lysate from wild type and Tmem128 knockout animals.

Quantification of a select group of proteins in western blots from whole brain lysates normalized to GAPDH levels reveals no significant differences between the genotypes.

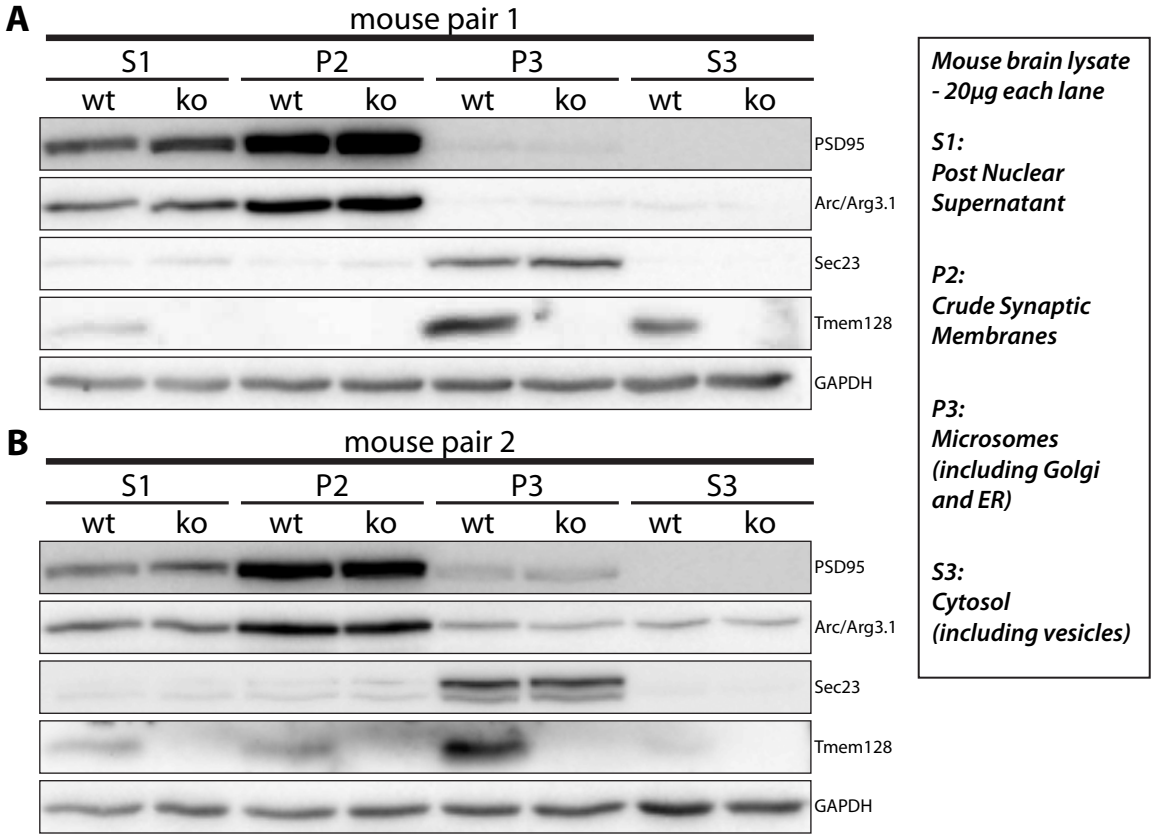

Figure 45: Synaptic localization of Tmem128.

Subcellular fractionation of brain lysates from wild type and Tmem128 knockout animals reliably shows Tmem128 presence in the microsomal fraction. (A) In one animal, Tmem128 is additionaly present in the cytosolic (small vesicle) fraction. (B) In most animals, however, Tmem128 is present in the cytosolic (small vesicle) fraction as well as in the crude synaptic membrane fraction, in addition to its enrichement in the microsomal fraction.

and in the synaptic membrane fraction (figure 45A). In one animal, however, Tmem128 could not be detected in the synaptic fraction, independent of loaded protein amount and western blot exposure times (figure 45B). The analysis of the purity of the individual fractions with PSD95, Sec23 and FMRP showed no differences between the two animals, indicating that differences between animals are due to biological variability and not due to impurities introduced during sample preparation.

I also observed no difference in the subcellular distribution of a large variety of neuronal and non-neuronal proteins, neither for soluble nor for transmembrane proteins (figure 46). There appeared to be a small increase in the GluA1 and GluA2 subunits of the AMPA-typye glutamate receptors in the P2 crude synaptic membrane fraction but detailed analysis and quantification showed no significant differences between wild type and Tmem128 knockout animals (figure 47).

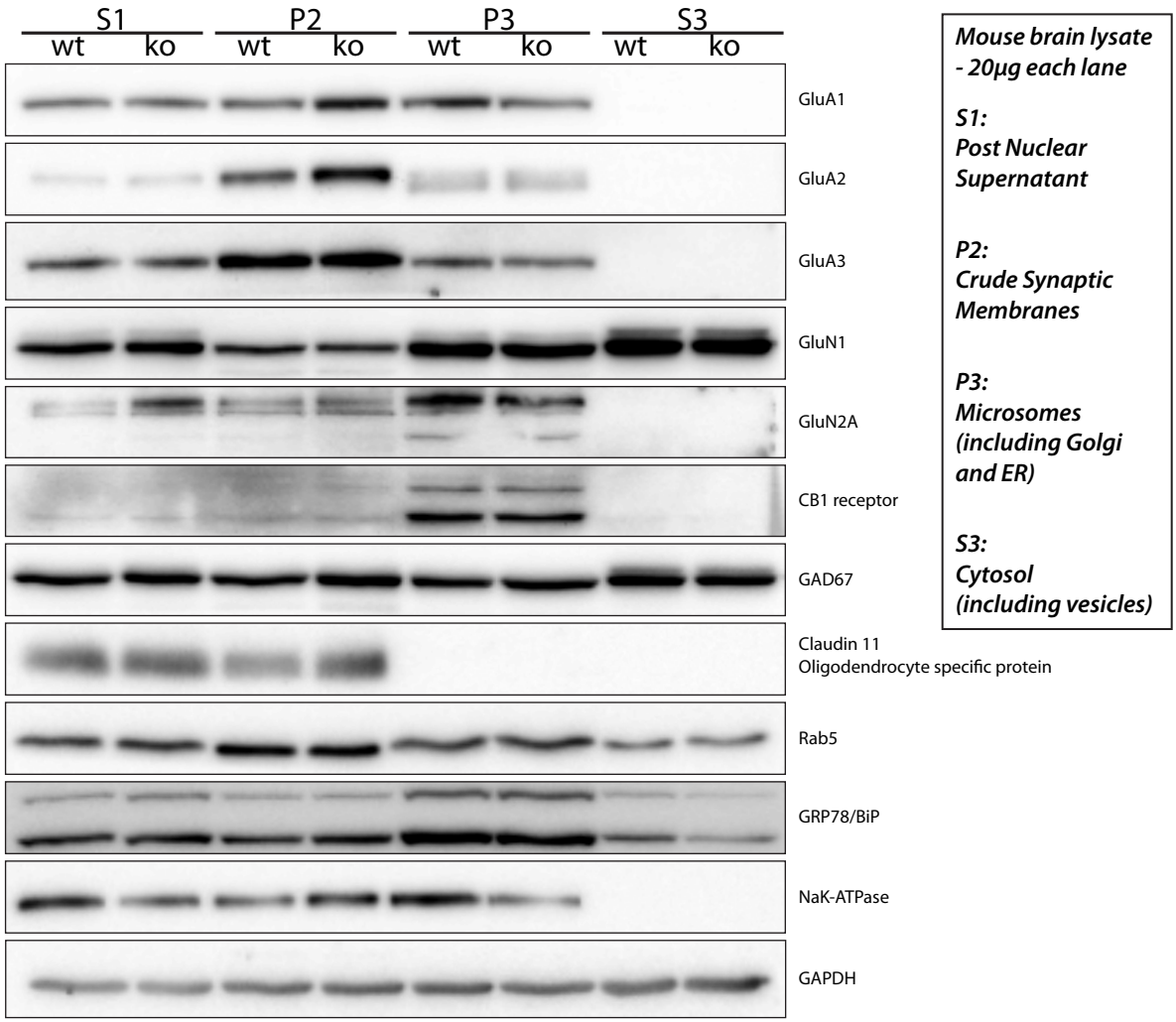

Figure 46: Biochemical analysis of protein expression in subcellular fractionation from brain lysates of wild type and Tmem128 knockout animals.

Analysis of the relative amounts of a select group of proteins distributed between different subcellular fractions. No obvious differences could be detected between wild type and knockout animals. Fractions were prepared from several mice pairs and assembled in one figure.

In previous experiments we could show the inducibility of Tmem128 mRNA by synaptic activity *in vitro* and *in vivo* (3.3.6) and we now aimed to confirm this result by investigating the changes of Tmem128 protein levels upon synaptic activity. We used the same stimulus as we had used previously for the induction of Tmem128 mRNA transcription, namely

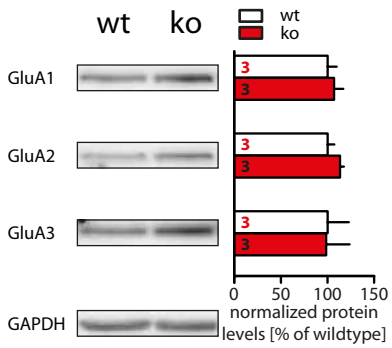

Figure 47: Biochemical analysis of protein expression in the synaptic membrane (P2) fraction of brain lysates from wild type and Tmem128 knockout animals.

Quantification of AMPA-type glutamate receptor subunit expression levels in western blots (normalized to GAPDH) reveals no significant differences between the genotypes.

kainic acid induced seizures. We analyzed lysates of mouse hippocampi at six diferent time points after seizure onset on western blot. Three animals were used for each time point and detection of Arc/Arg3.1 was used to select one animal for each time point, so that the induction of Arc/Arg3.1 matched the previously described induction profile for Arc/Arg3.1 (figure 48A). For the quantification, al animals were included in the analysis. Using this induction paradigm, we could show Tmem128 induction on the protein level (figure 48A). The induction follows a similar timecourse as the induction for Arc/Arg3.1, albeit with a longer lasting plateau. Overall induction is betwen 150% and 200% of baseline level (figure 48B), which is much weaker as Arc/Arg3.1 induction compared to baseline. Comparison of Tmem128 induction with GRP78/BiP showed, that the increase in Tmem128 protein level was not due to a generalized increase of all ER protein levels (data not shown).

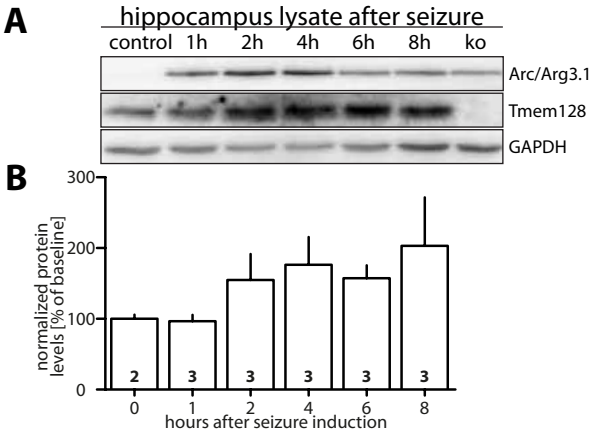

Figure 48: Expression analysis of Arc/Arg3.1 and Tmem128.

Western blot analysis of hippocampal lysates at different time points after kainic acid induced seizures. (A) Arc/Arg3.1 is induced after synaptic activity as previously described. Tmem128 expression is also induced. (B) Quantifiaction of Tmem128 expression after kainic acid induced seizures normalized to GAPDH.

4 Discussion

The goal of this study was the identification of novel Arc/Arg3.1 interaction partners using two different approaches. Both techniques have been optimized for special purposes. The Tandem Affinity Purification (TAP) potentially allows the isolation of large and intact protein complexes from native tissue, thus ensuring the identification of protein-protein interactions that are physiologically relevant. The Split-Ubiquitin modification of the classical yeast two hybrid screen (Y2H) allows the identification of interacting proteins that, due to their size or naturally occurring nuclear export signals, cannot translocate to the nucleus of the yeast cell, which is a major advantage over classical Y2H-techniques. With the introduction of another modification, the anchorage of the bait protein to the plasma membrane, we could specifically screen for membrane-near interactions of prey and bait proteins. While the identification of novel interaction partners for Arc/Arg3.1 with the TAP protocol and transgenic Tap-Arc/Arg3.1 mice has not been successful, we were able to identify several novel potential interaction partners for Arc/Arg3.1 with the Split-Ubiquitin approach. I have subsequently confirmed the interaction of Arc/Arg3.1 with two partners, namely RIP5 (Rab5 interacting protein) and Tmem128 (Transmembrane protein 128) with other techniques. In a next step, I have investigated these so far uncharacterized transmembrane proteins on a biochemical, cell biological, and genomic level. This allowed me to establish the putative topology of both proteins in the membrane of the endoplasmic reticulum (ER), where both proteins are localized. Moreover I could show that Tmem128 is alternatively spliced and that one splice variant is transcriptionally and translationally induced following synaptic activity. To better study RIP5 and Tmem128 I have generated antibodies against both proteins and I have generated a knockout mouse line for Tmem128. I have then analyzed the brains of the mice lacking Tmem128 on a morphological and biochemical level.

To my knowledge this is the first description of RIP5 and Tmem128 and the first time that both proteins have been implicated as interaction partners of Arc/Arg3.1. I will thus start the discussion by critically reviewing the experimental results obtained in this thesis. I will then put these results into the context of our current knowledge about Arc/Arg3.1 function with a special emphasis on the role of Arc/Arg3.1 in neuronal sorting and trafficking events.

4.1 Identification of novel Arc/Arg3.1 interaction partners

Using transgenic mice that express TAP-Arc/Arg3.1 for Tandem Affinity Purification (TAP) did not lead to the expected result of identifying novel interaction partners and signaling complexes of Arc/Arg3.1. This may be due to different reasons. One of them is the fact that Arc/Arg3.1 is expressed in the adult mouse brain at very low levels under non-stimulated conditions (Link et al. 1995; Lyford et al. 1995). The strategy employed to generate the transgenic TAP-Arc/Arg3.1 animals was a pro-nucleus injection of a transgenic construct that lead to the random integration of the TAP-Arc/Arg3.1 construct in the mouse genome. In order to mimic the low expression of wild type Arc/Arg3.1, the promoter driving the transgenic

construct was chosen to be a low level expressing promoter as well, namely the murine Thy-1 promoter. Unfortunately this low expression level led to considerable difficulties in obtaining enough brain material containing TAP-Arc/Arg3.1 fusionprotein. Thus a successful purification of Arc/Arg3.1 and its binding partners in the tandem affinity procedure could not be achieved. Furthermore, the transcription and translation of Arc/Arg3.1 is highly and transiently induced after patterned synaptic activity. This can potentially result in a high number of protein-protein interactions involving Arc/Arg3.1 that are transient and possibly weak in nature. Therefore, a knock-in animal where the TAP-Arc/Arg3.1 is under the control of the natural, inducible, Arc/Arg3.1 promoter would have led to larger amounts of Arc/Arg3.1 containing protein complexes and thus a higher chance of successfully identifying interaction partners.

The alternative method that we employed to identify novel Arc/Arg3.1 interaction partners was the Split-Ubiquitin variant of the standard Y2H screen. Since we are especially interested in the potential role of Arc/Arg3.1 in the trafficking and intracellular sorting of neuronal transmembrane proteins, we used an additional variation, namely the anchorage of the bait protein Arc/Arg3.1 to the plasma membrane. For this purpose, Arc/Arg3.1 was expressed as a fusion construct with the yeast membrane protein Ost4. This allowed us to specifically screen for interactions that take place near or at the plasma membrane. Using this approach we identified several novel interaction partners for Arc/Arg3.1, many of them transmembrane proteins. Surprisingly we did not identify any previously described interaction partners, some of which are known to act in membrane dynamics. Unfortunately, the libraries containing the prey proteins, that are available for the Split-Ubiquitin technique, do not have the same degree of complexity as the ones for the classical Y2H. As discussed above, the individual protein-protein interactions involving Arc/Arg3.1 are possibly rather weak and transient or may need to be stabilized by other neuronal proteins. It is therefore conceivable that not all protein-protein interactions involving Arc/Arg3.1 can be identified in a yeast screen where the individual yeast cells express only a small part of the library and often only fragments of the individual prey proteins. However, we identified six potential interaction partners for Arc/Arg3.1 which we analyzed further.

4.2 Validation of RIP5 and Tmem128 as interaction partners

The six potential interaction partners were tested in a HEK cell-based co-immunoprecipitation assay to validate their interactions with Arc/Arg3.1. In this assay, only two of the six proteins, namely RIP5 and Tmem128, showed consistent binding to Arc/Arg3.1. However, RIP5 binding to Arc/Arg3.1 was very weak. The interaction of Tmem128 with Arc/Arg3.1 could additionally be validated in the mammalian-two-hybrid system. This screen uses the tagged intracellular N-termini of the proteins of interest to probe for protein-protein interactions. Since RIP5 and Tmem128 are proteins with several transmembrane domains,

their interaction with Arc/Arg3.1 could be dependent on their intracellular N-termini, their intracellular loops, their C-termini or a combination of the three. Seen in this light, it is not surprising that in the mammalian-2-hybrid analysis a positive interaction with Arc/Arg3.1 could only be seen for Tmem128 but not for RIP5. The fact that the previously published Arc/Arg3.1 interaction partner Dynamin2 (Chowdhury et al. 2006) could be validated with co-immunoprecipitations but not with the mammalian-2-hybrid analysis, shows that not all protein interactions can be validated using this system.

4.3 ER-localization and topology of RIP5 and Tmem128

Using fluorescently tagged versions of RIP5 and Tmem128 and different markers for subcellular compartments I could show that both RIP5 and Tmem128 are localized to the endoplasmic reticulum (ER) in Hek293 and HeLa cells as well as cultured cortical and hippocampal neurons.

The ectopic expression of proteins always carries the danger of mislocalization, even more so when dealing with tagged transmembrane proteins. The observed localization of RIP5 and Tmem128 to the ER could thus potentially be biased by overexpression and/or mislocalization. But the fact that this specific localization was observed in cells as different as HeLa and neurons, and that it was independent from the nature or position of the tag being used, leads us to the conclusion that the majority of translated RIP5 and Tmem128 are indeed localized to the ER. Furthermore, there are several classical ER localization signals present in the amino acid sequence of RIP5 and of Tmem128.

Whether the entire population of RIP5 always resides in the ER or is being distributed in small amounts to other membranous compartments or the plasma membrane remains to be investigated. Since we have a working antibody against Tmem128 for western blot analysis, we could use this tool to study the distribution of Tmem128 in different membranes. Subcellular fractionation of mouse brain homogenate provides us with different subcellular samples for western blot analysis: The crude synaptic membrane fraction, including the pre- and postsynapse, the microsomal fraction, as well as the cytosolic fraction. Tmem128 is enriched in the microsomal fraction, but is also occasionally detectable in the postsynaptic membrane fraction as well as the cytosolic fraction (presumably in small vesicles). The presence of the plasma membrane marker NaK-ATPase as well as several neuronal transmembrane proteins in the microsomal fraction indicates that this fraction contains plasma membrane in addition to the membranes of the ER and Golgi apparatus. Thus the population of Tmem128 in this fraction cannot unequivocally be attributed to a specific subcellular compartment. As is indicated by the presence of the ligand gated ion channel subunit GluN1, the cytosolic fraction contains not only soluble proteins, but also transmembrane proteins, presumably in the membranes of small vesicles. The occasional presence of Tmem128 in this fraction

indicates that a small amount of Tmem128 also resides in small vesicles but it has yet to be determined under which conditions Tmem128 is present in the postsynaptic or small vesicle fraction in addition to the microsomal fraction.

The localization of RIP5 and Tmem128 to specific ER subdomains like ER exit sites, where cargo leaves the ER in small vesicles for the Golgi apparatus, is difficult to study. Visualization of this kind of localization is only possible in immuno electron microscopy, a technique that is dependent on highly specific antibodies, or with multiple fluorescent labeling and confocal visualization in well resolved cell types. With their elongated morphology, very thin neurites and little cytoplasm, neurons do not fall into this category. But the localization to ER-subdomains in other, non-neuronal, cells might very well be artificial and not comparable to the situation in neurons. Thus, further investigating the localization of RIP5 and Tmem128 to ER subdomains or other membranous compartments could not be carried out in this study but might prove helpful in future experiments aiming at obtaining information on their possible functions.

Using the Digitonin based immunocytochemical assay allowed me to establish the likely topology for RIP5 and Tmem128 in the membrane of the ER. The N- and C-termini of both proteins face the cytoplasm and the first loops, connecting the first and second transmembrane domains, face the lumen of the ER. Establishing the likely topology for Tmem128 in the membrane of the endoplasmic reticulum with the second luminal loop close to or entirely embedded in the lipid bilayer may allow an additional conclusion. The stretch of amino acids comprising this part of Tmem128 (WSFFTP) is highly conserved from zebra fish to humans. Comparing these amino acids to proteoms of other organisms (using protein BLAST), shows that proteins belonging to the family of solute carriers (SLC), specifically the subfamily SLC6A of amino acid transporters, contain the WSFFTP motif in their 11th transmembrane domain. It matches perfectly with the motif found in two GABA transporters (SLC6A family members 1 and 13) as well as in the creatine transporter (SLC6A family member 8) where it is conserved from mouse to human. And it matches to a lesser degree to a similar motif found in the 11th transmembrane domain of other members of this protein family.

While these proteins are very large, contain 12 transmembrane domains and share little homology with Tmem128 apart from the WSFFTP motif, it is still very intriguing that Tmem128 might play a role in the transport of solutes across membranes.

4.4 Expression of RIP5 and Tmem128

Analysis of the mRNA levels of RIP5 and the Tmem128 splice variants in developing neurons in culture suggests that RIP5 and Tmem128-E5 are not regulated during neuronal maturation. Tmem128-E6 expression was, however, variable and was subject to non-time locked fluctuations in all cultures analyzed.

Using the anti Tmem128 antibody we were able to also analyze protein levels for Tmem128 in developing mouse brains. Here we found that Tmem128 levels are high during early postnatal development and subsequently decrease from infancy to adulthood. The two experimental settings for mRNA and protein analysis cannot be directly compared because neuronal development in culture is very different from postnatal brain development *in vivo*. Also, mRNA and protein levels might be differentially regulated. It would be interesting to know whether the decreasing expression observed in brain tissue is solely dependent on intrinsic signals present during brain development or whether it may be triggered by external stimuli provided during infancy. It is conceivable that the Tmem128 protein seen during brain development is translated from the non-inducible Tmem128-E5 mRNA and that the Tmem128 protein seen in adult mouse brains at varying levels is translated from the inducible Tmem128-E6 mRNA, which is the predominant mRNA in adult mouse brain, as we know from our northern blot analysis. An investigation of the mechanisms governing the transcriptional regulation of Tmem128, however, was beyond the scope of this study.

Analyzing the expression patterns of RIP5 and Tmem128 mRNA using radioactive in situ hybridization on adult mouse brain sections and sections of mouse embryos (day 16.5), we found both proteins to be expressed in a variety of tissues and brain regions at relatively low levels. It would, however, be wrong to immediately conclude from the mRNA levels, that RIP5 and Tmem128 protein levels are equally low. It is possible that both proteins have a long half-life, as might be expected for transmembrane proteins, and that actual protein levels are higher than the mRNA levels suggest.

The signal distribution seen for RIP5 and Tmem128 in the embryonic in situ hybridizations does not match entirely with the mRNA levels for different tissues seen on the northern blots. This is most likely due to the different ages at which the analyzed samples were prepared. The in situ hybridizations were carried out on embryonic section (E16.5), while the RNAs used for the northern blots were obtained from adult animals. Nevertheless we can conclude that RIP5 and Tmem128 are expressed at low levels in various tissues of embryonic and adult mice.

4.5 Induction of Tmem128-E6 by neuronal activity

Using KCl stimulation of primary neuronal cultures with subsequent RT-PCR as well as kainic acid stimulation of adult animals with subsequent in situ hybridization analysis, I could show that the expression of Tmem128-E6 mRNA levels is induced by neuronal activity. However, we were not able to show a lack of induction of the second Tmem128 splice variant, Tmem128-E5, due to technical constraints. The uninducible and the inducible Tmem128 mRNAs differ only in their 3'UTR. The probe that we used for the detection of Tmem128-E6 corresponds to the 564 nucleotides of exon 6, which is relatively short for an in situ probe. And the even shorter length of exon 5 of only 210 nucleotides prevented us from attempting to use in situ hybridization to confirm the lack of induction of Tmem128-E5 that we have seen with RT-PCR on cultured neurons after activity.

The time course of induction was different between the *in vitro* and the *in vivo* experiment: The kainate in situ hybridizations show increased Tmem128 transcription in the dentate gyrus 2h after seizure onset and in the CA1 region 4h after seizure onset. The induction of mRNA in the culture was generally faster, which might be due to a stronger stimulation in the *in vitro* experiment. Modulatory network effects in the intact brain used for the *in vivo* experiment can also not be excluded. Concerning the time difference of induction in DG and CA1 *in vivo*, it is hard to judge whether this represents a genuine expression pattern with time delayed expression of Tmem128 along the trisynaptic synapse path after stimulation, or whether it is caused by a delay in seizure activity between the two regions.

4.6 Antibody generation against RIP5 and Tmem128

The antibodies that we generated for RIP5 and Tmem128 did not entirely fulfill our expectations. The very weak performance of the anti RIP5 antibodies in all tested paradigms as well as the high concentration that was needed of the anti Tmem128 antibody, and the low signal to noise ratio that is a result of this, can have several reasons. Technical constraints forced us to use N-terminally tagged versions of the intracellular N-termini of RIP5 and Tmem128 for immunization. In order to fold correctly under physiological conditions a non-tagged N-terminus might be crucial for both proteins. Additional factors determined by the cytoplasmic milieu could potentially also be crucial for correct folding. It is thus possible that the antibodies generated against the N-terminally tagged fusion proteins do not recognize the physiological conformation of RIP5 and Tmem128. It is also possible that the expressed fragments of RIP5 and Tmem128 in *E.coli* lacked posttranslational modifications that are specific for eukaryotes and that might be needed for optimal antigen presentation.

4.7 Generation and characterization of the Tmem128 knockout mouse line

The use of targeted embryonic stem cells for the generation of a constitutive, and later conditional, Tmem128 knockout mouse line was very successful. Using southern blot analysis I confirmed the insertion of the targeting cassette into the genomic locus of Tmem128 and using our self-made antibody I also confirmed the knockout on the protein level. The knockout mice show no morphological difference to their wild type littermates and they develop normally. The only obvious difference was the low breeding efficiency compared to wild type matings, though the distribution of genotypes in litters from homozygous matings was in accordance with Mendelian laws of inheritance. All other parameters like postnatal growth, macroscopic and microscopic brain morphology were not different between wild type and Tmem128 knockout mice. Analysis of the expression levels and subcellular distribution of a number of proteins, including neuron specific proteins like the neurotransmitter subunits GluA1-3 and GluN1, did not reveal notable differences between the genotypes. Considering the structural similarity between RIP5 and Tmem128 as well as the large degree of colocalization, and also considering that both proteins physically associate and potentially form a complex *in vivo*, it is possible that the knockout of Tmem128 induces a compensatory upregulation or functional rescue by RIP5. This could be an explanation for absence of an obvious phenotype in the Tmem128 knockout mice. Unfortunately, an upregulation of RIP5 on the protein level could not be analyzed due to the low specificity of the RIP5 antibody that we generated. An interesting future experiment would be the shRNA induced knockdown of RIP5 in specific brain regions of the Tmem128 knockout mice.

Given the expression of Tmem128 in all analyzed brain regions (figures 22D and 44) and its presence in the synapse (figure 41D and 45B), it would be prudent to continue this project with a series of electrophysiological and behavioral studies to analyze the influence of the Tmem128 knockout on basic synaptic transmission and different forms of potentiation as well as general and learning related behavior.

In general, the lack of an obvious phenotype in the Tmem128 knockout mice with the above mentioned analyses is reminiscent of the phenotype of the Arc/Arg3.1 knockout mice themselves. These mice also show no aberrant morphology or baseline physiology and their behavior is entirely normal unless challenged in long term-memory paradigms. The investigations used to analyze the Tmem128 knockout animals would not have detected a phenotype in the Arc/Arg3.1 knockout mice either. This leads me to the conclusion that the loss of Tmem128 in mice likely leads to a more subtle behavioral phenotype, comparable to the Arc/Arg3.1 knockout mice and will likely only be detected with more specialized behavioral tests.

4.8 RIP5 and Tmem128 in the context of the neuronal endoplasmic reticulum

The endoplasmic reticulum fulfills several vital functions in neurons, not only under steady state conditions, but also under high demand and in plasticity related circumstances. There was so far no known link between Arc/Arg3.1 and the ER, but the newly identified interaction partners RIP5 and Tmem128 open up exciting new possibilities to envision the organizing role that Arc/Arg3.1 plays in intracellular sorting in neurons.

It is well described that several plasticity related events in single synapses and entire neurons rely on the precise regulation of intracellular calcium levels (Bardo et al. 2006; M. K. Park et al. 2008). As a release site for stored intracellular calcium and also as the organelle responsible for clearance of excess intracellular calcium, the ER is a prime candidate for regulation of calcium dependent synaptic plasticity. Although it is unlikely that the relatively small RIP5 and Tmem128 form homo- or heteromeric channels, it is possible that they act as modulatory proteins for calcium channels that are located in the membrane of the ER. In order to test this hypothesis, high resolution calcium imaging of individual spines of Tmem128 knockout neurons or wild type neurons overexpressing RIP5 and/or Tmem128 can be used. Absence or increased expression of both proteins might influence baseline or stimulus triggered calcium signals.

The capacity of the ER to produce novel transmembrane proteins, like neurotransmitter receptors and ion channels, is another site of possible influence by the ER on synaptic function. Therefore, local protein synthesis at ER-exit sites near synaptic spines can strongly influence a spines capacity to react to plasticity inducing stimuli. In addition to novel protein synthesis, the surface expression of several important synaptic proteins is known to be regulated by either ER retention/retrieval signals or ER export signals present in their cytoplasmic tails. Among them are voltage gated Ca^{2+} channels (Bichet et al. 2000), GABA receptors (Margeta-Mitrovic et al. 2000), K^{+} channels (Ma et al. 2001), as well as NMDA receptors (Scott et al. 2001). Upon a specific stimulus these signals get masked or unmasked and the proteins can exit the ER towards the Golgi apparatus and their final destination. In this light it is possible that RIP5 and Tmem128 fulfill this masking function for a subset of synaptic proteins and that the interaction with Arc/Arg3.1 acts as a trigger to capture or release these proteins at ER-exit sites. Although the subcellular fractionation of brains from Tmem128 knockout animals did not hint at a function for Tmem128 in organizing the subcellular distribution of transmembrane proteins, repeating these experiments under different conditions of synaptic activity could lead to a greater insight in a possible chaperone function of Tmem128.

RIP5 and Tmem128 could also be involved in the protein translation machinery. Although in neurons the ribosome studded rER is mainly found in the soma and proximal dendrites. While the sER is mainly localized to distal dendrites. Any protein involved in the regulation of novel protein synthesis in the ER is expected to preferentially localize to rER containing

areas. This is not what we found for RIP5 and Tmem128. Fluorescently tagged versions of both proteins were localized throughout the entire neuron, although this localization might be a result of the strong overexpression. Additionally, the transmembrane proteins synthesized at the rER are cell biologically complex proteins with hydrophobic as well as hydrophilic domains. The requirements for protein folding are therefore very high and a number of specialized chaperones are expressed in the ER to aid nascent polypeptides co-translationally or post-translationally to achieve the correct secondary and tertiary structure. If either of the proteins analyzed in this study were essential components in the protein folding machinery, it would be highly unlikely not to see a morphological phenotype in cells overexpressing or not expressing one of these proteins.

A well-established theory of synapse maturation postulates, that spine morphology and function are tightly connected and that spine size is correlated with transmission efficacy (Nägerl et al. 2004; Grunditz et al. 2008; Kasai et al. 2010). The lipid synthesizing properties of the ER are indispensable when considering spine growth as an aspect of synaptic plasticity. But if RIP5 and Tmem128 were involved in this metabolic pathway, strong overexpression, and in case of Tmem128 also a knockout, should have led to a visible morphological phenotype in cultured neurons.

Instead of being directly involved in one of the several ER associated functions, RIP5 and Tmem128 could also be important for the structure and morphology of the ER and so indirectly influence its function. In order to generate the high degree of stable curvature seen in ER tubules, the outer membrane leaflet must be expanded by additional lipids or proteins and must have a surface area of at least 110% of inner leaflet (Zimmerberg and Kozlov 2006). Therefore, membrane shaping proteins, and also proteins responsible for the branched architecture of the ER tubules, must be very abundant. Judging by the in situ hybridizations, this is not the case for RIP5 or Tmem128. Also we did not observe aberrations in ER morphology in HeLa cells and neurons overexpressing RIP5 and Tmem128. But this has been observed for other proteins involved in shaping the ER-membrane (Voeltz et al. 2006; J. Hu et al. 2009).

It is still possible, that RIP5 and/or Tmem128 are involve in any of the above mentioned processes under specific and specialized circumstances and that we have so far not been able to identify these circumstances and thus have not been able to see a phenotype during overexpression or knockout. Another possibility is that both proteins function in cellular processes, whose disturbance has no visible influence on cell morphology or survival. Peptide homology between Tmem128 and other murine proteins point in the direction of transmembrane transport of amino acids or other solutes.

It is also possible that RIP5 and Tmem128 function lies outside of the ER and that, similar to the gamma secretase components Presenilin1 and Pen2, the masking or unmasking of specific export is needed in order to promote ER export. The large ER resident pool of

these proteins occludes the small functional pool that resides in the plasma membrane end endosomal structures (Pasternak et al. 2003; Fassler et al. 2010). The large degree of colocalization between ectopically expressed Presenilin1 and Tmem128 in cultures neurons is especially interesting in this context.

An interesting finding from this study was the identification of two alternative splice variants, of which one is inducible by neuronal activity. Alternative splicing is a versatile genetic tool that allows cells to generate a large variety of proteins from a limited subset of pre-mRNAs and thus is a major contributor to proteomic diversity. This mechanism is especially prevalent in the mammalian nervous system, where 40%-60% of neuronal pre-mRNAs are alternatively spliced (Yeo et al. 2004). Prime examples for alternative splicing during neuronal development are Neurexins and Neuroligins. These are presynaptic and postsynaptic receptors that engage in transsynaptic interactions and function in synapse development (Ushkaryov et al. 1992; Ichtchenko et al. 1995; M. Yamagata et al. 2003). Alternative splicing of both proteins determines their affinity for each other and thus the speed and specificity of synapse formation (Boucard et al. 2005; K. Shen and Scheiffele 2010). Examples for alternative splicing in the adult nervous system include Homer1A, a synaptic scaffolding protein whos mRNA can be alternatively spliced to generate a truncated, dominant negative protein (Bottai et al. 2002), that destabilizes spines in an activity dependent manner (Sala et al. 2003). Ionotropic glutamate receptors are also subjected to alternative splicing. Splicing events influence AMPAR receptor synthesis and trafficking (Coleman et al. 2006; Greger and José A Esteban 2007) and activity dependent alternative splicing controls ER-export and synaptic delivery of the NMDAR (Mu et al. 2003).

Alternative splicing that does not affect the encoded protein, but rather the untranslated and presumably regulatory regions of the pre-mRNA, have also been described in the literature. The complex exon structure of the brain derived neurotrophoc factor (BDNF) gene together with alternative use of transcription start sites and polyadenylation sites can potentially give rise to 18 different splice variants, which all encode the same protein (Aid et al. 2007; Pruunsild et al. 2007). Activity induced alternative splicing of mutually exclusive 3'UTRs has been reported as an additional modulatory mechanism (Hermey et al, submitted). Although the biological significance of these complex splicing events is far from clear, they provide intriguing examples for regulatory events in which the "where" and "when" of protein expression are regulated, rather than the encoded amino acid sequence itself.

Taken together, the findings described in this thesis expand our knowledge of Arc/Arg3.1 interaction partners and open new ways for the interpretation of Arc/Arg3.1 function in the context of the neuronal endoplasmic reticulum and different forms of synaptic plasticity.

5 Appendix

5.1 References

Aid, T., Kazantseva, A., Piirsoo, M., Palm, K. & Timmusk, T. (2007) Mouse and rat BDNF gene structure and expression revisited. Journal of Neuroscience Research 535,525–535.

Alberi, L., Liu, S., Wang, Y., Badie, R., Smith-Hicks, C., Wu, J., Pierfelice, T. J., Abazyan, B., Mattson, M. P., Kuhl, D., et al. (2011) Activity-induced Notch signaling in neurons requires Arc/Arg3.1 and is essential for synaptic plasticity in hippocampal networks. Neuron 69,437–44.

Altar, C. A., Laeng, P., Jurata, L. W., Brockman, J. a, Lemire, A., Bullard, J., Bukhman, Y. V, Young, T. a, Charles, V. & Palfreyman, M. G. (2004) Electroconvulsive seizures regulate gene expression of distinct neurotrophic signaling pathways. J Neuroscience 24,2667–77.

Amaral, D. & Witter, M. P. (1989) The Three-Dimensional Organization of the Hippocampal Formation: A Review of Anatomical Data. Neuroscience 31,571–591.

Araque, a, Parpura, V., Sanzgiri, R. P. & Haydon, P. G. (1999) Tripartite synapses: glia, the unacknowledged partner. Trends in neurosciences 22,208–15.

Aridor, M., Guzik, A. K., Bielli, A. & Fish, K. N. (2004) Endoplasmic reticulum export site formation and function in dendrites. J Neuroscience 24,3770–6.

Arthur, J. S. C., Fong, A. L., Dwyer, J. M., Davare, M., Reese, E., Obrietan, K. & Impey, S. (2004) Mitogen- and stress-activated protein kinase 1 mediates cAMP response element-binding protein phosphorylation and activation by neurotrophins. J Neuroscience 24,4324–32.

Bailey, D., Urena, L., Thorne, L. & Goodfellow, I. (2012) Identification of protein interacting partners using tandem affinity purification. Journal of visualized experiments : JoVE 5–9

Banke, T. G., Bowie, D., Lee, H-K, Huganir, R. L., Schousboe, A. & Traynelis, S. F. (2000) Control of GluR1 AMPA receptor function by cAMP-dependent protein kinase. J Neuroscience 20,89–102.

Bardo, S., Cavazzini, M. G. & Emptage, N. (2006) The role of the endoplasmic reticulum Ca2+ store in the plasticity of central neurons. Trends in pharmacological sciences 27,78–84.

Barria, A., Muller, D., Derkach, V. A., Griffith, L. C. & Soderling, T. R. (1997) Regulatory Phosphorylation of AMPA-Type Glutamate Receptors by CaM-KII During Long-Term Potentiation. Science 276,2042–2045.

Baumann, O. & Walz, B. (2001) Endoplasmic reticulum of animal cells and its organization into structural and functional domains. International review of cytology 205,149–214.

Béïque, J.-C., Na, Y., Kuhl, D., Worley, P. F. & Huganir, R. L. (2011) Arc-dependent synapse-specific homeostatic plasticity. PNAS 108,816–821.

Benke, T. A., Lüthi, A., Isaac, J. T. R. & Collingridge, G. L. (1998) Modulation of AMPA receptor unitary conductance by synaptic activity. Nature 393,793–797.

Berridge, M. J. (1998) Neuronal Calcium Signaling. Neuron 21,13–26.

Bezprozvanny, I., Watras, J. & Ehrlich, B. E. (1991) Bell-shaped calcium-response curves of lns (l, 4, 5) P3-and calcium-gated channels from endoplasmic reticulum of cerebellum. Nature 351,751–754.

Bichet, D., Cornet, V., Geib, S., Carlier, E., Volsen, S., Hoshi, T., Mori, Y. & De Waard, M. (2000) The I-II loop of the Ca2+ channel alpha1 subunit contains an endoplasmic reticulum retention signal antagonized by the beta subunit. Neuron 25,177–90.

Biedler, J. L., Helson, L. & Spengler, B. A. (1973) Morphology and growth, tumorigenicity, and cytogenetics of human neuroblastoma cells in continuous culture. Cancer research 33,2643–52.

De Bivort, B. L., Guo, H.-F. & Zhong, Y. (2009) Notch signaling is required for activity-dependent synaptic plasticity at the Drosophila neuromuscular junction. Journal of neurogenetics 23,395–404.

Bliss, T. V. P. & Collingridge, G. L. (1993) A synaptic model of memory: long-term potentiation in the hippocampus. Nature 361,31–39.

Bliss, T. V. P. & Lomo, T. (1973) Long-Lasting Potentiation of Synaptic transmission in the dentate area of the anaesthetized rabbit following stimulation of the peforant path. Journal of Physiology 232,331–356.

Bottai, D., Guzowski, J. F., Schwarz, M. K., Kang, S. H., Xiao, B., Lanahan, A., Worley, P. F. & Seeburg, P. H. (2002) Synaptic activity-induced conversion of intronic to exonic sequence in Homer 1 immediate early gene expression. J Neuroscience 22,167–75.

Boucard, A. a, Chubykin, A. a, Comoletti, D., Taylor, P. & Südhof, Thomas C. (2005) A splice code for trans-synaptic cell adhesion mediated by binding of neuroligin 1 to alpha- and beta-neurexins. Neuron 48,229–36.

Buchan, D. W. A., Ward, S. M., Lobley, A. E., Nugent, T. C. O., Bryson, K. & Jones, D. T. (2010) Protein annotation and modelling servers at University College London. Nucleic acids research 38,W563–8.

Cajigas, I. J., Will, T. & Schuman, E. M. (2010) Protein homeostasis and synaptic plasticity. EMBOJ 29,2746–52.

Carrel, D., Masson, J., Al Awabdh, S., Capra, C. B., Lenkei, Z., Hamon, M., Emerit, M. B. & Darmon, M. (2008) Targeting of the 5-HT1A serotonin receptor to neuronal dendrites is mediated by Yif1B. J Neuroscience 28,8063–73.

Chan, S. L., Mayne, M., Holden, C. P., Geiger, J. D. & Mattson, M. P. (2000) Presenilin-1 mutations increase levels of ryanodine receptors and calcium release in PC12 cells and cortical neurons. JBC 275,18195–200.

Chawla, S., Vanhoutte, P., Arnold, F. J. L., Huang, C. L.-H. & Bading, H. (2003) Neuronal activity-dependent nucleocytoplasmic shuttling of HDAC4 and HDAC5. Journal of Neurochemistry 85,151–159.

Cheung, K.-H., Mei, L., Mak, D.-O. D., Hayashi, I., Iwatsubo, T., Kang, D. E. & Foskett, J. K. (2010) Gain-of-function enhancement of IP3 receptor modal gating by familial Alzheimer's disease-linked presenilin mutants in human cells and mouse neurons. Science signaling 3,ra22.

Cheung, K.-H., Shineman, D., Müller, M., Cárdenas, C., Mei, L., Yang, J., Tomita, T., Iwatsubo, T., Lee, V. M.-Y. & Foskett, J. K. (2008) Mechanism of Ca2+ disruption in Alzheimer's disease by presenilin regulation of InsP3 receptor channel gating. Neuron 58,871–83.

Chowdhury, S., Shepherd, J. D., Okuno, H., Lyford, G. L., Petralia, R. S., Plath, N., Kuhl, D., Huganir, R. L. & Worley, P. F. (2006) Arc/Arg3.1 interacts with the endocytic machinery to regulate AMPA receptor trafficking. Neuron 52,445–459.

Cole, A. J., Saffen, D. W., Baraban, J. M. & Worley, P. F. (1989) Rapid increase of an immediate early gene messenger RNA in hippocampal neurons by synaptic NMDA receptor activation. Nature 340,474–476.

Coleman, S. K., Möykkynen, T., Cai, C., Von Ossowski, L., Kuismanen, E., Korpi, E. R. & Keinänen, K. (2006) Isoform-specific early trafficking of AMPA receptor flip and flop variants. J Neuroscience 26,11220–9.

Collingridge, G. L., Isaac, J. T. R. & Wang, Y. T. (2004) Receptor trafficking and synaptic plasticity. Nature Reviews Neuroscience 5,952–62.

Cooney, J. R., Hurlburt, J. L., Selig, D. K., Harris, K. M. & Fiala, J. C. (2002) Endosomal compartments serve multiple hippocampal dendritic spines from a widespread rather than a local store of recycling membrane. J Neuroscience 22,2215–24.

Corkin, S. (1984) Lasting consequences of bilateral medial temporal lobectomy: Clinical course and experimental findings in HM. Seminars in Neurology 4,249–259.

Costa, R. M., Honjo, T. & Silva, A. J. (2003) Learning and memory deficits in Notch mutant mice. Current Biology 13,1348–1354.

Csordás, G., Várnai, P., Golenár, T., Roy, S., Purkins, G., Schneider, T. G., Balla, T. & Hajnóczky, G. (2010) Imaging interorganelle contacts and local calcium dynamics at the ER-mitochondrial interface. Molecular cell 39,121–32.

Cui-Wang, T., Hanus, C., Cui, T., Helton, T. D., Bourne, J. N., Watson, D., Harris, K. M. & Ehlers, M. D. (2012) Local zones of endoplasmic reticulum complexity confine cargo in neuronal dendrites. Cell 148,309–21.

Dash, P. K., Hochner, B. & Kandel, E. R. (1990) Injection of the cAMP-responsive element into the nucleus of Aplysia sensory neurons blocks long-term facilitation. Nature 345,718–721.

Derkach, V. A., Oh, M. C., Guire, E. S. & Soderling, T. R. (2007) Regulatory mechanisms of AMPA receptors in synaptic plasticity. Nature Reviews Neuroscience 8,101–113.

Dityatev, A. & Rusakov, D. A. (2011) Molecular signals of plasticity at the tetrapartite synapse. Current Opinion in Neurobiology 21,353–9.

Ehlers, M. D. (2000) Reinsertion or degradation of AMPA receptors determined by activity-dependent endocytic sorting. Neuron 28,511–25.

Eichenbaum, H. (2000) A cortical–hippocampal system for declarative memory. Nature Reviews Neuroscience 1,1–10.

Eichenbaum, H. (2013) What H.M. taught us. Journal of cognitive neuroscience 25,14–21.

Esteban, José A. (2003) AMPA receptor trafficking: a road map for synaptic plasticity. Molecular interventions 3,375–85.

Fassler, M., Zocher, M., Klare, S., Guzman de la Fuente, A., Scheuermann, J., Capell, A., Haass, C., Valkova, C., Veerappan, A., Schneider, D., et al. (2010) Masking of transmembrane-based retention signals controls ER export of gamma-secretase. Traffic 11,250–8.

Flavell, S. W., Cowan, C. W., Kim, T.-K., Greer, P. L., Lin, Y., Paradis, S., Griffith, E. C., Hu, L. S., Chen, C. & Greenberg, M. E. (2006) Activity-dependent regulation of MEF2 transcription factors suppresses excitatory synapse number. Science 311,1008–12.

Flexner, J. B., Flexner, L. B. & Stellar, E. (1963) Memory in mice as affected by intracerebral puromycin. Science 141,57–59.

Friedman, J. R. & Voeltz, G. K. (2011) The ER in 3D: a multifunctional dynamic membrane network. Trends in cell biology 21,709–17.

Frischknecht, R. & Gundelfinger, E. D. (2012) The brain's extracellular matrix and its role in synaptic plasticity edited by Michael R. Kreutz and Carlo Sala. Advances in Experimental Medicine and Biology 970,153–171.

Fujino, T., Lee, W.-C. A. & Nedivi, E. (2003) Regulation of cpg15 by signaling pathways that mediate synaptic plasticity. Molecular and cellular neurosciences 24,538–54.

Fusi, S., Drew, P. J. & Abbott, L. F. (2005) Cascade models of synaptically stored memories. Neuron 45,599–611.

Gandy, S. (2005) The role of cerebral amyloid β accumulation in common forms of Alzheimer disease. Journal of Clinical Investigation 115,1121–1129.

Gey, G. O., Coffman, W. D. & Kubicek, M. T. (1952) Tissue culture studies of the proliferative capacity of cervical carcinoma and normal epithelium. Cancer research 12,264–265.

Glenner, G. G. & Wong, C. W. (1984) Alzheimer's disease: initial report of the purification and characterization of a novel cerebrovascular amyloid protein. Biochemical and biophysical research communications 120,885–890.

Goldgaber, D., Lerman, M. I., McBride, O. W., Saffiotti, U. & Gajdusek, D. C. (1987) Characterization and chromosomal localization of a cDNA encoding brain amyloid of Alzheimer's disease. Science 394,877–880.

Graham, F. L., Smiley, J., Russell, W. C. & Nairn, R. (1977) Characteristics of a human cell line transformed by DNA from human adenovirus type 5. The Journal of general virology 36,59–74.

Grant, S. G. N. (2010) Targeted TAP tags, phosphoproteomes and the biology of thought. Expert review of proteomics 7,169–71.

Gray, E. (1959) Electron microscopy of synaptic contacts on dendrite spines of the cerebral cortex. Nature 183,1592–1593.

Greenberg, M. E. & Ziff, E. B. (1984) Stimulation of 3T3 cells induces transcription of the c-fos proto-oncogene. Nature 311,433–438.

Greer, P. L. & Greenberg, M. E. (2008) From synapse to nucleus: calcium-dependent gene transcription in the control of synapse development and function. Neuron 59,846–60.

Greger, I. H. & Esteban, José A. (2007) AMPA receptor biogenesis and trafficking. Current Opinion in Neurobiology 17,289–97.

Grunditz, A., Holbro, N., Tian, L., Zuo, Y. & Oertner, T. G. (2008) Spine neck plasticity controls postsynaptic calcium signals through electrical compartmentalization. J Neuroscience 28,13457–66.

Gundelfinger, E. D., Frischknecht, R., Choquet, D. & Heine, M. (2010) Converting juvenile into adult plasticity: a role for the brain's extracellular matrix. The European journal of neuroscience 31,2156–65.

Guzowski, J. F., Timlin, J. A., Roysam, B., Worley, P. F. & Barnes, C. A. (2005) Mapping behaviorally relevant neural circuits with immediate-early gene expression. Current Opinion in Neurobiology 15,599–606.

Hammond, A. T. & Glick, B. S. (2000) Dynamics of transitional endoplasmic reticulum sites in vertebrate cells. Molecular biology of the cell 11,3013–30.

Hayward, W. S., Neel, B. G. & Astrin, S. M. (1981) Activation of a cellular onc gene by promoter insertion in ALV-induced lymphoid leukosis. Nature 290,475–480.

Hebb, D. O. (1949) The Organization of behavior: A neuropsychological theory. John Wiley & Sons, New York

Herculano-Houzel, S. (2012) The remarkable, yet not extraordinary, human brain as a scaled-up primate brain and its associated cost. PNAS 109,10661–10668.

Hermey, G., Mahlke, C., Schwake, M., & Sommer, T. (2010). Der Experimentator - Neurowissenschaften. Heidelberg: Spektrum Akademischer Verlag.

Hermey, G., Mahlke, C., Gutzmann, J. J., Schreiber, J., Blüthgen, N & Kuhl, D. (submitted). Genome-wide profiling of the synaptic activity-dependent hippocampal transcriptome.

Holbro, N., Grunditz, A. & Oertner, T. G. (2009) Differential distribution of endoplasmic reticulum controls metabotropic signaling and plasticity at hippocampal synapses. PNAS 106,15055–60.

Hollmann, M. & Heinemann, S. (1994) Cloned glutamate receptors. Ann. Rev. Neurosci. 17,31–108.

Hong, S. J., Li, H., Becker, K. G., Dawson, V. L. & Dawson, T. M. (2004) Identification and analysis of plasticity-induced late-response genes. PNAS 101,2145–50.

Horton, A. C. & Ehlers, M. D. (2003) Dual modes of endoplasmic reticulum-to-Golgi transport in dendrites revealed by live-cell imaging. J Neuroscience 23,6188–99.

Hu, J., Shibata, Y., Zhu, P.-P., Voss, C., Rismanchi, N., Prinz, W. A., Rapoport, T. A. & Blackstone, C. (2009) A class of dynamin-like GTPases involved in the generation of the tubular ER network. Cell 138,549–61.

Ichtchenko, K., Hata, Y., Nguyen, T., Ullrich, B., Missler, M., Moomaw, C. & Südhof, T C. (1995) Neuroligin 1: a splice site-specific ligand for beta-neurexins. Cell 81,435–43.

Jeyifous, O., Waites, C. L., Specht, C. G., Fujisawa, S., Schubert, M., Lin, E. I., Marshall, J., Aoki, C., De Silva, T., Montgomery, J. M., et al. (2009) SAP97 and CASK mediate sorting of NMDA receptors through a previously unknown secretory pathway. Nature Neuroscience 12,1011–9.

Ju, W., Morishita, W., Tsui, J., Gaietta, G., Deerinck, T. J., Adams, S. R., Garner, C. C., Tsien, R. Y., Ellisman, M. H. & Malenka, R. C. (2004) Activity-dependent regulation of dendritic synthesis and trafficking of AMPA receptors. Nature neuroscience 7,244–53.

Kaang, B.-K., Kandel, E. R. & Grant, S. G. N. (1993) Activation of cAMP-responsive genes by stimuli that produce long-term facilitation in Aplysia sensory neurons. Neuron 10,427–35.

Kang, H. & Schuman, E. M. (1996) A requirement for local protein synthesis in neurotrophin-induced hippocampal synaptic plasticity. Science 273,1402–6.

Kasai, H., Fukuda, M., Watanabe, S., Hayashi-Takagi, A. & Noguchi, J. (2010) Structural dynamics of dendritic spines in memory and cognition. Trends in neurosciences 33,121–9.

Kato, A., Ozawa, F., Saitoh, Y., Hirai, K. & Inokuchi, K. (1997) vesl, a gene encoding VASP/Ena family related protein, is upregulated during seizure, long-term potentiation and synaptogenesis. FEBS Letters 412,183–189.

Kawashima, T., Okuno, H., Nonaka, M., Adachi-Morishima, A., Kyo, N., Okamura, M., Takemoto-Kimura, S., Worley, P. F. & Bito, H. (2009) Synaptic activity-responsive element in the Arc/Arg3.1 promoter essential for synapse-to-nucleus signaling in activated neurons. PNAS 106,316–21.

Kelly, K., Cochran, B. H., Stiles, C. D. & Leder, P. (1983) Cell-specific regulation of the c-myc gene by lymphocyte mitogens and platelet-derived growth factor. Cell 35,603–10.

Kimberly, W. T., LaVoie, M. J., Ostaszewski, B. L., Ye, W., Wolfe, M. S. & Selkoe, D. J. (2003) Gamma-secretase is a membrane protein complex comprised of presenilin, nicastrin, Aph-1, and Pen-2. PNAS 100,6382–7.

Kojro, E. & Fahrenholz, F. (2005) The non-amyloidogenic pathway: structure and function of alpha-secretases. Sub-cellular biochemistry 38,105–27.

Lee, Hey-Kyoung, Takamiya, K., Han, J.-S., Man, H., Kim, C.-H., Rumbaugh, G., Yu, S., Ding, L., He, C., Petralia, R. S., et al. (2003) Phosphorylation of the AMPA receptor GluR1 subunit is required for synaptic plasticity and retention of spatial memory. Cell 112,631–43.

Li, H., Gu, X., Dawson, V. L. & Dawson, T. M. (2004) Identification of calcium- and nitric oxide-regulated genes by differential analysis of library expression (DAzLE). PNAS 101,647–52.

Lin, Y., Bloodgood, B. L., Hauser, J. L., Lapan, A. D., Koon, A. C., Kim, T.-K., Hu, L. S., Malik, A. N. & Greenberg, M. E. (2008) Activity-dependent regulation of inhibitory synapse development by Npas4. Nature 455,1198–204.

Link, W., Konietzko, U., Kauselmann, G., Krug, M., Schwanke, B., Frey, U. & Kuhl, D. (1995) Somatodendritic expression of an immediate early gene is regulated by synaptic activity. PNAS 92,5734–5738.

Linseman, D. A., Bartley, C. M., Le, S. S., Laessig, T. A., Bouchard, R. J., Meintzer, M. K., Li, M. & Heidenreich, K. A. (2003) Inactivation of the myocyte enhancer factor-2 repressor histone deacetylase-5 by endogenous Ca2+/calmodulin-dependent kinase II promotes depolarization-mediated cerebellar granule neuron survival. JBC 278,41472–81.

Llano, I., González, J., Caputo, C., Lai, F. A, Blayney, L. M., Tan, Y. P. & Marty, A. (2000) Presynaptic calcium stores underlie large-amplitude miniature IPSCs and spontaneous calcium transients. Nature neuroscience 3,1256–65.

Lord, C., Ferro-Novick, S. & Miller, E. A. (2013) The Highly Conserved COPII Coat Complex Sorts Cargo from the Endoplasmic Reticulum and Targets It to the Golgi. Cold Spring Harbor perspectives in biology 5.

Lyford, G. L., Yamagata, K., Kaufmann, W. E., Barnes, C. A., Sanders, L. K., Copeland, N. G., Gilbert, D. J., Jenkins, N. A., Lanahan, A. A. & Worley, P. F. (1995) Arc, a Growth Factor and Activity-Regulated Gene, Encodes a Novel Cytoskeleton-Associated Protein That Is Enriched in Neuronal Dendrites. Neuron 14,433–445.

Ma, D., Zerangue, N., Lin, Y.-F., Collins, A., Yu, M., Jan, Y. N. & Jan, L. Y. (2001) Role of ER export signals in controlling surface potassium channel numbers. Science 291,316–9.

Malenka, R. C. & Bear, M. F. (2004) LTP and LTD: an embarrassment of riches. Neuron 44,5–21.

Malenka, R. C., Kauer, J. A., Zucker, R. S. & Nicoll, R. A. (1988) Postsynaptic calcium is sufficient for potentiation of hippocampal synaptic transmission. Science 242,81–4.

Malinow, R. & Malenka, R. C. (2002) AMPA receptor trafficking and synaptic plasticity. Annual review of neuroscience 25,103–26.

Man, H.-Y., Sekine-Aizawa, Y. & Huganir, R. L. (2007) Regulation of {alpha}-amino-3-hydroxy-5-methyl-4-isoxazolepropionic acid receptor trafficking through PKA phosphorylation of the Glu receptor 1 subunit. PNAS 104,3579–84.

Maniatis, T., Fritsch, E. F. & Sambrook, J. (1982) Molecular Cloning. A Laboratory Manual. Cold Spring Harbor, New York

Margeta-Mitrovic, M., Jan, Y. N. & Jan, L. Y. (2000) A Trafficking Checkpoint Controls GABA B Receptor Heterodimerization. Neuron 27,97–106.

Martone, M. E., Zhang, Y., Simpliciano, V. M., Carragher, B. O. & Ellisman, M. H. (1993) Three-dimensional visualization of the smooth endoplasmic reticulum in Purkinje cell dendrites. J Neuroscience 13,4636–4646.

Mattson, M. P. (2010) ER calcium and Alzheimer's disease: in a state of flux. Science signaling 3,pe10.

Mayer, M. L., Benveniste, M., Patneau, D. K. & Vyklicky Jr., L. (1992) Pharmacologic properties of NMDA receptors. Annals of the New York Academy of Sciences 648,194–204.

Mayford, M., Siegelbaum, S. A. & Kandel, E. R. (2012) Synapses and memory storage. Cold Spring Harbor perspectives in biology 4.

Mayor, M. L., Westbrook, G. L. & Guthrie, P. B. (1984) Voltage dependent block by Mg2+ of NMDA responses in spinal cord neurons. Nature 309,261–263.

McKinsey, T. A., Zhang, C. L. & Olson, E. N. (2002) MEF2: a calcium-dependent regulator of cell division, differentiation and death. Trends in biochemical sciences 27,40–7.

Meldolesi, J. (2001) Rapidly exchanging Ca2+ stores in neurons: molecular, structural and functional properties. Progress in neurobiology 65,309–38.

Mikhaylova, M., Sharma, Y., Reissner, C., Nagel, F., Aravind, P., Rajini, B., Smalla, K.-H., Gundelfinger, E. D. & Kreutz, M. R. (2006) Neuronal Ca2+ signaling via caldendrin and calneurons. Biochimica et biophysica acta 1763,1229–37.

Miyata, M., Finch, E. a, Khiroug, L., Hashimoto, K., Hayasaka, S., Oda, S. I., Inouye, M., Takagishi, Y., Augustine, G. J. & Kano, M. (2000) Local calcium release in dendritic spines required for long-term synaptic depression. Neuron 28,233–44.

Morgan, J. I., Cohen, D. R., Hempstead, J. L. & Curran, T. (1987) Mapping patterns of c-fos expression in the central nervous system after seizure. Science 237,192–7.

Mu, Y., Otsuka, T., Horton, A. C., Scott, D. B. & Ehlers, M. D. (2003) Activity-dependent mRNA splicing controls ER export and synaptic delivery of NMDA receptors. Neuron 40,581–94.

Nägerl, U. V., Eberhorn, N., Cambridge, S. B. & Bonhoeffer, T. (2004) Bidirectional activity-dependent morphological plasticity in hippocampal neurons. Neuron 44,759–67.

Nakamura, T., Lasser-Ross, N., Nakamura, K. & Ross, W. N. (2002) Spatial Segregation and Interaction of Calcium Signalling Mechanisms in Rat Hippocampal CA1 Pyramidal Neurons. The Journal of Physiology 543,465–480.

Nedivi, E., Hevroni, D., Naot, D., Israeli, D. & Citri, Y. (1993) Numerous candidate plasticity-related genes revealed by differential cDNA cloning. Nature 363,718–722.

Neves, G., Cooke, S. F. & Bliss, T. V. P. (2008) Synaptic plasticity, memory and the hippocampus: a neural network approach to causality. Nature Reviews Neuroscience 9,65–75.

Nowak, L., Bregestovski, P. & Ascher, P. (1984) Magnesium gates glutamate-activated channels in mouse central neurones. Nature 307,462–465.

Oertner, T. G. & Svoboda, K. (2002) Subliminal messages in hippocampal pyramidal cells. The Journal of Physiology 543,397–397.

Olmsted, J. B., Carlson, K., Klebe, R., Ruddle, F. & Rosenbaum, J. (1970) Isolation of microtubule protein from cultured mouse neuroblastoma cells. PNAS 65,129–36.

Opazo, P. & Choquet, D. (2011) A three-step model for the synaptic recruitment of AMPA receptors. Molecular and Cellular Neuroscience 46,1–8.

Opazo, P., Labrecque, S., Tigaret, C. M., Frouin, A., Wiseman, P. W., De Koninck, P. & Choquet, D. (2010) CaMKII triggers the diffusional trapping of surface AMPARs through phosphorylation of stargazin. Neuron 67,239–52.

Palade, G. E. & Porter, K. R. (1954) Studies on the endoplasmic reticulum. I. Its identification in cells in situ. Journal of experimental medicine 100,641–656.

Park, C. S., Gong, R., Stuart, J. & Tang, S.-J. (2006) Molecular network and chromosomal clustering of genes involved in synaptic plasticity in the hippocampus. JBC 281,30195–211.

Park, M. K., Choi, Y. M., Kang, Y. K. & Petersen, O. H. (2008) The endoplasmic reticulum as an integrator of multiple dendritic events. The Neuroscientist 14,68–77.

Pastalkova, E., Serrano, P., Pinkhasova, D., Wallace, E., Fenton, A. A. & Sacktor, T. C. (2006) Storage of spatial information by the maintenance mechanism of LTP. Science 313,1141–4.

Pasternak, S. H., Bagshaw, R. D., Guiral, M., Zhang, S., Ackerley, C. A., Pak, B. J., Callahan, J. W. & Mahuran, D. J. (2003) Presenilin-1, Nicastrin, Amyloid Precursor Protein, and -Secretase Activity Are Co-localized in the Lysosomal Membrane. JBC 278,26687–26694.

Pear, W. S., Nolan, G. P., Scott, M. L. & Baltimore, D. (1993) Production of high-titer helper-free retroviruses by transient transfection. PNAS 90,8392–6.

Plath, N., Ohana, O., Errington, M. L., Schmitz, D., Gross, C., Mao, X., Engelsberg, A., Mahlke, C., Welzl, H., Kobalz, U., et al. (2006) Arc/Arg3.1 Is Essential for the Consolidation of Synaptic Plasticity and Memories. Neuron 437–444.

Plutner, H., Davidson, H. W., Saraste, J., & Balch, W. E. (1992). Morphological analysis of protein transport from the ER to Golgi membranes in digitonin-permeabilized cells: role of the P58 containing compartment. JCB, 119(5), 1097–1116.

Porter, K. R. (1953) Observations on a submicroscopic basophilic component of cytoplasm. The Journal of experimental medicine 97,727–50.

Porter, K. R., Claude, A. & Fullam, E. F. (1945) A study of tissue culture cells by electron Microscopy. Journal of experimental medicine 81,233–246.

Pruunsild, P., Kazantseva, A., Aid, T., Palm, K. & Timmusk, T. (2007) Dissecting the human BDNF locus: bidirectional transcription, complex splicing, and multiple promoters. Genomics 90,397–406.

Puig, O., Caspary, F., Rigaut, G., Rutz, B., Bouveret, E., Bragado-nilsson, E., Wilm, M. & Séraphin, B. (2001) The tandem affinity purification (TAP) method: A general procedure of protein complex purification. Methods 24,218–229.

Qian, Z., Gilbert, M. E., Colicos, M. A., Kandel, E. R. & Kuhl, D. (1993) Tissue-plasminogen activator is induced as an immediate-early gene during seizure, kindling and long-term potentiation. Nature.

Ramanan, N., Shen, Y., Sarsfield, S., Lemberger, T., Schütz, G., Linden, D. J. & Ginty, D. D. (2005) SRF mediates activity-induced gene expression and synaptic plasticity but not neuronal viability. Nature neuroscience 8,759–67.

Ramírez, O. A., Vidal, R. L., Tello, J. A., Vargas, K. J., Kindler, S., Härtel, S. & Couve, A. (2009) Dendritic Assembly of Heteromeric gamma-Aminobutyric Acid Type B Receptor Subunits in Hippocampal Neurons. JBC 284,13077–13085.

Rial-Verde, E. M., Lee-Osbourne, J., Worley, P. F., Malinow, R. & Cline, H. T. (2006) Increased expression of the immediate-early gene Arc/Arg3.1 reduces AMPA receptor-mediated synaptic transmission. Neuron 52thisissu,461–474.

Rivera, V. M., Miranti, C. K., Misra, R. P., Ginty, D. D., Chen, R. H., Blenis, J. & Greenberg, M. E. (1993) A growth factor-induced kinase phosphorylates the serum response factor at a site that regulates its DNA-binding activity. Molecular and Cellular Biology 13,6260–6273.

Sala, C., Futai, K., Yamamoto, K., Worley, P. F., Hayashi, Y. & Sheng, M. (2003) Inhibition of dendritic spine morphogenesis and synaptic transmission by activity-inducible protein Homer1a. J Neuroscience 23,6327–37.

Sanger, F., Nicklein, S. & Coulson, A. R. (1977) DNA sequencing with chain-terminating inhibitors. PNAS 74,5463–5467.

Scott, D. B., Blanpied, T. A., Swanson, G. T., Zhang, C. & Ehlers, M. D. (2001) An NMDA receptor ER retention signal regulated by phosphorylation and alternative splicing. J Neuroscience 21,3063–72.

Scoville, W. B. & Milner, B. (1957) Loss of recent memory after bilateral hippocampal lesions. Journal of neurology, neurosurgery, and Psychiatry 20,11–21.

Sharp, A. H., McPherson, P. S., Dawson, T. M., Aoki, C., Campbell, K. P. & Snyder, S. H. (1993) Differential immunohistochemical localization of inositol 1, 4, 5-trisphosphate-and ryanodine-sensitive Ca2+ release channels in rat brain. J Neuroscience 13,3051–3063.

Shen, K. & Scheiffele, P. (2010) Genetics and cell biology of building specific synaptic connectivity. Annual review of neuroscience 33,473.

Sheng, M. & Greenberg, M. E. (1990) The Regulation and Function of c-fos and Other Immediate Early Genes in the Nervous System. Neuron 4,477–485.

Sheng, M., McFadden, G. & Greenberg, M. E. (1990) Membrane depolarization and calcium induce c-fos transcription via phosphorylation of transcription factor CREB. Neuron 4,571–82.

Sheng, M., Thompson, M. A. & Greenberg, M. E. (1991) CREB: a Ca(2+)-regulated transcription factor phosphorylated by calmodulin-dependent kinases. Science 252,1427–30.

Shepherd, J. D. & Huganir, R. L. (2007) The Cell Biology of Synaptic Plasticity: AMPA Receptor Trafficking. Annual review of cell and developmental biology 23,613–643.

Shepherd, J. D., Rumbaugh, G., Wu, J., Chowdhury, S., Plath, N., Kuhl, D., Huganir, R. L. & Worley, P. F. (2006) Arc/Arg3.1 mediates homeostatic synaptic scaling of AMPA receptors. Neuron 52,475–84.

Shi, S.-H., Hayashi, Y., Esteban, Jose A & Malinow, R. (2001) Subunit-specific rules governing AMPA receptor trafficking to synapses in hippocampal pyramidal neurons. Cell 105,331–43.

Shibata, Y., Voeltz, G. K. & Rapoport, T. A. (2006) Rough sheets and smooth tubules. Cell 126,435–9.

Sonnhammer, E. L., Von Heijne, G. & Krogh, A. (1998) A hidden Markov model for predicting transmembrane helices in protein sequences. ISMB: International Conference on Intelligent Systems for Molecular Biology 6,175–82.

Spacek, J. (1985) Three-dimensional analysis of dendritic spines. II. Spine apparatus and other cytoplasmic components. Anatomy and embryology 171,235–43.

Spacek, J. & Harris, K. M. (1997) Three-dimensional organization of smooth endoplasmic reticulum in hippocampal CA1 dendrites and dendritic spines of the immature and mature rat. J Neuroscience 17,190–203.

Stent, G. S. (1973) A physiological mechanism for Hebb's postulate of learning. PNAS 70,997–1001.

Van Strien, N. M., Cappaert, N. L. M. & Witter, M. P. (2009) The anatomy of memory: an interactive overview of the parahippocampal-hippocampal network. Nature Reviews Neuroscience 10,272–82.

Stump, G., Durrer, A., Klein, A.-L., Lütolf, S., Suter, U. & Taylor, V. (2002) Notch1 and its ligands Delta-like and Jagged are expressed and active in distinct cell populations in the postnatal mouse brain. Mechanisms of Development 114,153–9.

Swanger, S. A. & Bassell, G. J. (2012) Dendritic protein synthesis in the normal and diseased brain. Neuroscience 232,106–127.

Tanzi, R. E. & Bertram, L. (2005) Twenty years of the Alzheimer's disease amyloid hypothesis: a genetic perspective. Cell 120,545–55.

Terasaki, M., Slater, N. T., Fein, A., Schmidek, A. & Reese, T. S. (1994) Continuous network of endoplasmic reticulum in cerebellar Purkinje neurons. PNAS 91,7510–4.

Thinakaran, G. & Koo, E. H. (2008) Amyloid precursor protein trafficking, processing, and function. JBC 283,29615–9.

Toresson, H. & Grant, S. G. N. (2005) Dynamic distribution of endoplasmic reticulum in hippocampal neuron dendritic spines. The European journal of neuroscience 22,1793–8.

Treisman, R. (1987) Identification and purification of a polypeptide that binds to the c-fos serum response element. The EMBO journal 6,2711–7.

Turrigiano, G. G. (2008) The self-tuning neuron: synaptic scaling of excitatory synapses. Cell 135,422–35.

Tusnády, G. E. & Simon, I. (1998) Principles governing amino acid composition of integral membrane proteins: application to topology prediction. Journal of molecular biology 283,489–506.

Tusnády, G. E. & Simon, I. (2001) The HMMTOP transmembrane topology prediction server. Bioinformatics (Oxford, England) 17,849–50.

Ushkaryov, Y. a, Petrenko, a G., Geppert, M. & Südhof, T C. (1992) Neurexins: synaptic cell surface proteins related to the alpha-latrotoxin receptor and laminin. Science 257,50–6.

Vazdarjanova, A., McNaughton, B. L., Barnes, C. A, Worley, P. F. & Guzowski, J. F. (2002) Experience-dependent coincident expression of the effector immediate-early genes arc and Homer 1a in hippocampal and neocortical neuronal networks. J Neuroscience 22,10067–71.

Vlachos, A., Korkotian, E., Schonfeld, E., Copanaki, E., Deller, T. & Segal, M. (2009) Synaptopodin regulates plasticity of dendritic spines in hippocampal neurons. J Neuroscience 29,1017–33.

Voeltz, G. K., Prinz, W. A, Shibata, Y., Rist, J. M. & Rapoport, T. A. (2006) A class of membrane proteins shaping the tubular endoplasmic reticulum. Cell 124,573–86.

Wallace, C. S., Lyford, G. L., Worley, P. F. & Steward, O. (1998) Differential intracellular sorting of immediate early gene mRNAs depends on signals in the mRNA sequence. J Neuroscience 18,26–35.

Wang, K. H., Majewska, A., Schummers, J., Farley, B., Hu, C., Sur, M. & Tonegawa, S. (2006) In vivo two-photon imaging reveals a role of arc in enhancing orientation specificity in visual cortex. Cell 126,389–402.

Whitlock, J. R., Heynen, A. J., Shuler, M. G. & Bear, M. F. (2006) Learning induces long-term potentiation in the hippocampus. Science 313,1093–7.

Wisden, W. & Seeburg, P. H. (1993) Mammalian ionotropic glutamate receptors. Current Opinion in Neurobiology 3,291–8.

Won, J. & Silva, A. J. (2008) Molecular and cellular mechanisms of memory allocation in neuronetworks. Neurobiology of learning and memory 89,285–292.

Wu, J., Petralia, R. S., Kurushima, H., Patel, H., Jung, M., Volk, L., Chowdhury, S., Shepherd, J. D., Dehoff, M., Li, Y., et al. (2011) Arc/Arg3.1 regulates an endosomal pathway essential for activity-dependent β-amyloid generation. Cell 147,615–28.

Xia, Z., Dudek, H., Miranti, C. K. & Greenberg, M. E. (1996) Calcium influx via the NMDA receptor induces immediate early gene transcription by a MAP kinase/ERK-dependent mechanism. J Neuroscience 16,5425–36.

Yamagata, M., Sanes, J. R. & Weiner, J. A. (2003) Synaptic adhesion molecules. Current opinion in cell biology 15,621–32.

Yang, Y., Wang, X.-B., Frerking, M. & Zhou, Q. (2008) Delivery of AMPA receptors to perisynaptic sites precedes the full expression of long-term potentiation. PNAS 105,11388–93.

Yeckel, M. F. & Berger, T. W. (1990) Feedforward excitation of the hippocampus by afferents from the entorhinal cortex: redefinition of the role of the trisynaptic pathway. PNAS 87,5832–6.

Yeo, G., Holste, D., Kreiman, G. & Burge, C. B. (2004) Variation in alternative splicing across human tissues. Genome biology 5,R74.

Zimmerberg, J. & Kozlov, M. M. (2006) How proteins produce cellular membrane curvature. Nature reviews. Molecular cell biology 7,9–19.

5.2 Statement of Contribution

Extensive technical assistance with animal breeding and caring was provided by Eva Kronenberg and Hiltrud Voss. Cultivation and injection of embryonic stem cells as well as southern blot analysis of cells and mice was performed by Irm Hermans-Borgmeyer and Sarah Homann.

Genotyping of transgenic mice was done by several people including Navid Memarnia, Ute Süsens, Barbara Merz and the author. All competent bacteria used for molecular cloning were kindly provided by Ute Süsens.

Kainic acid injection for seizure induction were performed either by or under the supervision of PD Dr. Guido Hermey. Perfusions were carried out under the supervision of either PD Dr. Guido Hermey or Dr. Claudia Mahlke. Technical assistance by Ulla Kobalz, Anastasia Stawrakakis, Barbara Merz, Andrea Zeisser and Ute Süsens contributed to this work. Specifically 2DE (U.K.), molecular cloning (A.Z.), mammalian-2-hybrid analysis (A.Z.), Northern blot analysis (B.M.) as well as in situ hybridizations (B.M.).

5.3 Curriculum Vitae

For privacy reasons the CV is not included in the online version of this dissertation.

Aus datenschutzrechtlichen Gründen ist der Lebenslauf in der Online-Version der Dissertation nicht enthalten.

For privacy reasons the CV is not included in the online version of this dissertation.

Aus datenschutzrechtlichen Gründen ist der Lebenslauf in der Online-Version der Dissertation nicht enthalten.

Der experimentelle Teil dieser Arbeit wurde angefertigt unter der Betreuung durch Prof. Dr. Dietmar Kuhl von Mai 2008 bis Mai 2013 am Institut für Molekulare Neurobiologie der Freien Universität Berlin und am Zentrum für Molekulare Neurobiologie Hamburg (ZMNH) des Universitätsklinikums Hamburg-Eppendorf in Hamburg, Deutschland.

Ich versichere ausdrücklich, daß ich die Arbeit selbständig und ohne fremde Hilfe verfaßt, andere als die von mir angegebenen Quellen und Hilfsmittel nicht benutzt und die aus den benutzten Werken wörtlich oder inhaltlich entnommenen Stellen kenntlich gemacht habe.

Jakob Gutzmann 18.05.2013